(12) INTERNATIONAL APPLICATION PUBLISHED UNDER THE PATENT COOPERATION TREATY (PCT)

(19) World Intellectual Property Organization
International Bureau

(43) International Publication Date
01 July 2021 (01.07.2021)

WIPO | PCT

(10) International Publication Number
WO 2021/130505 A1

(51) International Patent Classification:
B06B 1/06 (2006.01) *G10K 11/02* (2006.01)
G10K 11/34 (2006.01) *G10K 11/22* (2006.01)
G10K 11/04 (2006.01)

(21) International Application Number:
PCT/GB2020/053373

(22) International Filing Date:
29 December 2020 (29.12.2020)

(25) Filing Language: English

(26) Publication Language: English

(30) Priority Data:
62/953,577 25 December 2019 (25.12.2019) US
62/954,171 27 December 2019 (27.12.2019) US

(71) Applicant: **ULTRALEAP LIMITED** [GB/GB]; The West Wing, Glass Wharf, Bristol, Bristol, BS2 OEL (GB).

(72) Inventors: **LONG, Benjamin John Oliver**; Ultraleap Limited, The West Wing, Glass Wharf, Bristol, Bristol, BS2 0EL (GB). **KAPPUS, Brian**; Ultraleap Limited, The West Wing, Glass Wharf, Bristol, Bristol, BS2 0EL (GB). **PRICE, Adam**; Ultraleap Limited, The West Wing, Glass Wharf, Bristol, Bristol, BS2 0EL (GB).

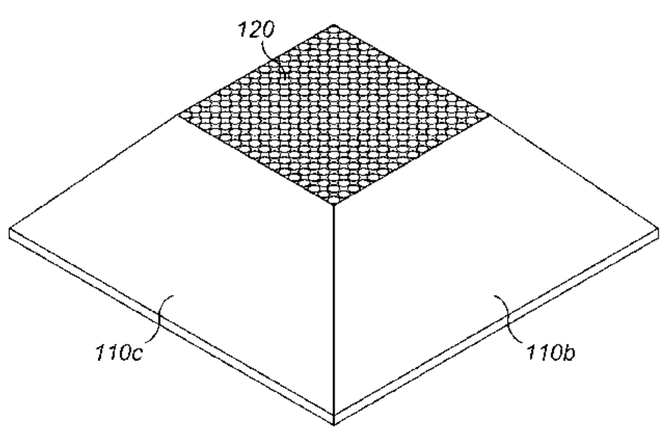
(74) Agent: **WITHERS & ROGERS LLP**; 4 More London Riverside, London, Greater London, SE1 2AU (GB).

(81) Designated States *(unless otherwise indicated, for every kind of national protection available)*: AE, AG, AL, AM, AO, AT, AU, AZ, BA, BB, BG, BH, BN, BR, BW, BY, BZ, CA, CH, CL, CN, CO, CR, CU, CZ, DE, DJ, DK, DM, DO, DZ, EC, EE, EG, ES, FI, GB, GD, GE, GH, GM, GT, HN, HR, HU, ID, IL, IN, IR, IS, IT, JO, JP, KE, KG, KH, KN, KP, KR, KW, KZ, LA, LC, LK, LR, LS, LU, LY, MA, MD, ME, MG, MK, MN, MW, MX, MY, MZ, NA, NG, NI, NO, NZ, OM, PA, PE, PG, PH, PL, PT, QA, RO, RS, RU, RW, SA, SC, SD, SE, SG, SK, SL, ST, SV, SY, TH, TJ, TM, TN, TR, TT, TZ, UA, UG, US, UZ, VC, VN, WS, ZA, ZM, ZW.

(84) Designated States *(unless otherwise indicated, for every kind of regional protection available)*: ARIPO (BW, GH, GM, KE, LR, LS, MW, MZ, NA, RW, SD, SL, ST, SZ, TZ, UG, ZM, ZW), Eurasian (AM, AZ, BY, KG, KZ, RU, TJ, TM), European (AL, AT, BE, BG, CH, CY, CZ, DE, DK, EE, ES, FI, FR, GB, GR, HR, HU, IE, IS, IT, LT, LU, LV, MC, MK, MT, NL, NO, PL, PT, RO, RS, SE, SI, SK, SM, TR), OAPI (BF, BJ, CF, CG, CI, CM, GA, GN, GQ, GW, KM, ML, MR, NE, SN, TD, TG).

(54) Title: ACOUSTIC TRANSDUCER STRUCTURES

(57) Abstract: Defining critical spacing is necessary for steering of parametric audio. Comparing steering measurements both with and without a waveguide leads to a conclusion that the diffuse phyllotactic grating lobe contributes audio and is to blame for poor steering. In addition, the waveguide needs to function with correct phase offsets to achieve the steering required for performance. Arranging tubes so that the array configuration changes from rectilinear to another distribution is useful when the waveguide is short of critical spacing or constrained for space. Array designs may also capitalize on rectilinear transducer design while having the benefits of a transducer tiling that has irrational spacing to promote the spread of grating lobe energy.



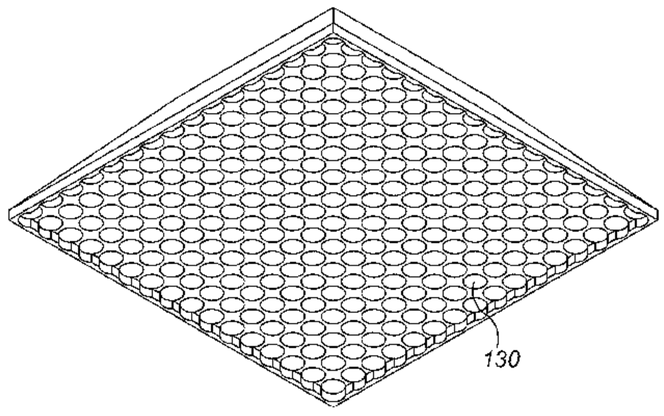


FIG. 1C

[Continued on next page]

WO 2021/130505 A1

Published:

— *with international search report (Art. 21(3))*

— *the filing date of the international application is within two months from the date of expiration of the priority period (Rule 26bis.3)*

ACOUSTIC TRANSDUCER STRUCTURES

PRIOR APPLICATIONS

[0001] This application claims the benefit of: (1) U.S. Provisional Patent Application No. 62/953,577, filed December 25, 2019; and (2) U.S. Provisional Patent Application No. 62/954,171, filed on December 27, 2019, both of which are incorporated by reference in its entirety.

FIELD OF THE DISCLOSURE

[0002] The present disclosure relates generally to improved techniques in acoustic transducer structures used in mid-air haptic systems.

BACKGROUND

[0003] As discussed herein, the term "phased array" refers to a group of transmitters which project into the same space and can be individually addressed. By selecting specific signals or, in the case of a monochromatic array, phases and amplitudes, the group of transmitters can shape the emitted field. In the case of an ultrasound phased array in air, the sound field can be focused, made to diverge, shaped into beams, and generally rearranged into many other forms. Uses for shaped and steered ultrasonic fields include mid-air haptics, directional audio, and the imaging of physical materials and scenes.

[0004] Steering via a phased array can encounter grating lobes when element spacing is above critical spacing. This results in sound energy being projected in unintended directions. To bring the array closer to critical spacing an acoustic waveguide structure can be used. Jager et al.(2017 IEEE) demonstrated beam steering using a waveguide structure. While Jager shows a reduction in grating lobes, it does not realize or demonstrate consequences with respect to haptics or parametric audio.

[0005] Further, described herein are array designs that are intended to capitalize on rectilinear transducer design, yet have the benefits of a transducer tiling that has irrational spacing to promote the spread of grating lobe energy.

[0006] Arranging the transducers of an emitting phased array system generates unwanted extra features depending on such parameters as wavelength, element size, separation distance between elements and geometric uniformity of spacing.

[0007] As the wavelength is decreased, the element size and separation distance when measured in wavelengths increases. Above a certain size, grating lobes appear and distort the output, which at the extremes creates extra output focus points that are unwanted.

[0008] For commercial reasons it may be necessary to set the frequency independently of the size and spacing of the elements, wherein with a structure with geometric uniformity of spacing, when actuated to produce a focus unwanted extra output focus points appear. In this case, the only modifiable parameter is the uniformity of the geometry. However, commercially, it is beneficial to create transducers that do not waste material, have high packing density and minimize the number and complexity of steps required for manufacture.

SUMMARY

[0009] One key innovation disclosed herein is recognizing that approaching critical spacing is necessary for steering of parametric audio. When looking at ultrasound simulation or measurement data, it is not apparent that the diffuse phyllotactic grating lobe contributes as much audio as it does. Nor does measurement of the audio alone lead to the conclusion that grating lobes are to blame for the poor steering. It takes comparing steering measurements both with and without a waveguide to come to that conclusion. In addition, the waveguide needs to be functioning with correct phase offsets to achieve the steering required for performance.

[0010] In addition, Jager et al. only demonstrates operation using equal-length tubes and does not discuss other possibilities. In this disclosure, different-length

tubes are equally functional and allow for a much wider variety of shapes. Also, arranging tubes so that the array configuration changes from rectilinear to another distribution is a non-obvious use and has benefits when the waveguide is short of critical spacing or constrained for space.

[0011] Further, this disclosure describes array designs intended to capitalize on rectilinear transducer design while having the benefits of a transducer tiling that has irrational spacing to promote the spread of grating lobe energy.

BRIEF DESCRIPTION OF THE DRAWINGS

[0012] The accompanying figures, where like reference numerals refer to identical or functionally similar elements throughout the separate views, together with the detailed description below, are incorporated in and form part of the specification, serve to further illustrate embodiments of concepts that include the claimed invention and explain various principles and advantages of those embodiments.

[0013] Figures 1A, 1B, and 1C show an arrangement of a waveguide.

[0014] Figure 2 shows a grating lobe suppression simulation.

[0015] Figure 3 shows a grating lobe suppression simulation.

[0016] Figure 4 shows laser doppler vibrometer scan images.

[0017] Figure 5 shows an arrangement of transducers as a phyllotactic spiral.

[0018] Figure 6 shows the effect of Figure 5 in simulation.

[0019] Figures 7A and 7B illustrate an ultrasonic acoustic simulation of a rectilinear array.

[0020] Figures 8A and 8B illustrate an ultrasonic acoustic simulation using an array in a phyllotactic spiral arrangement.

[0021] Figure 9 shows the audio steering performance of a tone production of an array arranged in a phyllotactic spiral.

[0022] Figure 10 shows the audio steering performance of a tone production of an array arranged in a phyllotactic spiral.

[0023] Figure 11 shows steering of a parametric audio beam using a rectilinear array.

[0024] Figure 12 shows steering of a parametric audio beam using a rectilinear array.

[0025] Figure 13 shows steering of a parametric audio beam using a rectilinear array.

[0026] Figure 14 shows a frequency response of parametric audio from a transducer array.

[0027] Figure 15 shows a Voronoi diagram of a point set in a phyllotactic spiral.

[0028] Figure 16 shows a plot having circular transducers arranged in a phyllotactic spiral.

[0029] Figure 17 shows a plot having square transducers arranged in a phyllotactic spiral.

[0030] Figure 18 shows a rectilinearly aligned arrangement of transducers.

[0031] Figure 19 shows a Bragg diffraction of a square lattice of transducer elements.

[0032] Figure 20 shows binary tiling of transducers.

[0033] Figures 21A and 21B show Bragg diffractions of binary tiling.

[0034] Figures 22A and 22B show pinwheel tiling and its Bragg diffraction.

[0035] Figure 23 shows a right-angled triangle motif present in the pinwheel fractal construction.

[0036] Figure 24 shows rectangular arrays designs for left- and right-handed 'domino' arrays having 1:2 aspect ratio.

[0037] Figure 25 shows designs for four variants of the 'square' arrays.

[0038] Figure 26 shows a simulation of eigenmodes using the Helmholtz equation.

[0039] Figure 27 shows a simulation of maximum z-deflection for a bending mode of piezoelectric actuator.

[0040] Figure 28 shows a simulation of maximum z-deflection for a bending mode of piezoelectric actuator.

[0041] Figure 29 shows a simulation that details the basic steps for arranging a square unit cell into a new arrangement.

[0042] Figure 30 shows a simulation that illustrates how Figure 29 may be recursively extended to build larger arrays of elements.

[0043] Figure 31 shows a simulation that illustrates variation possibilities provided by rotation or mirroring or both.

[0044] Figures 32A, 32B, 32C, and 32D show an example element array of square transducers constructed using rotation.

[0045] Figures 33A, 33B, 33C, and 33D show an example element array of square transducers constructed using mirroring.

[0046] Figures 34A, 34B, 34C, and 34D show an example element array of square transducers constructed using rotation and mirroring.

[0047] Figure 35 shows is a graph showing the simulated recursive offset arrays using square transducers.

[0048] Skilled artisans will appreciate that elements in the figures are illustrated for simplicity and clarity and have not necessarily been drawn to scale. For example, the dimensions of some of the elements in the figures may be exaggerated relative to other elements to help to improve understanding of embodiments of the present invention.

[0049] The apparatus and method components have been represented where appropriate by conventional symbols in the drawings, showing only those specific details that are pertinent to understanding the embodiments of the present invention so as not to obscure the disclosure with details that will be readily apparent to those of ordinary skill in the art having the benefit of the description herein.

DETAILED DESCRIPTION

[0050] I. Steering of an Ultrasonic Phased Array Using an Acoustic Waveguide Structure

[0051] A. Introduction

[0052] A limitation encountered when working with an ultrasonic phased array is the phenomena of grating lobes. This is the effect wherein certain arrangements of

transducers produce leakage of energy in unintended directions taking the form of an erroneous lobe of output. To illustrate this effect, consider a linear array of transducers with spacing a from center-to-center. When they are all producing ultrasound in phase, they produce a field similar to a line source, where a section taken perpendicularly to the array of transducers will reveal a circular diverging wave front, but in the plane of the transducers there will be a substantially linear wave front projecting directly away from the transducers. Now, consider another direction at angle θ from the vertical in that plane. The distance along that direction before an emitted spherically diverging wave front from one transducer connects with another transducer is given by $d = a \sin \theta$. When this distance is equal to one wavelength then along that direction every wave is adding constructively. The result of this constructive interference at that angle is a grating lobe. The angle this occurs is given by $\theta = \sin^{-1} \frac{\lambda}{a}$, where λ is the wavelength of the ultrasound. This illustrates that the grating lobe, in this instance, is dependent on the spacing a and how it compares to the wavelength λ. If, for instance, a is smaller than λ, a solution does not exist and therefore a grating lobe will not exist in this arrangement and emission scenario.

[0053] Grating lobes in phased arrays have been studied extensively and careful analysis shows that all grating lobes will be eliminated regardless of arrangement when the spacing of transducers is equal to or smaller than half of the wavelength ($\frac{1}{2}\lambda$) (Wooh & Shi, 1999). This is referred to as 'critical spacing'. A linear or planar array with transducers spaced at critical spacing will be able to achieve desired fields without grating lobe artefacts. As demonstrated above, grating lobes for a beam produced at a right angle directly away from the array, vanish as the system approaches a wavelength (λ) spacing, or double that of critical spacing. If moving or steering the beam in any direction other than directly perpendicular however, in that arrangement, grating lobes will immediately appear when the system starts to steer. In between wavelength spacing (λ) and critical spacing ($\frac{1}{2}\lambda$) there exists a class of arrays which can steer to increasingly larger angles without grating lobes. This could be beneficial if large steering angles are not

required as larger transducers tend to provide stronger acoustic fields. So, fewer would be required, simplifying the design of the system.

[0054] The geometry of ultrasonic transducers is dictated by many factors including the materials used, the actuating element, matching layers, resonant cavities, and many other aspects of the transducer element design. It can be difficult to design a transducing element which can achieve critical spacing. In addition, an oddly shaped elements may prevent arrangements which mitigate secondary focusing from grating lobes such as a phyllotactic spiral. The invention presented here is a series of tubes, or waveguide paths, which can be mounted directly atop a transducer or array of transducers which direct the acoustic output to a second aperture at the opposite end of the waveguide. From the perspective of the produced acoustic field, it is as if the transducer aperture has been substantially replaced by this second aperture in terms of the geometric arrangement of the phased array. In one such geometric arrangement, the waveguide can be used to adjust the spatial arrangement of transducers from, for example, rectilinear to a phyllotactic spiral. In another arrangement, the open aperture can be reduced so that critical spacing can be achieved.

[0055] Figures 1A, 1B, and 1C show an example arrangement 100 of this innovation in various views. Shown is a rectilinear array with tapering openings 120, 130 on the upper and lower sides with a cross section shown via A-A 140 in Figure 1A. These openings 120 130 are surrounded by members 110a, 110b, 110c, 110d as shown in Figures 1A, 1B, and 1C.

[0056] Specifically, this waveguide couples to a 16×16 rectilinear array 120 of 1cm diameter circular transducers spaced at 1.03cm which operate at 40kHz. The waveguide forms straight-line tapering paths to circular openings with 5mm spacing. At sea level and standard conditions, the wavelength of 40kHz is 8.6mm. The waveguide therefore transforms the apparent geometry of the array from 1.2λ spacing to $.58\lambda$ spacing, much closer to the 0.5λ critical spacing. In other words, this shows an example waveguide that transforms a 16 x 16 rectilinear array of 10 mm 40 kHz transducers to near critical (5 mm) spacing.

[0057] Figure 2 and Figure 3 show the effectiveness of this new, tighter spacing. Figure 2 shows a graph 200 of grating lobe suppression that is focused at [x,y,z] = [40mm,0,150mm]. The x-axis 210 is location in mm. The y-axis 220 is in db. A normal plot 230 is compared to a waveguide plot 240.

[0058] In Figure 2, a focus point is projected at $[x, y, z] = [40\text{mm}, 0, 150\text{mm}]$ and a microphone is swept across the x-dimension at $z = 150\text{mm}$. A clear focus point is observed at $x = 40\text{mm}$ in both the regular and waveguide arrangement. However, for the widely spaced regular arrangement, a secondary focus caused by the grating lobe is readily apparent at $x = -110\text{mm}$. The tighter spacing enabled by the waveguide prevents the creation of a secondary focus.

[0059] Figure 3 shows another example of grating lobe suppression via graph 300 of a similar experimental measurement with the focus projected at $x = 80\text{mm}$. The x-axis 310 is location in mm. The y-axis 320 is in db. A normal plot 330 is compared to a waveguide plot 340.

[0060] Figure 3 illustrates the necessity to approach critical spacing when steering to larger angles – in this case the secondary focus is nearly the same magnitude as the intended focus. Once again, the tight spacing enabled by the waveguide eliminates the grating lobe.

[0061] A further experimental verification is shown in Figure 4, which is a series 400 of a scanning laser doppler vibrometer scan images 410 430 of the acoustic field. This method directly images the acoustic field without potentially disturbing the field with a solid microphone. As with the microphone data, no grating lobe is observed without steering 420 and even when steered to a 45° angle 440

[0062] B. Waveguides for Focused Ultrasound

[0063] Mid-air haptics uses specialized high-pressure acoustic fields, typically modulated foci, to produce a vibrotactile sensation on the human body. Grating lobes can cause secondary fields which are also modulated, thereby creating haptics in unintended places.

[0064] One method to prevent grating lobes from forming secondary foci is to arrange the emitting array into a pseudo-random arrangement. Figure 5 shows one

such arrangement 500 of 7 mm transducers 530 as a phyllotactic spiral . The x-axis 510 and the y-axis 520 are in meters. The inset square 540 illustrates the extent of an array of the same transducers packed into a rectilinear arrangement. This arrangement contains no regular spatial frequencies and therefore prevents grating lobes from forming secondary foci.

[0065] Figure 6 shows the effect of Figure 5 in simulation 600. The x-axis 610 and y-axis 620 are in mm. The grayscale is in pressure (arbitrary) units. Here, the field in the x-y plane 640 parallel to the array at $z = 20\text{cm}$ is simulated when a focus 630 is placed at $x = 10\text{cm}$ and $z = 20\text{cm}$. The grating lobe focus in a rectilinear array of similar density would appear at approximately $x = 5\text{cm}$. The phyllotactic arrangement distributes this secondary focus to a large arc in the negative x domain. Without a tight focus, the grating lobe will not produce a haptic sensation.

[0066] One distinct downside of the phyllotactic arrangement is the large spacing required. The inset square 540 in Figure 5 shows the extent of an array if the same transducers were packed rectilinearly. The increased size of the phyllotactic spiral arrangement might prevent the use of such an array in integrations which are tight on space, as well as likely increase the cost of manufacture.

[0067] Using a waveguide structure, it is possible to use connect a rectilinear transducer array to a phyllotactic spiral-arranged or similarly pseudo-random exit pattern which distributes grating lobe energy. In one arrangement, design consists of a straight-line tube from each transducer to the closest exit aperture. Depending on the size and shape of the exit arrangement, this may require iterative design to prevent crossing of tubes. This will also likely create different length tubes requiring measured or simulated phase offsets to be included in steering calculations (discussed below).

[0068] A pseudo-random arrangement is not required, however, when the exit apertures are near critical spacing. For haptics, however, this can lead to some drawbacks. For instance, with a reduced exit aperture, the effective depth of focus will increase at similar distances. Without a tight focus, peak pressure will be

lower and potentially provide a reduced haptic effect. At the same time, with increased steering ability provided by the critical spacing, focus shape will be maintained through large steering angles close to the array. Depending on the application, a waveguide can be designed which optimizes the interplay between reduced grating lobes, depth of focus, and exit aperture size.

[0069] C. Waveguides for Parametric Audio

[0070] Parametric audio is an effect whereby audible sound is produced by nonlinear distortion in the air when ultrasound at varying frequencies is present. By controlling the short-wavelength field of ultrasound, the resulting audio can be controlled to a degree not possible using conventional loudspeakers.

[0071] The most common use of the parametric audio effect is to produce beams of audio which follow beams of ultrasound. Within the beam, audio is being produced in every volume element in proportion to the magnitude and relative frequencies present. After the audible sound is produced, it spreads out more due to its larger wavelength relative to the ultrasound. The largest magnitude of audible sound, however, will exist within the ultrasound beam, so only in a direction that will be reinforced through further parametric audio generation.

[0072] Figures 7A and 7B illustrate an ultrasonic acoustic simulation 700 of a rectilinear array at 1.2λ spacing producing a beam at 30° steering angle. A grating lobe beam is clearly visible, directed away from the steering direction. In Figure 7A, the simulation 730 shows two audio beams, each directed along its own ultrasonic beam. The net result will be two diverging audio beams which will limit the perceived directionality of the system and its ability to target specific users. In Figure 7B, the simulation 730 shows a grating lobe 770 that appears in the negative-y steering angle.

[0073] Figures 8A and 8B illustrate an ultrasonic acoustic simulation 800 using an array in a phyllotactic spiral arrangement with packing density comparable to a 1.2λ rectilinear array. Simulation of a phyllotactic-spiral arranged ultrasonic array above critical spacing projecting a beam in the positive-y direction at 30 degrees. In Figure 8A, the simulation 830 shows the pseudo-random arrangement of

transducers distributes the energy found in the grating lobe into a large arc. At first glance, it is not obvious that this diffuse, low-intensity, arc of ultrasound would be able to generate any significant parametric audio. In Figure 8B, the simulation 860 shows a grating lobe 870 is distributed and directed towards in the negative-y direction but is much more diffuse when compared to the rectilinear arrangement.

[0074] Figure 9 and Figure 10 show the audio steering performance of 1kHz tone production of a 61kHz array arranged in a phyllotactic spiral with packing density of about 1.2λ at 10° and 30° respectively. The graph 900 in Figure 9 has a plot 930 where the x-axis 910 is angle (degrees) and the y-axis 920 is SPL (db). The graph 1000 in Figure 10 has a plot 1030 where the x-axis 1010 is angle (degrees) and the y-axis 1020 is SPL (db).

[0075] This measurement shows the audio sound level measured at a given angle with respect to the normal of the array in a large room. Even with a relatively small 10° steering angle (Figure 9) the measured audio emitted is not symmetric about the array, which one would expect if the grating beam were not present. When steered to a more extreme angle such as 30° (Figure 10), the polar profile shows sound is coming out at unintended angles, at around about -20°, and at a greater amplitude than even the intended +30° steering. This roughly corresponds to the angle of the grating beam/arc simulated in Figure 8. This unexpected result is created because while the grating beam has a lower peak pressure spatially, its size and spatial extent make up for this lack of intensity. As discussed above, when parametric audio is generated, due to its larger wavelength, it diffracts and spreads out more readily than the ultrasound. Therefore, at any given cross-section, and entire arc of low-intensity sources in the grating beam are contributing to parametric audio in that general direction. As a result, phyllotactic spiral-arranged arrays not only do not help, but actively hurt parametric audio steering performance from ultrasonic phased arrays due to their lower packing density compared to rectilinear or hexagonal-packed arrays.

[0076] Fortunately, arrays approaching critical spacing do help with steering parametric audio due to their complete lack of grating lobe energy.

[0077] Figure 11 shows a graph 1100 with an x-axis 1110 of angle (degrees) and a y-axis 1120 in dB having a normal plot 1130 and a waveguide plot 1140. Specifically, Figure 11 shows steering of a parametric audio beam to +10 degrees using a rectilinear array at 1.2 lambda (normal) and the .58 lambda waveguide illustrated in Figure 1.

[0078] Figure 12 shows a graph 1200 with an x-axis 1210 of angle (degrees) and a y-axis 1220 in dB having a normal plot 1230 and a waveguide plot 1240. Specifically, Figure 12 shows steering of a parametric audio beam to + 20 degrees using a rectilinear array at 1.2 lambda (normal) and the .58 lambda waveguide illustrated in Figure 1.

[0079] Figure 13 shows a graph 1300 with an x-axis 1310 of angle (degrees) and a y-axis 1320 in dB having a normal plot 1330 and a waveguide plot 1340. Specifically, Figure 13 shows steering of a parametric audio beam to + 40 degrees using a rectilinear array at 1.2 lambda (normal) and the .58 lambda waveguide illustrated in Figure 1.

[0080] Figure 13 shows a graph 1400 with an x-axis 1410 of frequency (Hz) and a y-axis 1420 in SPL (dB) having a normal plot 1430 and a waveguide plot 1440. Specifically, Figure 14 shows frequency response of parametric audio from a 16 x 16 40 kHz transducer array with and without a waveguide.

[0081] Thus Figure 11, Figure 12, and Figure 13 show the parametric audio steering performance of the waveguide shown in Figure 1 compared to a bare 1.2λ-spaced 40kHz array. As is readily observed, the near-critically-spaced exit apertures of the waveguide eliminate the grating lobe beam and its resulting audio. This shows that the invention presented here enables aggressive steering of parametric audio to arbitrary angles from any size transducer by enabling critical spacing. In addition, the frequency response is virtually unaffected as shown in Figure 14.

[0082] D. Waveguide Design and Operation

[0083] Enabling proper operation of a phased array with a waveguide requires adjusting the output to compensate for the waveguide itself. In other words, just like the phase of each and amplitude for each transducer must be coordinated and driven precisely, any relative change caused by a waveguide path must also be compensated for. For instance, if one waveguide path causes a phase offset of $\pi/4$ while another in for the same array causes a $\pi/2$ shift, then this offset must be subtracted from the desired phase of each transducer respectively when calculating activation coefficients for a given field. If both amplitude and phase for each transducer are considered as a complex number, and the attenuation and phase delay of the waveguide tube a further complex number, then the application of the correction factor for the waveguide may be realized as the division of the first by the second. Without this compensation, the field will be malformed and distorted by the waveguide. In addition, if activation coefficients are produced using a model which accounts for time-of-flight, any time-delay caused by the waveguide must be compensated for as coefficients are calculated.

[0084] Phase offsets and time-delays can be derived using empirical or simulated methods. The simplest approach, albeit time-consuming, is to measure the phase offsets and time-delays associated with each waveguide path directly. In one arrangement, phase can be measured with continuous, monochromatic drive with reference to a control signal, while time delay can be measured with an impulse, chirp or comparison to a control path. Another approach is to calculate the phase and time delay with simulation. This could be done with something as sophisticated as a finite element model (FEA) or an analytic model of a pipe or appropriate structure. In the data presented in previous sections, the phase offsets were calculated using the length of each waveguide path, where this was divided through by the wavelength of the ultrasonic excitation in free air resulting in a remainder that describes the appropriate phase offset. This was then refined by measuring the strength and location of a focus generated directly above the array at 15cm and compared to a model. Increasing the effective length of each tube by

8% resulted in a good fit to simulation. As stated above, without this compensation, the waveguide structure will not produce the expected field.

[0085] Most of the discussion here has been about waveguides for transmit, but they also work for receive. A receiver placed at one end of a waveguide will only receive and produce a signal when ultrasound is directed at the aperture at the opposing end of the waveguide. A receive system at critical spacing will be free from aliased ghost images created by grating lobe artefacts. In addition, shaping the open aperture of the waveguide into a horn or similar structure could provide increased sensitivity compared to the receive element in open air.

[0086] The waveguide shown in Figure 1 represents only one arrangement possible from this invention. The waveguide paths, in this case decreasing radius straight-line tubes, need not be straight, decreasing radius, circular in cross-section, or even void of material. As long as the ultrasonic acoustic wave can propagate down the waveguide path and its phase offset and time delay can be well characterized and consistent, then it can be used to manipulate the array. For instance, a waveguide which transforms a rectilinear array into a phyllotactic pseudo-random arrangement will certainly not involve straight-line tubes and will likely incorporate non-circular cross-sections. In another arrangement, a waveguide could be used to bend the acoustic field around a corner with each waveguide path bending around to have an exit aperture at 90 degrees relative to the original waveguide. In another arrangement, the cross-section of the waveguide path can narrow before flaring out again near the exit aperture. This narrowing can provide increased acoustic impedance to the transducer, improving its acoustic output, as well as providing a horn-like exit aperture to increase the coupling to open air. In another arrangement, a variety of transducers could be utilized within the same array, say mixed frequency or emitting power, and a waveguide can bring them all into a unified emitting region.

[0087] The waveguide can be composed of a variety of materials. This includes metals, plastic, and even flexible polymers. The acoustic impedance of the construction material needs to be sufficiently higher than that of air to prevent

ultrasound from passing from one waveguide path to another (cross talk within the array). This is not difficult as most solids are at least two orders of magnitude higher acoustic impedance compared to air. This enables the possibility of using flexible materials such as plastic tubing as a portion of the waveguide. For instance, an exit aperture array, composed of metal or hard plastic could be coupled to an input array of transducers with plastic or polymer tubing. Then each could be mounted independently, allowing the flexible tubes to bridge the connection. The polymer tubes could remain flexible during their operating life or be cured in some way (UV for instance) after installation. Given that the length and shape will be fixed during assembly, the phase offset and time delay should remain mostly unchanged regardless of the exact details of placement, within reason. Extreme angles or pinched/obstructed tubes will obviously cause distortions. If more accuracy is required, measurement or simulation could provide the 2^{nd}-order corrections necessary.

[0088] In addition to plastic or polymers, metal can be used for a portion or all of the waveguide. Metal has the benefit of acting as a heat-sink as the waveguide can readily trap air, causing excessive heat storage.

[0089] The waveguide cross-section need not be a decreasing-radius curve or act as a simple tube. It is possible to design a relatively sudden decrease in radius along a waveguide path to produce a Helmholtz resonator-like design. Using this methodology, the larger-volume chambers could provide a boost to the output efficiency of the transducers while the exit apertures could be packed together to approach critical spacing.

[0090] The volume within the waveguide paths need not be completely empty. Filling material such as Aerogel could be packed into the waveguide to provide a different acoustic impedance if so desired. Besides acoustic impedance matching, different materials could provide environmental proofing like water resistance.

[0091] Manufacturing the waveguides can be done with a variety of techniques. The array design shown in Figure 1—and proven experimentally—was produced with an additive manufacturing technique (FDM 3D printing). Other possible

options include injection molding, where each waveguide path is formed by a removable pin. Symmetry can be exploited for waveguide production as well. For instance, the waveguide shown in Figure 1 has 4-fold symmetry and 4 identical pieces could be connected together to form the final product. Another manufacturing arrangement involves connecting many straight polymer tubes of appropriate lengths into a form then heating them near their glass transition temperature. Then a form can be applied externally to push the collection of tubes into their final waveguide form. This external force can be similar to a vacuum bag or even water pressure in the case of metal tubing. It is also possible to produce one waveguide tube at a time and then glue/fuse them into the final result.

[0092] The disclosure presented here allows for the transformation of ultrasonic phased arrays to transform from one arrangement to another without significant loss of output or field-synthesis ability. This enables critically spaced or pseudo-random arrangements from arbitrary-sized transducing elements.

[0093] The goal of this disclosure is to produce an estimate of the acoustic pressure from an ultrasound phased array which reasonably matches the measurement of a stationary or slow-moving microphone at a similar location.

[0094] There are methods that detail ways to calculate instantaneous pressure or intensity or other metrics in the field. Here a series of algorithms efficiently use computational resources to calculate time-averaged metrics. These are useful for determining and regulating hot spots and higher-than desired pressure.

[0095] Estimating the field strength from an ultrasonic phased array can be done by summing the contribution of each transducer to the point of interest. This contribution is already calculated when creating a converging spherical wave. We can reuse this calculation to add a virtual microphone to the system. By monitoring this microphone and moving it along with new focus points, a robust system of field estimates and regulation can be established.

[0096] E. <u>Additional Disclosure</u>

[0097] 1. An ultrasonic array consisting of:

A) A plurality of ultrasonic transducers;

B) An operating acoustic wavelength;

C) A plurality of acoustic cavities;

D) Wherein each cavity has a input opening and an exit opening;

E) Wherein each input opening accepts ultrasound from a single transducer;

F) Wherein at least 2 of the geometric centers of the cavity exit openings are situated less than one wavelength from one another;

G) Wherein the ultrasound emerging from the exit opening has a phase offset relative to when it entered the input opening; and

H) Wherein at least 2 cavities have different phase offsets.

[0098] 2. The apparatus as in ¶ 1, wherein the phase offset for at least one cavity is inverted and applied to the phase of at least one transducer drive before emission.

[0099] 3. The apparatus as in ¶ 2, wherein the ultrasound is modulated to produce audible sound.

[00100] 4. The apparatus as in ¶ 2, wherein the ultrasound is modulated to produce a mid-air haptic effect.

[00101] 5. The apparatus as in ¶ 2, wherein the ultrasound is used to levitate an object.

[00102] 6. The apparatus as in ¶ 2, wherein the ultrasound emerging from the exit opening has a different amplitude relative to when it entered the input opening.

[00103] 7. The apparatus as in ¶ 6, wherein the amplitude offset is used to modify the amplitudes of at least one transducer before emission.

[00104] 8. The apparatus as in ¶ 3, wherein the exit openings are substantially co-planar.

[00105] 9. The apparatus as in ¶ 8, wherein the audio is directed at an angle greater than 15 degrees from the normal to the plane.

[00106] 10. The apparatus as in ¶ 8, wherein the audio is directed at an angle greater than 30 degrees from the normal to the plane.

[00107] 11. The apparatus as in ¶ 8, wherein the audio is directed at an angle greater than 45 degrees from the normal to the plane.

[00108] 12. The apparatus as in ¶ 8, wherein the audio is directed at an angle greater than 60 degrees from the normal to the plane.

[00109] 13. The apparatus as in ¶ 6, wherein the amplitude offset is within 2dB.

[00110] 14. The apparatus as in ¶ 1, wherein the cavities consist of straight cylinders with a decreasing radius from input to exit opening.

[00111] 15. The apparatus as in ¶ 14, wherein the wavelength is less than 9mm.

[00112] 16. The apparatus as in ¶ 14, wherein the pitch of the exit cavities is less than 6mm.

[00113] 17. The apparatus as in ¶ 2, wherein the phase offsets are stored in memory on the apparatus.

[00114] 18. The apparatus as in ¶ 6, wherein the amplitude offsets are stored in memory on the apparatus.

[00115] II. Transducer Sub-Tiles of Different Chirality

[00116] Previous disclosures have described the phyllotactic spiral as an example of a non-uniform structure that splits the grating lobe structures into many pieces. However, for ease of manufacture it is difficult to use, as can be seen when looking at the Voronoi diagram of the point set 1500, as shown in Figure 15.

[00117] As can be seen form this Voronoi diagram of a point set in a phyllotactic spiral, the 'seed shape' moves between a diamond-like shape and a hexagon-like shape in bands that appear to roughly follow the Fibonacci sequence in thickness. As there is no one single shape in the limit, it is clear that there is no one optimal transducer shape for a design based on this approach.

[00118] While the continuously changing shape of the Voronoi cells results in a reasonable design for an array of transducing elements which are non-resonant with a broadband response as the function of output will then vary little with this small change in shape, when narrowband resonant structures are considered, this would require careful tuning of each structure which is currently commercially infeasible. Resonant devices cover a large proportion of existing technologies,

including devices based on the piezoelectric effect; passing electricity through crystal structures to create mechanical bending.

[00119] Shown in Figure 16 is a plot 1600 showing circular transducers 1640 arranged in a phyllotactic spiral are relatively densely packed in the center square 1630, but circular transducers may be more expensive to manufacture. The x-axis 1610 is in meters; the y-axis 1620 is in meters. Previous disclosures have also shown how circular transducers may be arranged in a phyllotactic spiral as in Figure 16, but to reduce cost transducers are more likely to have rectilinear elements in their design or layout.

[00120] Square transducers are more difficult to position as a simple arrangement that does not require rotation yields the arrangement shown in Figure 17.

[00121] Shown in Figure 17 is a plot 1700 showing square transducers 1740 arranged in a phyllotactic spiral that are relatively densely packed in the center square 1730. The x-axis 1710 is in meters; the y-axis 1720 is in meters. The result of a rectilinear positioning of square transducers in the configuration of a phyllotactic spiral. The uniform packing without gaps is overlaid as the larger square 1730.

[00122] Using singulated unit transducers in a phyllotactic arrangement, only allowing rectilinear alignment of the set of square transducers, results in a configuration that is over twice the area of the equivalent uniform square packing that has no wasted space. This is a problem, because the power output of the array is reduced by this factor per unit area. The greater the packing density, the less energy per unit area is lost to the unoccupied regions.

[00123] This can be improved if the singulated units are allowed to rotate, breaking the rectilinearly aligned arrangement, as shown in Figure 18. Here, the simulation 1800 shows results of positioning transducers with corners pointing towards the center of the spiral within square 1810. To increase the density further, the phyllotactic pattern has been built inwards and in cases where the square elements overlap, the angular position has been incremented until the overlap is resolved. The power has also been modified slightly downwards to an

exponent of .4392 rather than the .5 that is more traditional to describe distance from the center. However, even in this configuration, there is around 40% extra area used over the densely packed alternative, leading to a drop in output at a focus from an area limited array of around 3 dB. As this is unwanted, finding an entirely dense packing of transducers is preferred. This would be beneficial from a manufacturing perspective as it could be designed to be produced as a sheet or roll. However, it is difficult to find a dense packing that also fulfils the requirement of a non-uniform arrangement.

[00124] A dense packing of transducers mounted on a surface is equivalent to a tiling of the plane. As the grating effects that need to be reduced or removed are effectively the result of wave phenomena interacting with the 'lattice' of transducer emission locations, so the effect can be determined ahead of time by taking the Fourier transform of the arrangement, yielding an equivalent to a modelled Bragg diffraction pattern. Then, to find a pattern that is effective, a 'lattice' of transducer emission locations must be found that has a weak and disperse Bragg diffraction pattern.

[00125] The Bragg diffraction of the rectilinear system yields the corresponding grating lobe configuration with the central focus surrounded by extra false images separated again by the rectilinear grid, as shown in Figure 19. Figure 19 shows a Bragg diffraction 1900 of a square lattice of transducer elements, showing the grating lobe configuration produced by this geometric layout.

[00126] As many interesting planar aperiodic tilings of the plane have been studied due to their properties as molecular models of crystalline systems and especially as models of quasi-crystals and mixtures of metals, there is literature that describes the Bragg diffractions of tilings as analogues of problems in X-ray crystallography. Due to this, considering the paper, Senechal, M. "Tilings, Diffraction and Quasi-crystals", the most interesting two tiling systems studied alongside their Bragg diffractions are the binary and pinwheel systems for tiling the plane.

[00127] The first system considered is that of the 'binary' tiling, where transducing elements may take the two shapes of the fat and thin rhombus present in the tiling, as shown in Figure 20. Figure 20 shows "binary" tiling 2000. An aperiodic tiling with pentagonal symmetries, related to the Penrose rhombus tilings. Used originally to model chemical mixtures, it is made of two different types of rhombus'.

[00128] Shown in Figures 21A and 21B are Bragg diffraction of the "binary" tiling. Figure 21A shows binary tiling and choice of elements 2100 for a potential transducer array. Figure 21B shows five-fold pentagonal symmetry in the diffraction 2150 that appears here to be more decagonal symmetry. When considering the Bragg diffraction of the system shown in Figure 21, it is mostly well spread out. However, manufacturing two different fat and thin rhombus transducer designs, in terms of their different acoustic properties, as well as tuning their frequency responses may prove time consuming and could involve different processes, e.g., thicknesses of bending structure. Furthermore, there is no pattern that can be easily tiled to construct larger sets of elements.

[00129] Shown in Figures 22A and 22B are pinwheel tiling and its Bragg diffraction. Figure 22A shows pinwheel tiling 2200 and the element chosen as representative transducer tiles. Figure 22B shows the Bragg diffraction 2250 of this configuration. This second system is the pinwheel tiling, where each transducing element is comprised of a right-angle triangle with sides measuring 1, 2 and $\sqrt{5}$ in ratio as shown in Figure 22. As can be seen from the Bragg diffraction, the frequency distribution of elements of the pinwheel tiling is substantially disordered in the frequency domain. Of the two finalist tilings described earlier, this is more attractive for manufacture. This is firstly because there is only one species of shape to be produced in this design, but also secondly because the right-angled triangle can be realized as a rectangle with aspect ratio 1:2 cut diagonally, which can allow for manufacture in aspect ratio 1:2 rectangles and cut, allowing for processes for rectilinear elements to be used for the most part.

[00130] The pinwheel tiling is also a fractal in that there is a set of five right angle triangles with sides measuring ratios of 1, 2 and √5 which fit perfectly in the area of a single triangle of the same shape but with five times the area of one of these fitted triangles.

[00131] Shown in Figure 23 are triangles 2300 that may also be set again inside of those, any integer power of five may be constructed into a right-angle triangle in this way (5, 25, 125, etc.), to produce a larger array in the shape of the right-angled triangle motif present in the pinwheel fractal construction. These are designs for left- and right-handed triangular arrays. The top-most 2310 and mid-bottom 2330 rows show possible piezoelectric material positioning while the mid-top 2320 and bottom-most 2340 rows show potential top plate structures.

[00132] Also shown are the left and right chiral constructions of the fractal pinwheel tiling, and also shown is the format that allows for complete structures to be potentially fabricated from a single sheet or attached together at the points shown. Further shown are lightly shaded locations to which a vibrating plate may be attached to generate a wave or may alternatively topologically illustrate a potential method to choose vent locations. If they are manufactured singly, then these right-angle triangle fractal tiles have the drawback that they do not use an equal number of left and right-handed right angle single elements, which may cause logistical difficulties if not considered.

[00133] The larger fractal tiles which by nature also have sides measuring ratios of 1, 2 and √5 may be reconstructed into rectangular arrays with 1:2 aspect ratio as shown in Figure 24. Figure 24 shows designs 2400 for left- and right-handed ‘domino’ arrays. The name ‘domino’ is appropriate because the configuration is involved in a related tiling pattern colloquially named ‘kite & domino’ (and kite shaped arrays may instead be created by flipping the direction of one of the two right angle triangle array elements along their shared hypotenuse, to produce arrays with the same number of elements). The top-most 2410 and mid-bottom 2430 rows show possible piezoelectric material positioning while the mid-top 2420 and bottom-most 2440 rows show potential top plate structures.

[00134] These arrays may contain an integer power of five multiplied by two elements (10, 50, 250 etc.) as shown and because they are purely asymmetric must require an equal number of left and right-handed triangles. This is preferable in the case of single element manufacture, as there are then fewer special cases to consider during processing.

[00135] Figure 25 shows designs 2500 for all four variants of the 'square' arrays. Notice that the achiral antisymmetric designs require very different numbers of left- and right-handed elements which are highlighted via the difference in shading between single elements.

[00136] From these rectangular sub-tiles of different chirality 2510 2520 2530 2540 2550 2560 2570 2580 shown in Figure 25, there may be four different square array configurations symmetric and asymmetric variants of a left- and right-handed configuration. However, there is a trade-off in that the asymmetric variant uses a different number of individual elemental left and right chirality transducers, but only left sub-tiles, but the symmetric variants uses left and right sub-tiles, but an equal number of left and right elements. These effects may be traded off to achieve an optimized manufacturing procedure depending on the relative cost of each step in the required processing. These square arrays result in an element count that is four multiplied by an integer power of five elements (20, 100, 500, etc.). The result of this is that either left and right sub-tiles must be manufactured, or the amount of piezoelectric crystal pieces consumed with different chirality is different, although with a native pinwheel tiling piezoelectric crystal cutting approach this would not be a problem.

[00137] These aforementioned array tiling designs should not preclude any partial tessellations as produced by taking a subsection of the pinwheel tiling to use for its superior diffraction characteristics.

[00138] The one remaining barrier to this design is that if the edges of the transducing element are clamped and there is a boundary condition, the structure bonded to the piezoelectric crystal may not flex with sufficient displacement to produce efficient output.

[00139] By simulating the eigenmodes using the Helmholtz equation as shown in Figure 26 we can consider the displacement generated by a unit impulse. Simulating the displacement of a piezoelectric plate makes it clear that it is viable to create a piezoelectric transducer that fits the desired shape, as shown in Figure 27. Cutting a slot makes the displacement increase, but decreases the resonant frequency as shown in Figure 28.

[00140] Specifically, Figure 26 shows eigenmodes 2800 of the solutions to the Helmholtz equation on the triangle 2810a 2810b 2810c 2180d 2180e 2180f 2180g 2180h 2180i which yield the harmonic modes of vibration. For each mode, the shape of the Helmholtz solution may be extrapolated to describe the acoustic far field actuated by the mode. This may also be used in reverse, as a pattern of directivity of a receiving element at a similar frequency. As it can be seen that each mode may generate a field that is complicated, taking the combination of multiple harmonics spanning different frequencies, the reception or transmission into the far field can identify spatial offsets into the far field, especially in angle, which may be parameterized into azimuth and elevation. Due to the nature of the asymmetry in the individual transducer element this is possible, but the effect may be strengthened further by coupling this with the irrational and non-repeating frequency behavior of the tiling. By actuating and/or receiving using these shapes, their tilings and their harmonics, potentially across multiple elements, exact positions of objects intersecting the far field of the acoustic generated by such an element or group of elements may be deduced by algorithmically or otherwise examining signals received by these elements or by microphones. Equally, the signal may be emitted by a simple transducer and received by an array such as is earlier described. The result of this is that by using all of the harmonics and receiver can track its angular location relative to potentially even an individual transducer.

[00141] Shown in Figure 27 is a simulation 2600 of maximum z-deflection for bending mode of piezoelectric actuator in the right-angle triangle shape 2640 for insertion into the pinwheel tiling. The x-axis 2610 is in millimeters; the y-axis

2630 is in millimeters; the z-axis 2620 is in micrometers. The scaling is shown on the right bar 2650.

[00142] Shown in Figure 28 is a simulation of maximum z-deflection for bending mode of piezoelectric actuator in the right-angle triangle shape 2740 for insertion into the pinwheel tiling. This has a slot cut to accentuate the bending mode but reducing the resonant frequency of the tile. The x-axis 2710 is in millimeters; the y-axis 2730 is in millimeters; the z-axis 2720 is in micrometers. The scaling is shown on the right bar 2750.

[00143] As any device that behaves with the correct center of mass may make use of this tiling procedure, it is in this case only required to create a wave generating technology with this physical footprint. The exact technology is not required to be piezoelectric transducing elements, and may be electrostatic, MEMs, CMUTs, PMUTs or any other prevailing technology or process. This invention may be applied to any transducer process to produce a complete or partial spatial packing of a two-dimensional plane with substantially reduced or eliminated element-to-element gaps.

[00144] Additional disclosure includes: 1. An array of triangular transducers wherein the locations of physical features can be described by barycentric coordinates applied to a triangle with sides forming the ratio 1:2:$\sqrt{5}$.

2. The array of ¶ 1, wherein the transducers comprise acoustic transducers.

3. The array of ¶ 1, wherein the transducers comprise an array of antennae for beamforming electromagnetic signals.

4. The array of ¶ 1, wherein the triangles whose sides form the ratio 1:2:$\sqrt{5}$ to which the barycentric coordinates are applied to yield the feature locations are themselves subdivisions of other triangles whose sides form the ratio 1:2:$\sqrt{5}$.

[00145] 5. An array comprising one or more tiles of transducers each comprised of many square transducers in a partial phyllotactic spiral pattern wherein two opposite corners of the transducer and a point in space common to the acoustic transducer elements on the tile are collinear.

6. The array of ¶ 5, wherein the transducers comprise acoustic transducers.

7. The array of ¶ 5, wherein the transducers comprise an array of antennae for beamforming electromagnetic signals.

8. The array of ¶ 5, wherein the common point in space collinear to opposite corners of each transducer does not lie on the tile of transducer elements.

[00146] 9. A device comprising one or more asymmetric transducers, wherein the field generated at a plurality of frequencies from a plurality of stable asymmetric resonant modes is used to localize a transducer detecting the field at a plurality of frequencies.

10. The device of ¶ 9, wherein the transducers comprise acoustic transducers.

11. The device of ¶ 9, wherein the transducers comprise an array of antennae for beamforming electromagnetic signals.

12. The device of ¶ 9, wherein the transducer is of a triangular shape, wherein the locations of physical features can be described by barycentric coordinates applied to a triangle with sides forming the ratio 1:2:$\sqrt{5}$.

13. The device of ¶ 9, wherein the transducer detecting the field is also an asymmetric transducer with a plurality of stable asymmetric resonant modes which are capable of detecting the field at a plurality of frequencies.

14. The device of ¶ 9, wherein the acoustic field detected using a plurality of stable asymmetric resonant modes at a plurality of resonant frequencies of the detector may be any arbitrary acoustic field.

[00147] III. Transducer Placement Using Recursive Techniques

[00148] Square shaped transducers are ideal for rectilinear arrangements resulting in zero wasted area. They can suffer from grating lobes, however, if they are of comparable size to the emitted wavelength. Placing square transducers into a phyllotactic spiral can break up secondary foci but necessities a reduction in packing density of at least 40%. To achieve the 40% parameter, individual transducers need to be singulated which increases cost of manufacture.

[00149] The invention presented here details a recursive technique to adjust the placement of square transducers in order to achieve an adjustable balance between packing density and effectiveness of reducing grating lobe magnitude.

[00150] Shown in Figure 29 is a simulation 2900 that details the basic steps for arranging a square unit cell into a new arrangement. Starting with rectilinear placing 2910, cells 1 and 2 are displaced to the right by an amount 'a' 2920. Next, unit cells 2 and 3 are adjusted down by amount 'b' 2930. This is followed by 3 and 4 moving left by 'c' 2940 and 1 and 4 moving up by 'd' 2950. With the size of one edge of the square unit cell given by 2r, this changes the location of unit cell centers to:

Unit 1 = [-r+a,r+d]

Unit 2 = [r+a,r-b]

Unit 3 = [r-c,-r-b]

Unit 4 = [-r-c,-r+d],

where the notation is given by [x-location, y-location]. Careful choices of the adjustment parameters (a,b,c,d) can give arrangements of all the elements which breaks symmetry.

[00151] Shown in Figure 30 is a simulation 3000 that illustrates how this method is recursively extended to build larger arrays of elements. Specifically, this is an illustration of a 4 x 4 tile recursively enumerated into a 16 x 16 element array 3010. The offset values (a' 3020, b' 3030, c' 3040, d' 3050) can be repeated from the previous round of recursion or generated anew.

[00152] Shown in Figure 31 is a simulation 3100 that illustrates some variation possibilities provided by rotation 3110 or mirroring 3120 or both 3130. This can provide more randomness into the arrangement to increase performance at a given packing density. This shows variation on simple offset tiling. As each tile is duplicated it can be mirrored or rotated. Like the offset values, these techniques can be recursively repeated to larger and larger arrays.

[00153] Determining which arrangements are most effective must be done through simulation. This can be as computationally sophisticated as a full non-linear finite-element approach or as simple as a linear Huygens model. As an example, array activation coefficients can be calculated so that a focus is steered to [x,y,z] = [40mm,0,200mm], and a Huygens model calculates the field to some

large extent in that plane. If the array is less dense than critical-spacing, a grating lobe secondary focus will appear somewhere in that plane. If the array arrangement is effective, this focus will be distributed in space and the peak secondary pressure (not the focus) will be low compared to the focus. The contrast between the focus pressure and the peak secondary pressure forms a metric for comparison of different arrangements. One can search through a large number of skew values with and without rotation or mirroring and pick the best performer for a given packing density.

[00154] Figures 32-34 illustrate a few examples of pseudo-random arrangements which effectively distribute grating lobe energy and prevent secondary foci using 7 mm square transducers operating at 61 kHz.

[00155] Figures 32A, 32B, 32C, and 32D show an example 256 element array of 7 mm square transducers constructed using rotation 3200 3210 3220 3230. In this example [a,b,c,d] = [1.6mm,1.3mm,1.1mm,0.7mm] for each round of recursion.

[00156] Figures 33A, 33B, 33C, and 33D show an example 256 element array of 7 mm square transducers constructed using rotation and mirroring 3300 3310 3320 3330. In this example [a,b,c,d] = [1.6mm,1.3mm,1.1mm,0.7mm] for each round of recursion just as figure 17 but with improved results.

[00157] Figures 34A, 34B, 34C, and 34D show an example 256 element array of 7 mm square transducers constructed using rotation and mirroring 3400 3410 3420 3430. In this example [a,b,c,d] = [0,1.9mm,0,0] for the first two rounds of recursion then no added offsets and only rotation for the last two.

[00158] One advantage of this technique compared to a phyllotactic spiral arrangement is that the array can be built in tiles. Each recursive arrangement step which quadruples the array size uses the previous unit cell as its basis – only rotating, mirroring, and skewing the arrangement as its placed into a new square. As a result, this unit cell (and its mirror, if used) can be manufactured as a unit and assembled into the larger array.

[00159] While this technique generates square arrays, when a satisfactory square arrangement is found, it can be sectioned to non-square sub-arrays which will be

nearly as effective at spreading out grating lobe foci as the original square arrangement. These non-square arrangements can be used together to make larger non-square shapes. Only when the number of sub-units starts is comparable to the number of transducers within each sub-unit does the possibility of grating lob problems resurfacing become an issue.

[00160] The key advantage of the invention presented here is that the search space for effective solutions is far reduced compared to random, arbitrary placement. The parameters which can vary in this system are the offsets for each round of recursion and the decision to mirror, rotate, or both. This allows for a tightly bounded search space and reduces the computation required to a manageable subset.

[00161] Figure 35 is a graph 3500 showing the best simulated recursive offset arrays using 256, 7 mm square transducers at 61 kHz. The y-axis 3520 is the difference between the focus pressure and peak grating lobe pressure. The x-axis 3510 shows the total area of each array. The 'best 1-tile results' line 3530 shows that through only rotation (as mirroring would require a 'second-tile' to be manufactured) solutions can be found whose performance ranges from closely-packed rectilinear to phyllotactic spiral-performance, albeit with lower density. The 'best 2-tile results' line 3540 shows that by adding mirroring, solutions within 1.5 dB of phyllotactic-spiral performance can be achieved at similar packing density, without the necessity of singulation or rotating individual elements. In addition, if space is limited for the array, for a given area an effective solution is generated which distributes grating lobe energy.

[00162] Other points included on the plot are closely-packed rectilinear (square array 3550), a phyllotactic spiral with rotated square elements (square rotated sunflower 3580), and estimates 3 triangle-element arrays 3560 (discussed elsewhere) with equal emission to the squares, as well as decreased emission at -3 dB 3570 and -4 dB 3590.

[00163] Additional disclosure includes: 1. An array comprising of many tiles comprising of a plurality of transducers wherein the physical transducer locations

are perturbed through rigid transformations such that the new footprint of each element intersects the footprint before the transformation is applied, wherein the original footprint of each comprises a uniform layout of acoustic transducers.

2. The array of ¶ 1, wherein the transducers comprise acoustic transducers.

3. The array of ¶ 5, wherein the transducers comprise an array of antennae for beamforming electromagnetic signals.

4. The array of ¶ 1, wherein the physical tile locations are perturbed through rigid transformations, wherein the new footprint of each tile intersects the footprint before the transformation is applied.

5. The array of ¶ 1, wherein the transformations are applied recursively to smaller tile arrangements that make up larger tile arrangements.

6. The array of ¶ 1, wherein a single tile is replicated to produce a plurality of tiles, which are then arranged using rigid transformations to produce an array.

7. The array of ¶ 1, wherein the transformed arrangement reduces grating lobe intensity.

[00164] IV. Conclusion

[00165] In the foregoing specification, specific embodiments have been described. However, one of ordinary skill in the art appreciates that various modifications and changes can be made without departing from the scope of the invention as set forth in the claims below. Accordingly, the specification and figures are to be regarded in an illustrative rather than a restrictive sense, and all such modifications are intended to be included within the scope of present teachings.

[00166] Moreover, in this document, relational terms such as first and second, top and bottom, and the like may be used solely to distinguish one entity or action from another entity or action without necessarily requiring or implying any actual such relationship or order between such entities or actions. The terms "comprises," "comprising," "has", "having," "includes", "including," "contains", "containing" or any other variation thereof, are intended to cover a non-exclusive

inclusion, such that a process, method, article, or apparatus that comprises, has, includes, contains a list of elements does not include only those elements but may include other elements not expressly listed or inherent to such process, method, article, or apparatus. An element proceeded by "comprises …a", "has …a", "includes …a", "contains …a" does not, without more constraints, preclude the existence of additional identical elements in the process, method, article, or apparatus that comprises, has, includes, contains the element. The terms "a" and "an" are defined as one or more unless explicitly stated otherwise herein. The terms "substantially", "essentially", "approximately", "about" or any other version thereof, are defined as being close to as understood by one of ordinary skill in the art. The term "coupled" as used herein is defined as connected, although not necessarily directly and not necessarily mechanically. A device or structure that is "configured" in a certain way is configured in at least that way but may also be configured in ways that are not listed.

[00167] The Abstract of the Disclosure is provided to allow the reader to quickly ascertain the nature of the technical disclosure. It is submitted with the understanding that it will not be used to interpret or limit the scope or meaning of the claims. In addition, in the foregoing Detailed Description, various features are grouped together in various embodiments for the purpose of streamlining the disclosure. This method of disclosure is not to be interpreted as reflecting an intention that the claimed embodiments require more features than are expressly recited in each claim. Rather, as the following claims reflect, inventive subject matter lies in less than all features of a single disclosed embodiment. Thus, the following claims are hereby incorporated into the Detailed Description, with each claim standing on its own as a separately claimed subject matter.

CLAIMS

We claim:

1. An apparatus comprising:

a plurality of ultrasonic transducers;

an operating acoustic wavelength;

a plurality of acoustic cavities, wherein each of the plurality of acoustic cavities has an input opening and an exit opening, the input opening having an entering ultrasound, the exit opening having a geometric center and having exiting ultrasound;

wherein each input opening accepts ultrasound from one of the plurality of transducers;

wherein at least two of the geometric centers of the exit openings are distanced from one another less than the operating acoustic wavelength;

wherein for a first of the plurality of acoustic cavities, a first exiting ultrasound has a first phase offset relative to a first entering ultrasound;

wherein for a second of the plurality of acoustic cavities, a second exiting ultrasound has a second phase offset relative to a second entering ultrasound;

wherein the first phase offset is different than the second phase offset.

2. The apparatus as in claim 1, wherein the first phase offset is inverted and applied to a phase of at least one transducer drive before emission.

3. The apparatus as in claim 2, wherein the first exiting ultrasound is modulated to produce audible sound.

4. The apparatus as in claim 2, wherein the first exiting ultrasound is modulated to produce a mid-air haptic effect.

5. The apparatus as in claim 2, wherein the first exiting ultrasound is used to levitate an object.

6. The apparatus as in claim 2, wherein the first exiting ultrasound has an amplitude offset relative to the first entering ultrasound.

7. The apparatus as in claim 6, wherein the amplitude offset is used to modify amplitudes of at least one transducer before emission.

8. The apparatus as in claim 3, wherein the exit openings are substantially co-planar.

9. The apparatus as in claim 8, wherein the audible sound is directed at an angle greater than 15 degrees normal to a plane.

10. The apparatus as in claim 8, wherein the audible sound is directed at an angle greater than 30 degrees normal to a plane.

11. The apparatus as in claim 8, wherein the audible sound is directed at an angle greater than 45 degrees normal to a plane.

12. The apparatus as in claim 8, wherein the audible sound is directed at an angle greater than 60 degrees normal to a plane.

13. The apparatus as in claim 6, wherein the amplitude offset is within 2dB.

14. The apparatus as in claim 1, wherein the plurality of acoustic cavities comprise straight cylinders with a decreasing radius from the input opening to the exit opening.

15. The apparatus as in claim 14, wherein the operating acoustic wavelength is less than 9 mm.

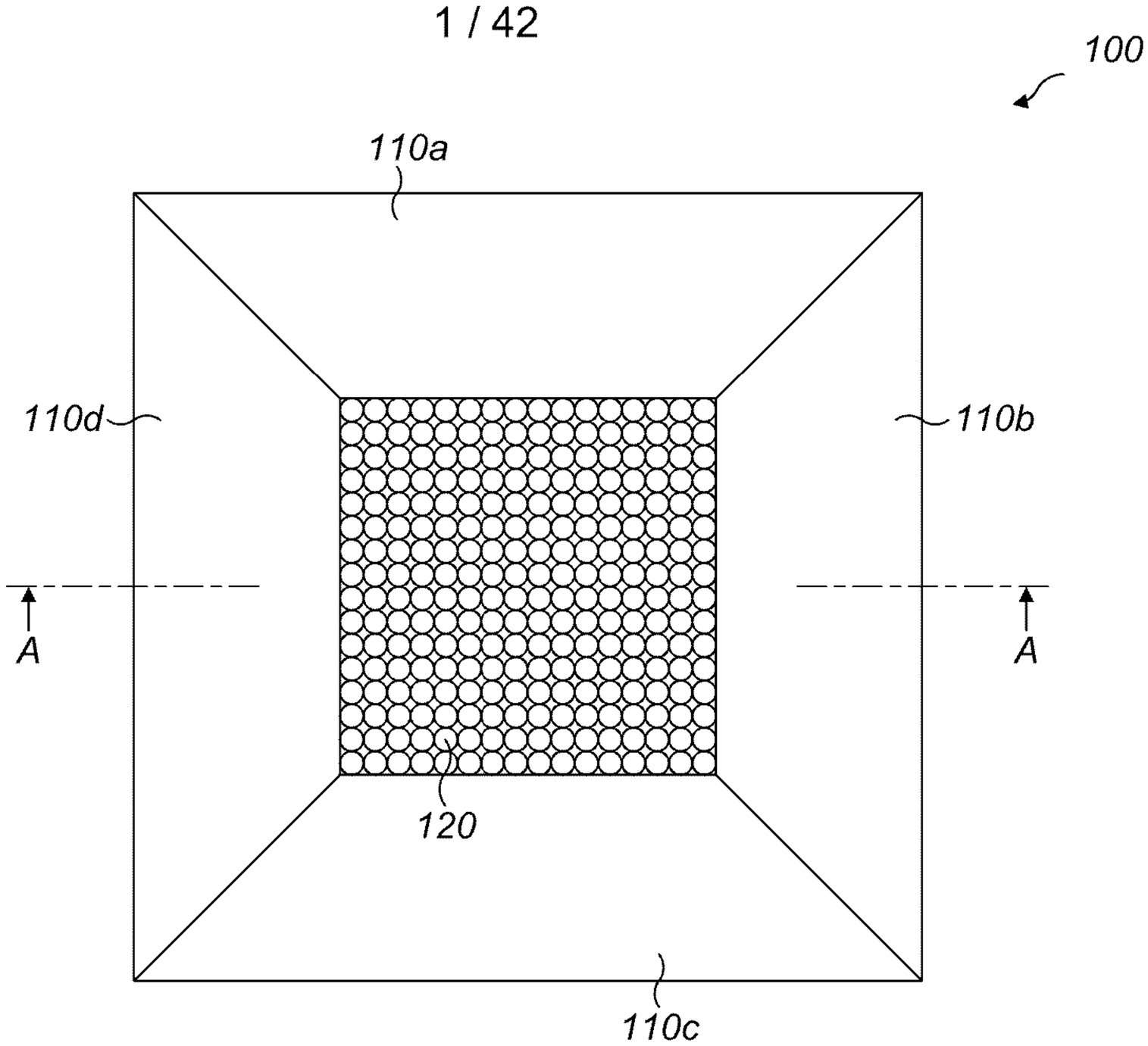
16. The apparatus as in claim 14, wherein a pitch of the exit opening is less than 6 mm.

17. The apparatus as in claim 2, wherein the first phase offset and the second phase offset are stored in memory.

18. The apparatus as in claim 6, wherein the amplitude offset is stored in memory.

19. The apparatus as in claim 2, wherein the exit openings are arranged to create grating lobe intensity.

20. The apparatus as in claim 19, wherein the exit openings have a horn-like exit aperture to increase coupling to open air.



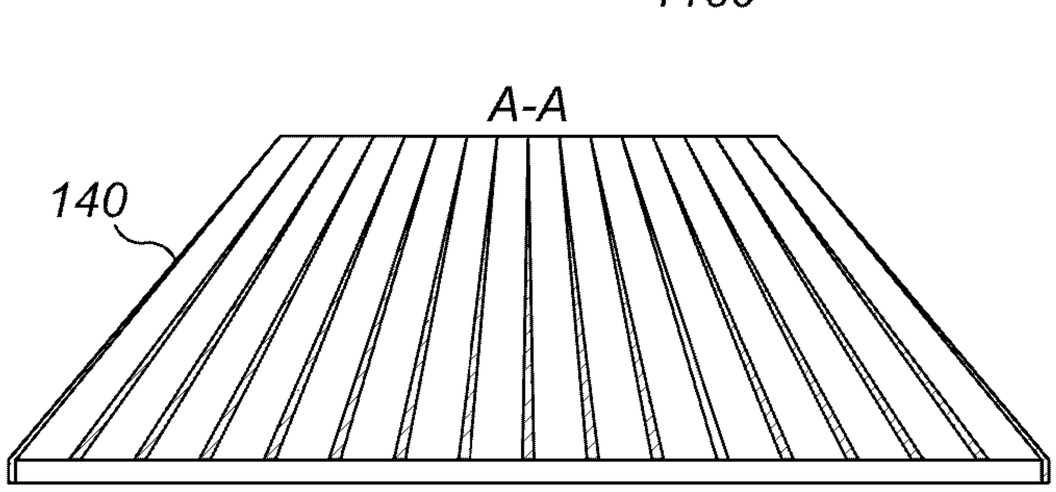


FIG. 1A

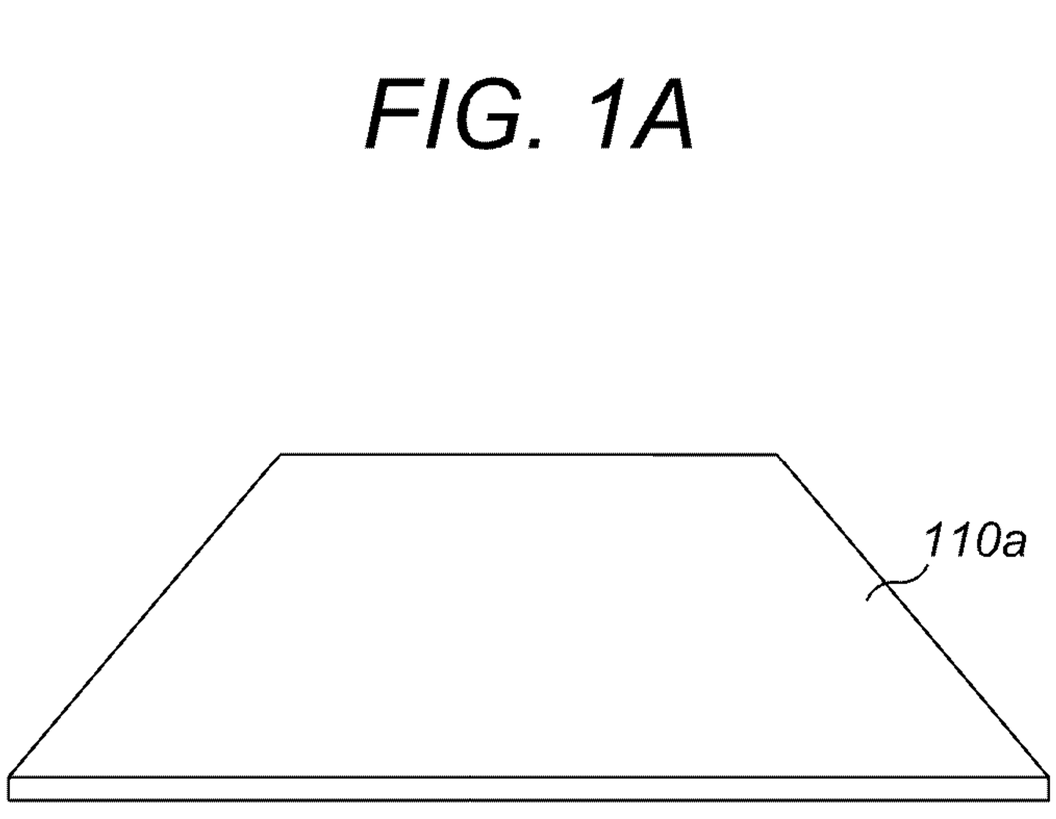


FIG. 1B

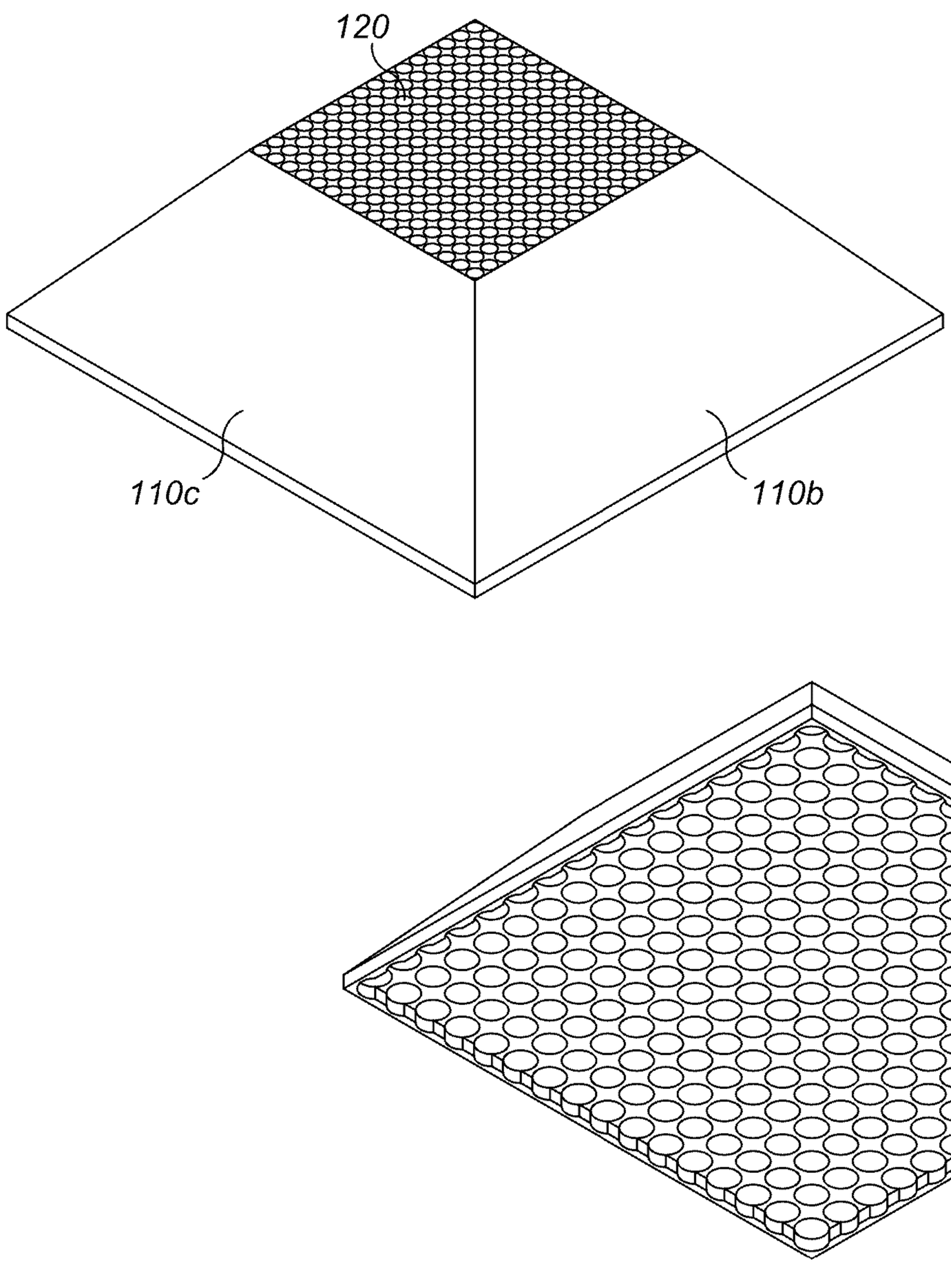


FIG. 1C

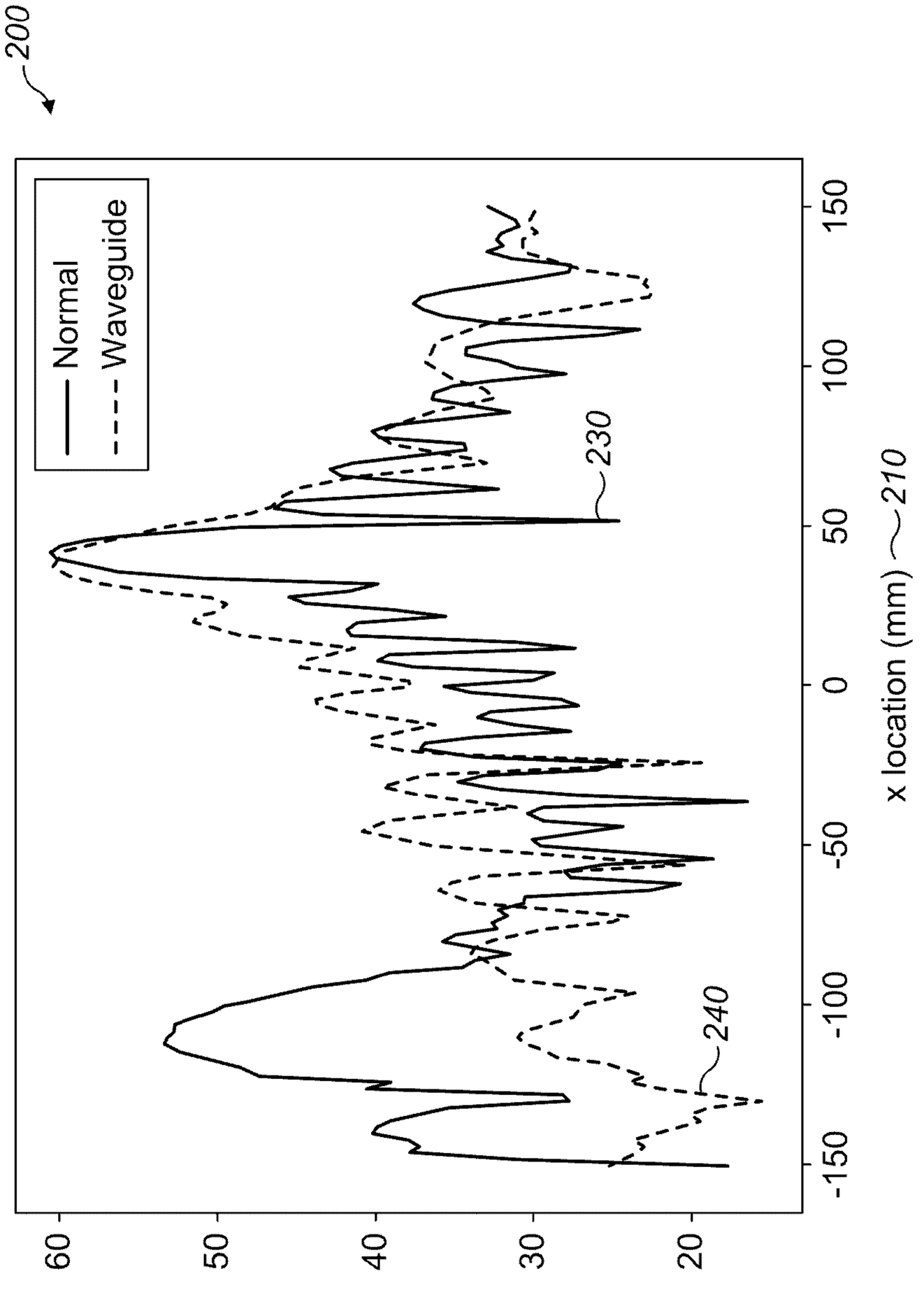

200
Normal
Waveguide
230
240
60
50
40
30
20
dB
220
-150
-100
-50
0
50
100
150
x location (mm)
210

FIG. 2

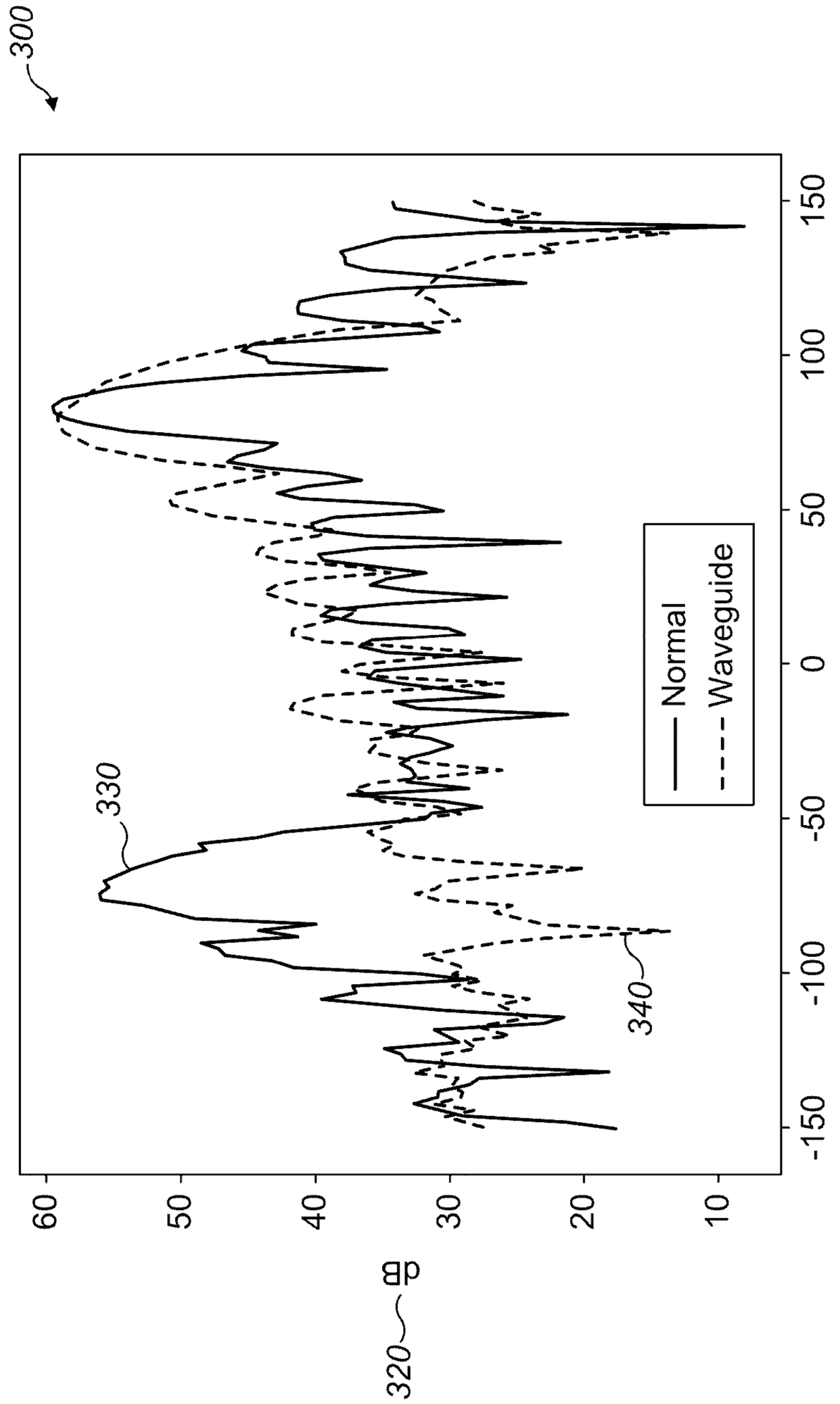

300
330
340
Normal
Waveguide
x location (mm)
310
150
100
50
0
-50
-100
-150
60
50
40
30
20
10
dB
320

FIG. 3

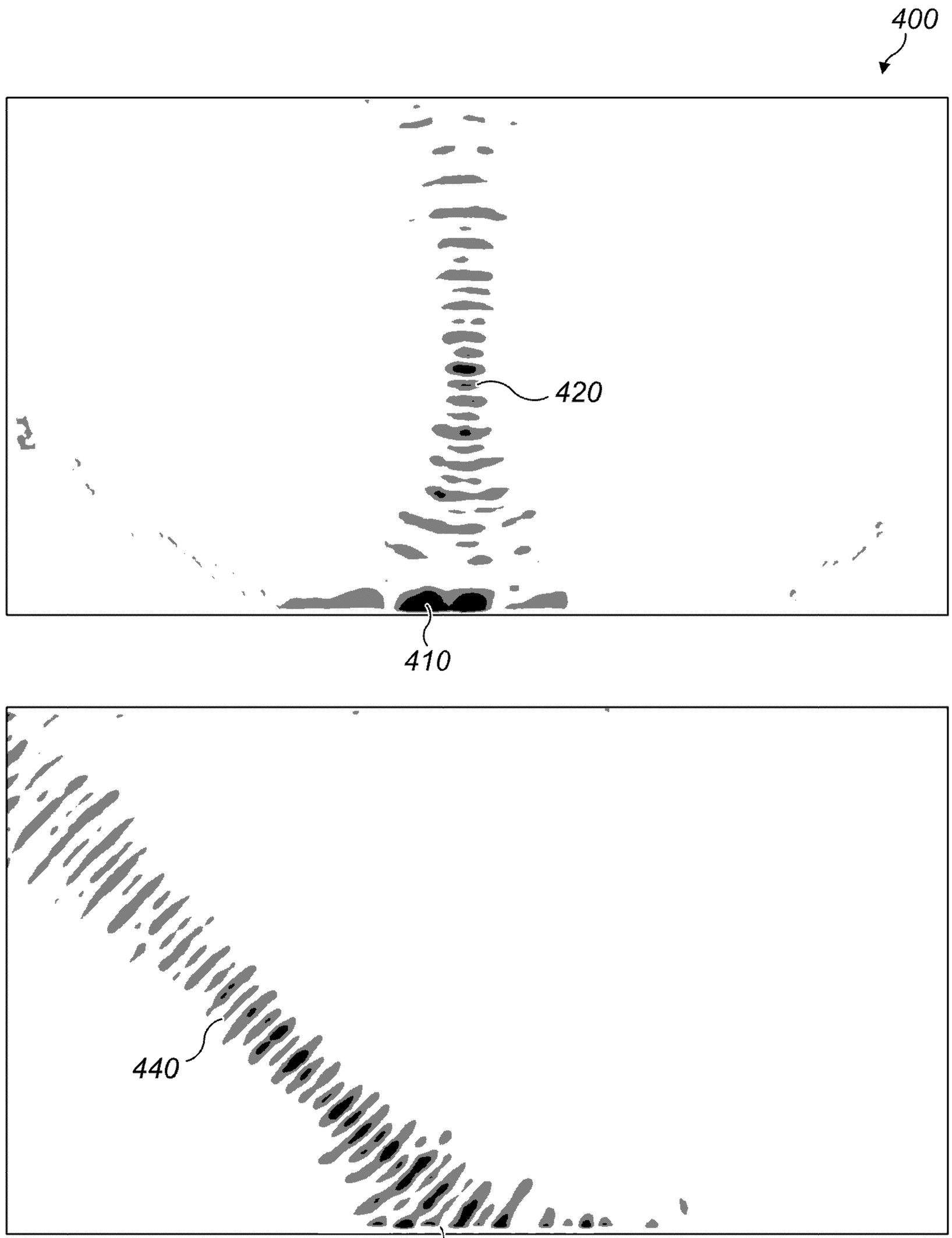


FIG. 4

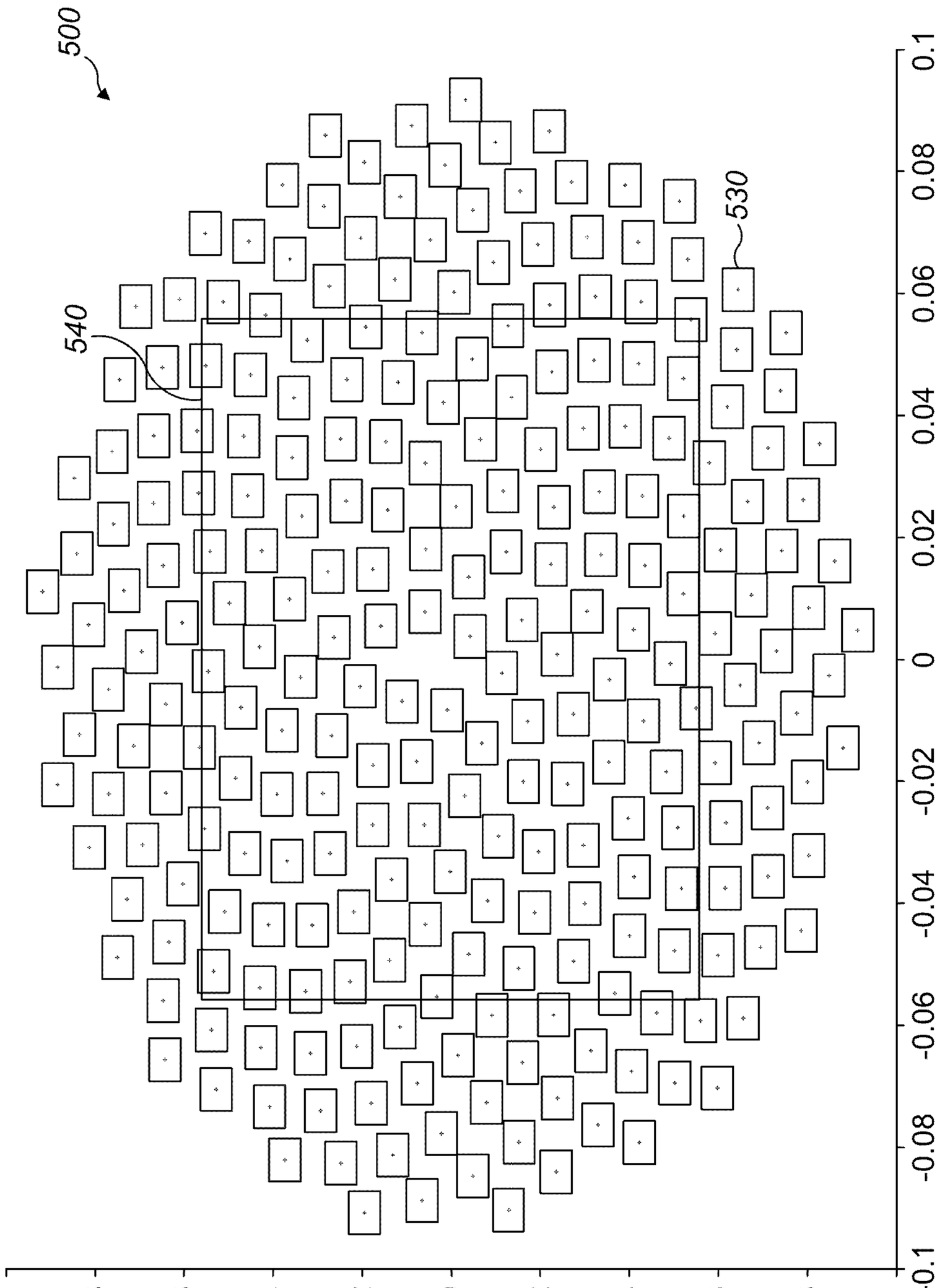


FIG. 5

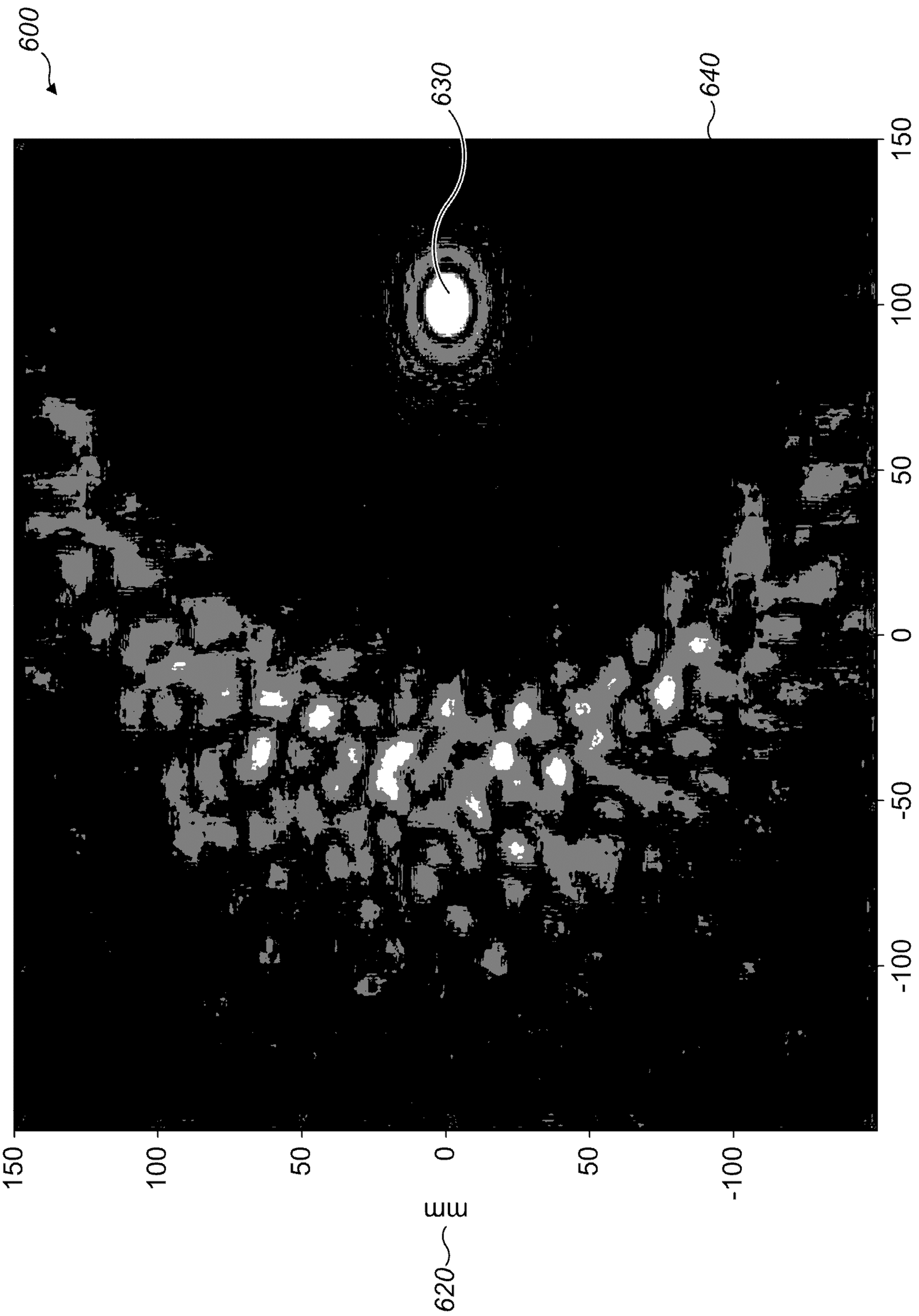


FIG. 6

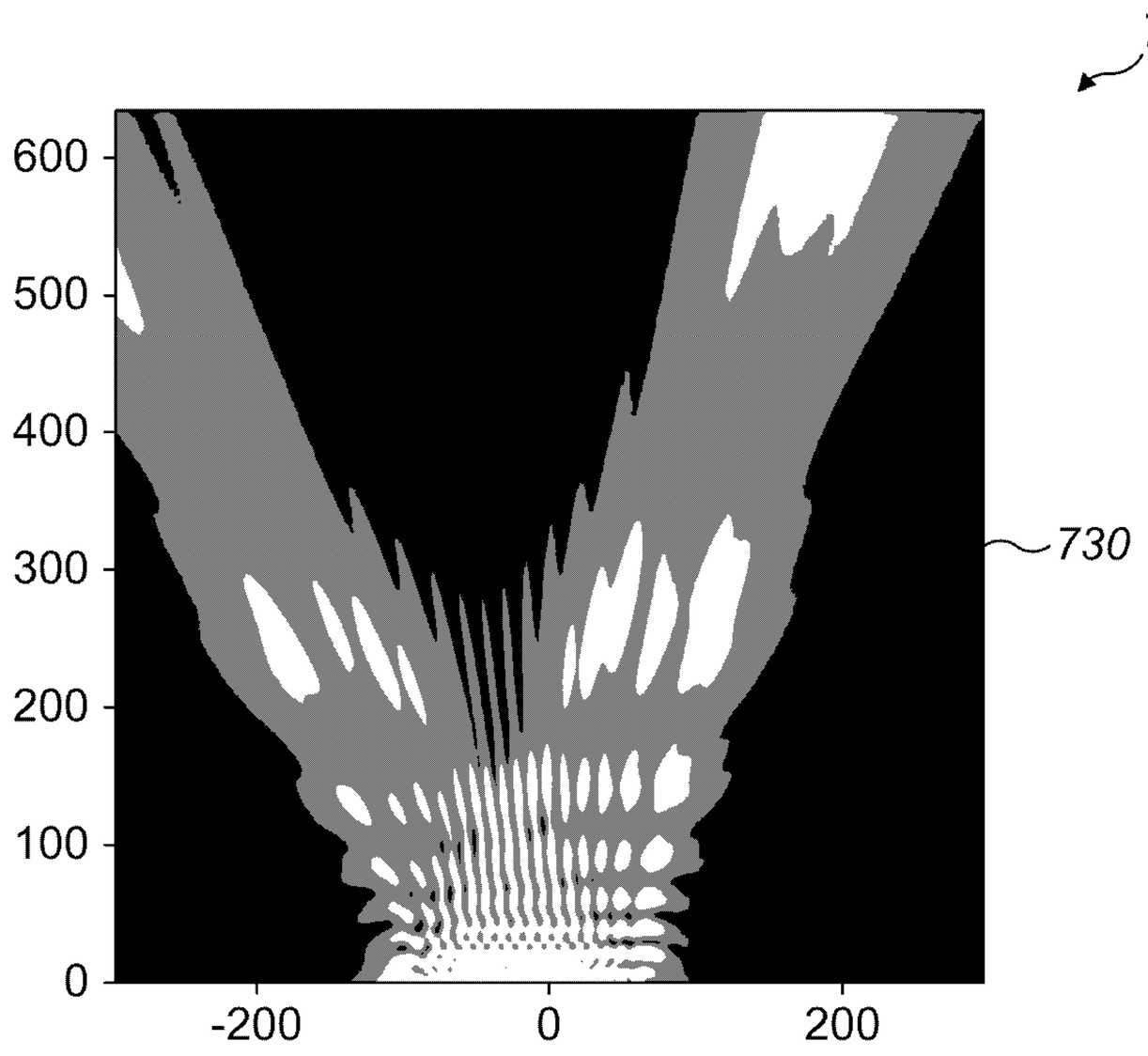

700
600
500
400
300
200
100
0
-200
0
200
730

FIG. 7A

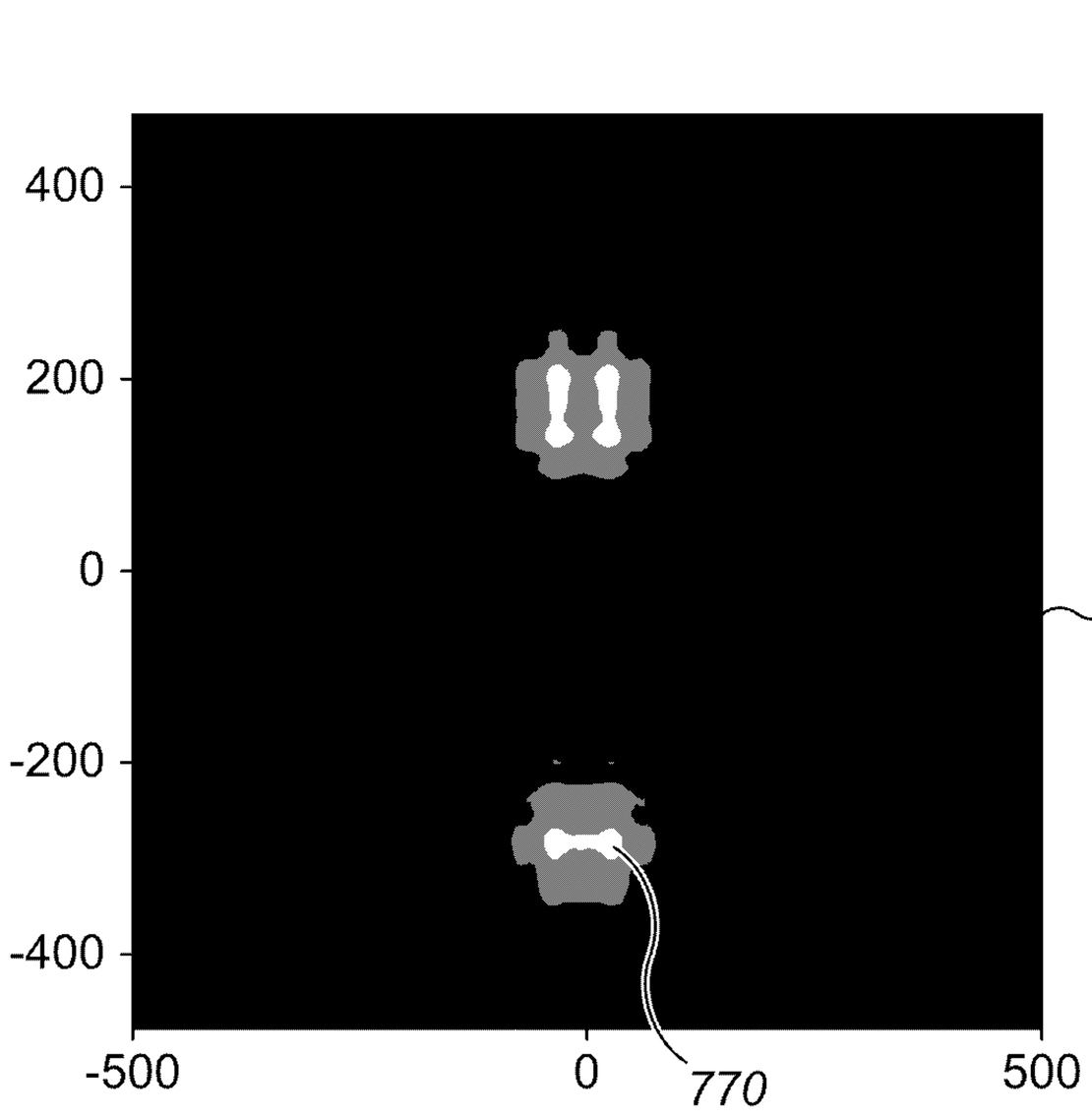

700
400
200
0
-200
-400
-500
0
500
710
770

FIG. 7B

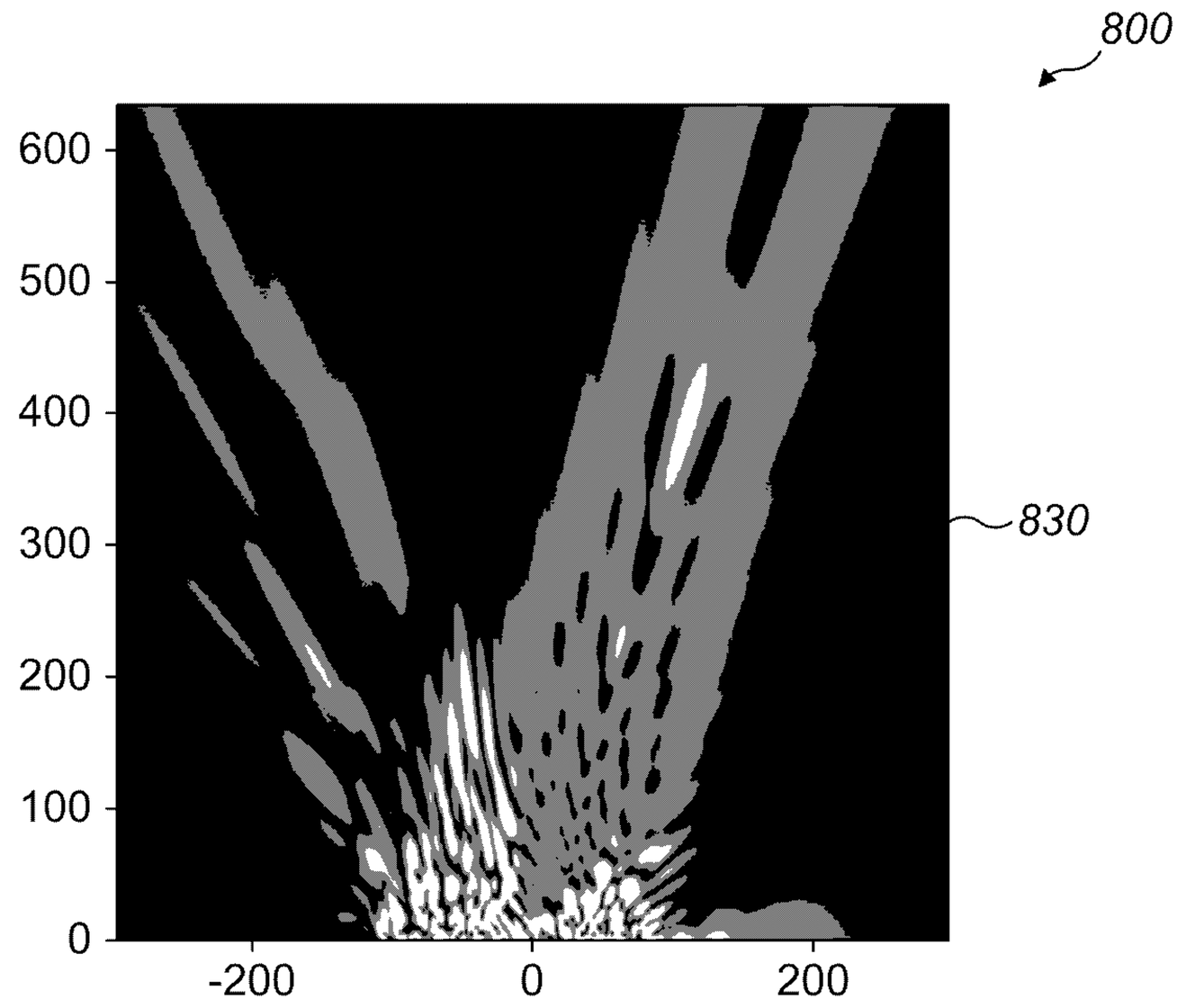

800
600
500
400
300
200
100
0
-200
0
200
830

FIG. 8A

800
400
200
0
-200
-400
-500
0
500
860
870

FIG. 8B

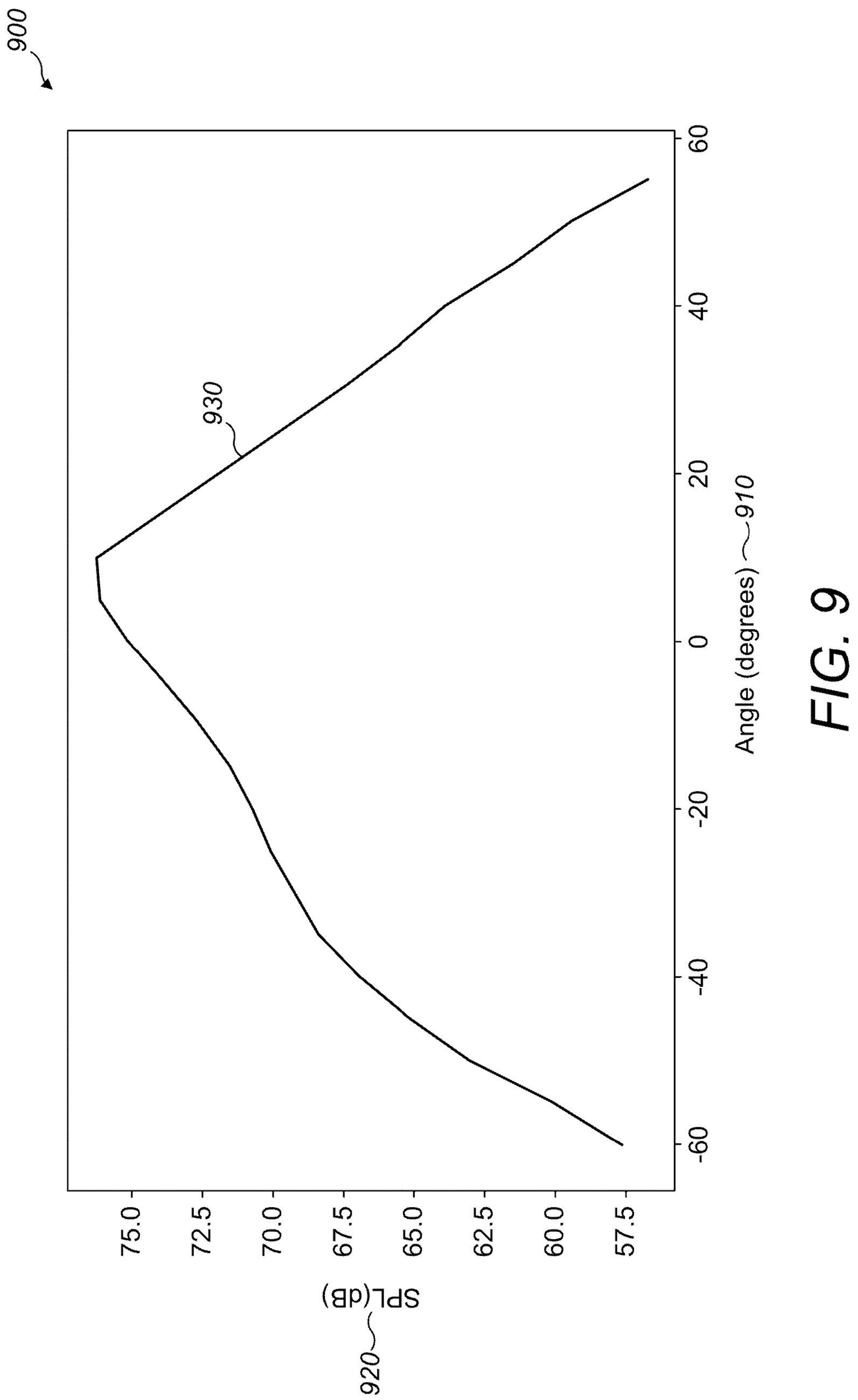

900
930
60
40
20
0
-20
-40
-60
Angle (degrees) 910
75.0
72.5
70.0
67.5
65.0
62.5
60.0
57.5
SPL(dB)
920

FIG. 9

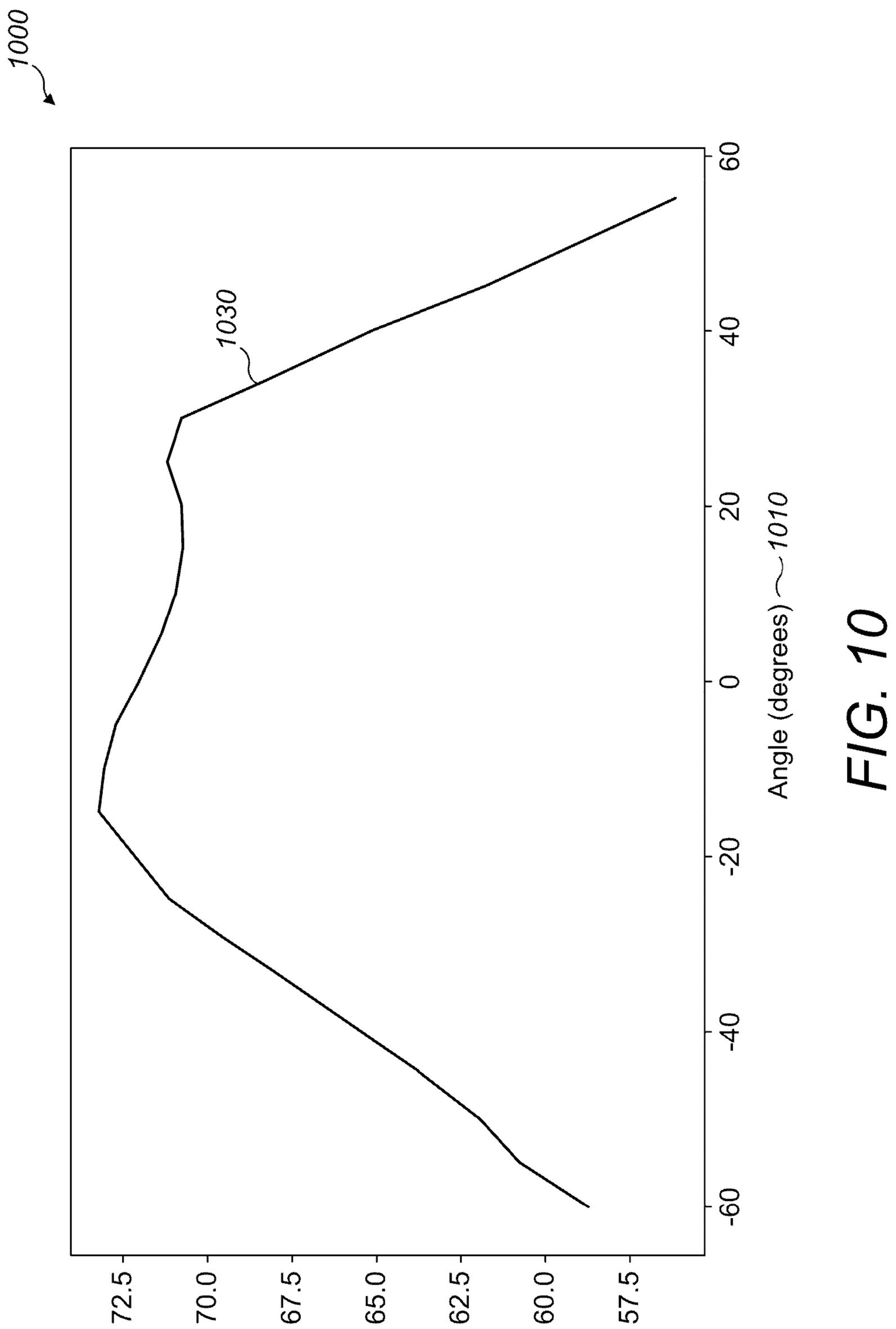

1000
1030
1010
1020
Angle (degrees)
SPL(dB)
60
40
20
0
-20
-40
-60
72.5
70.0
67.5
65.0
62.5
60.0
57.5

FIG. 10

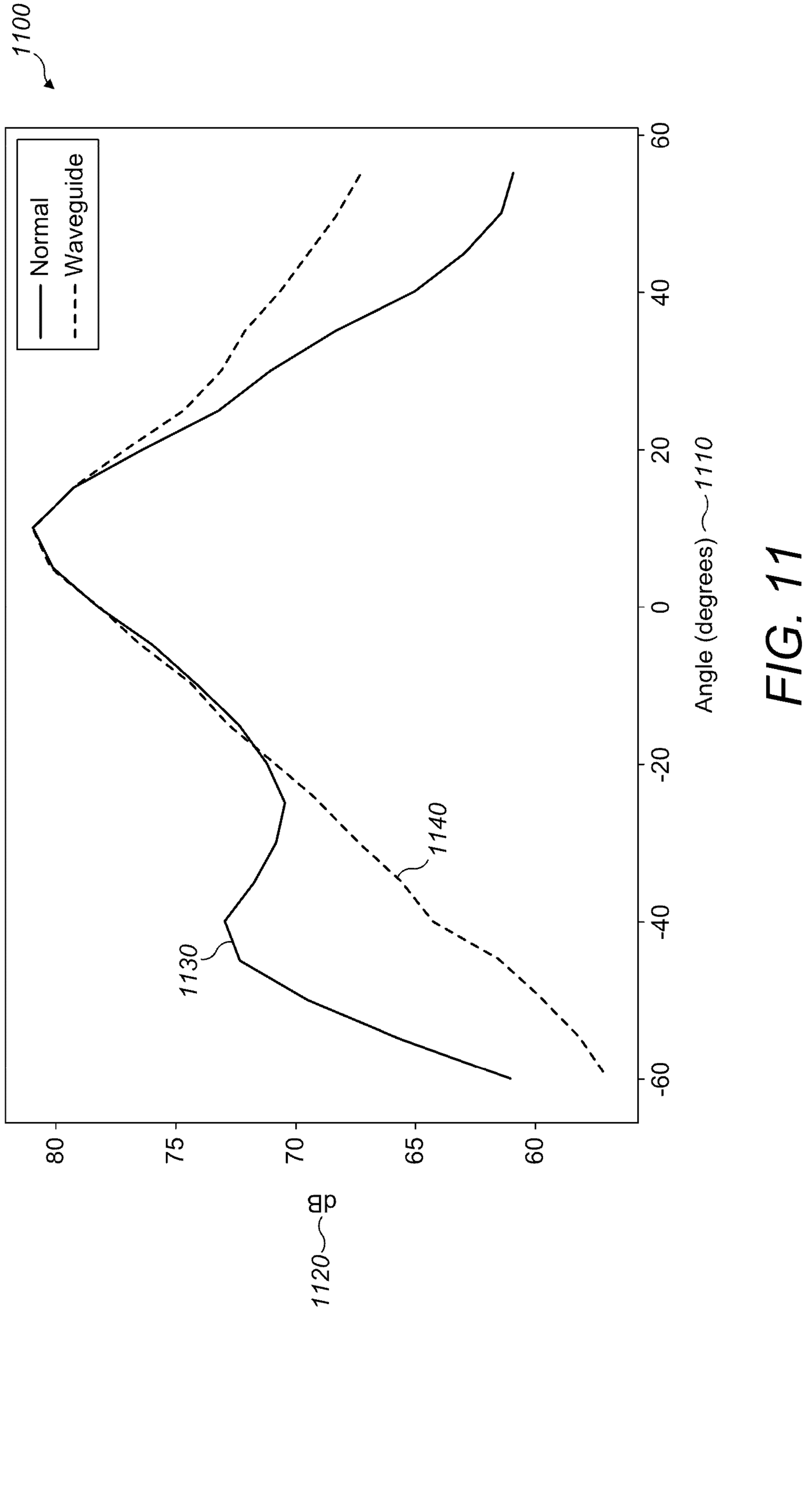

1100
Normal
Waveguide
60
40
20
0
-20
-40
-60
Angle (degrees)
1110
1130
1140
80
75
70
65
60
dB
1120

FIG. 11

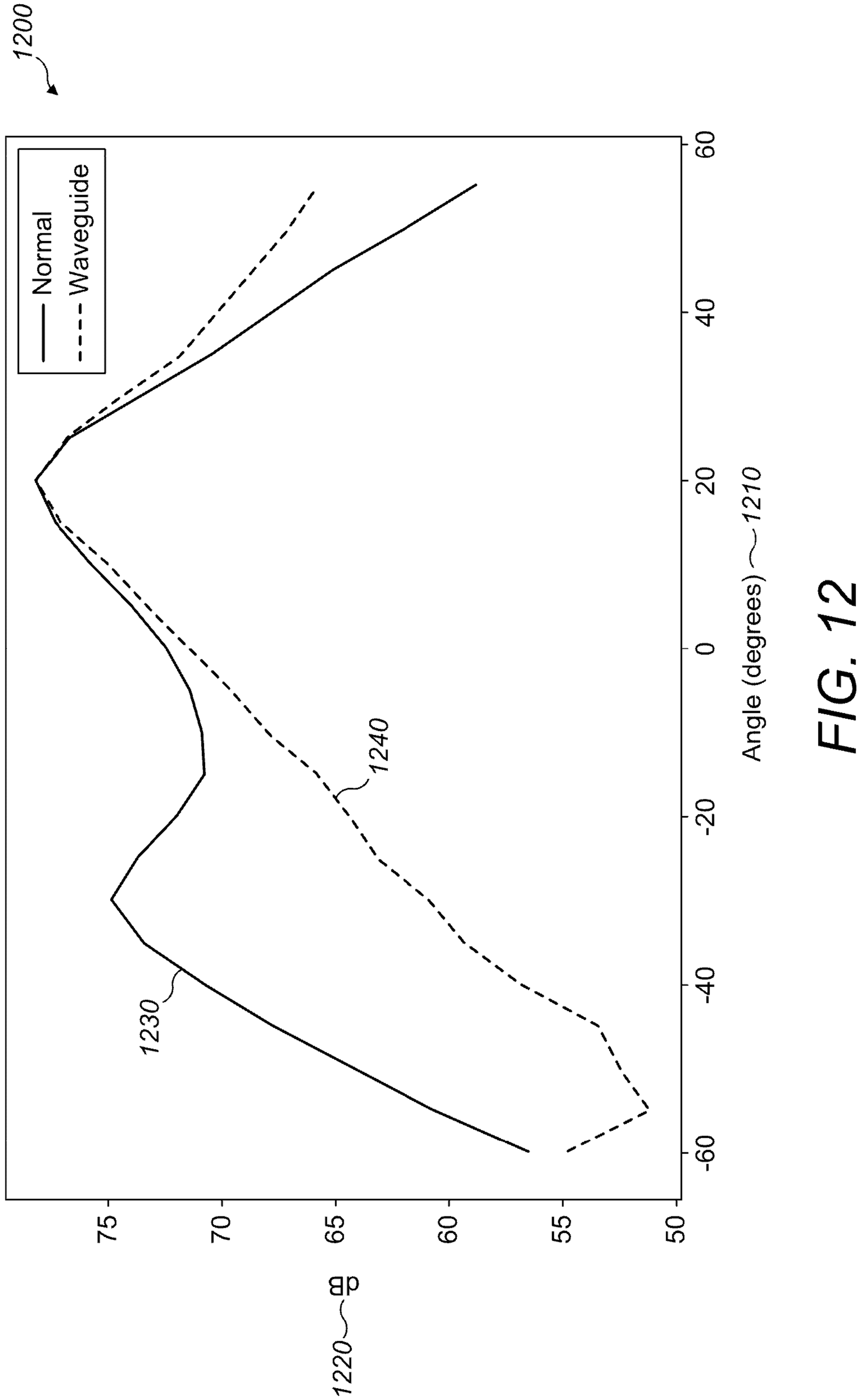

1200
Normal
Waveguide
1230
1240
1210
1220
dB
Angle (degrees)
75
70
65
60
55
50
-60
-40
-20
0
20
40
60

FIG. 12

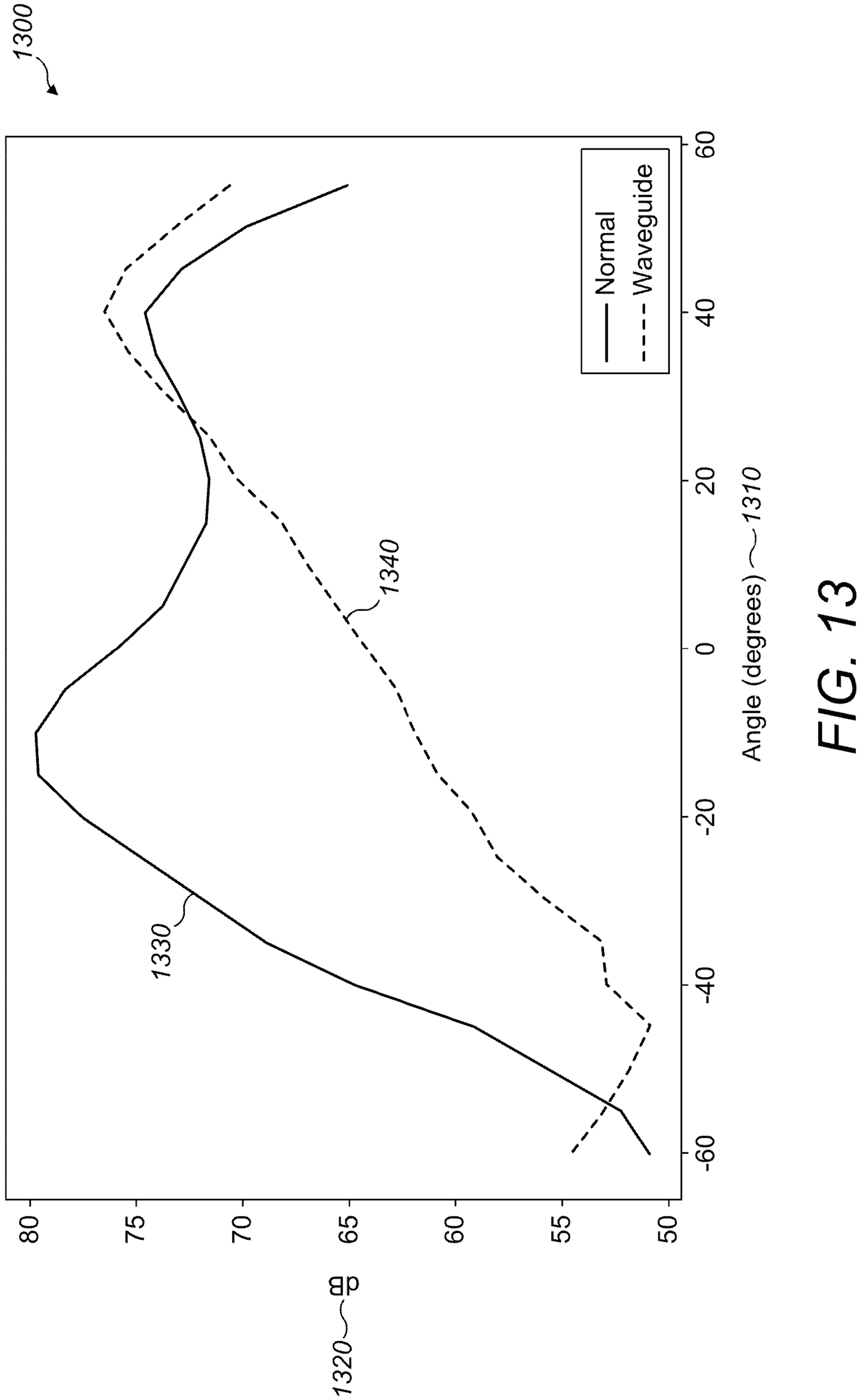

1300
Normal
Waveguide
1340
1330
1320
1310
Angle (degrees)
80
75
70
65
60
55
50
60
40
20
0
-20
-40
-60

FIG. 13

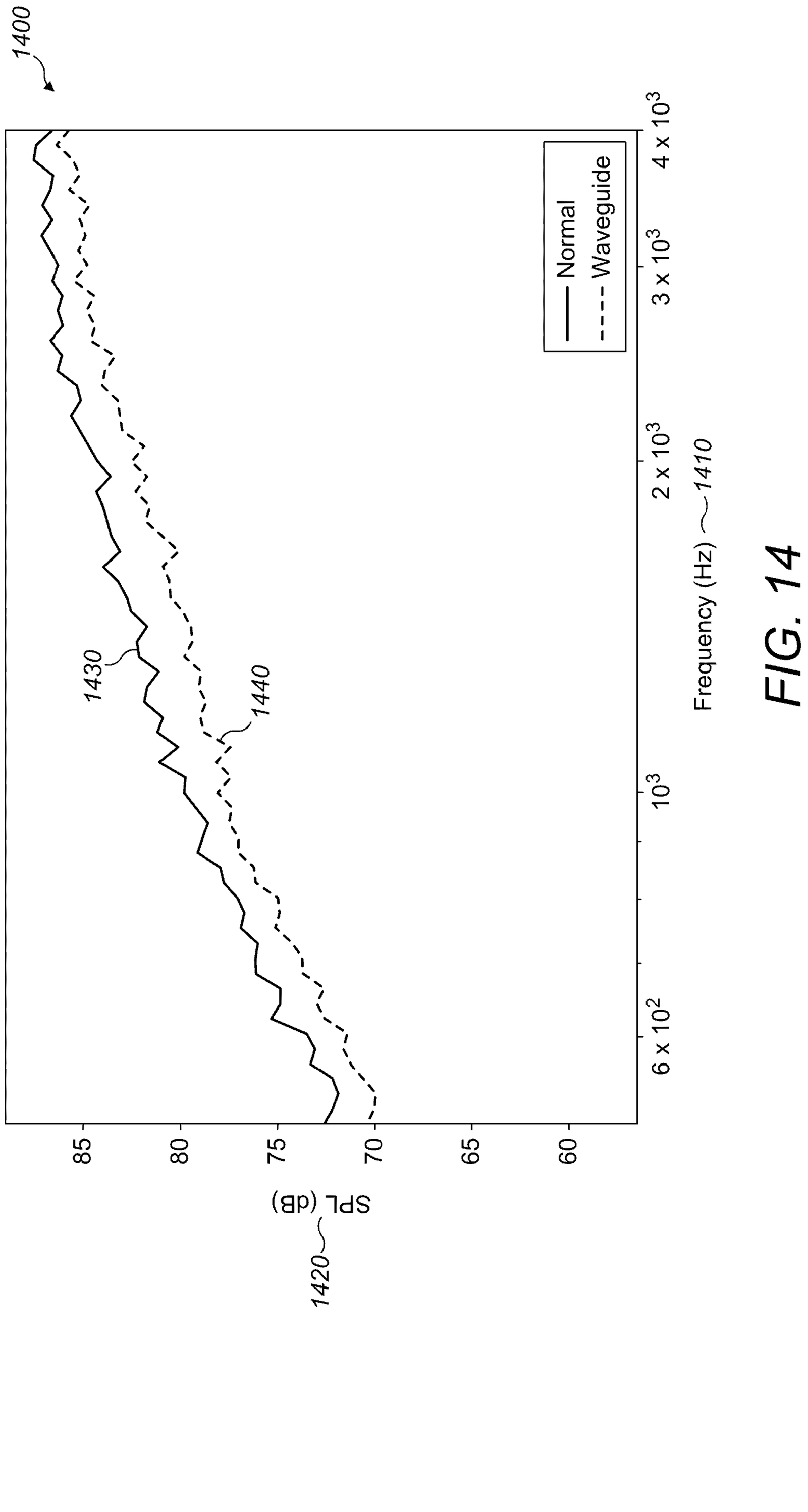

1400
SPL (dB)
1420
85
80
75
70
65
60
Frequency (Hz)
1410
6 x 10^2
10^3
2 x 10^3
3 x 10^3
4 x 10^3
Normal
Waveguide
1430
1440

FIG. 14

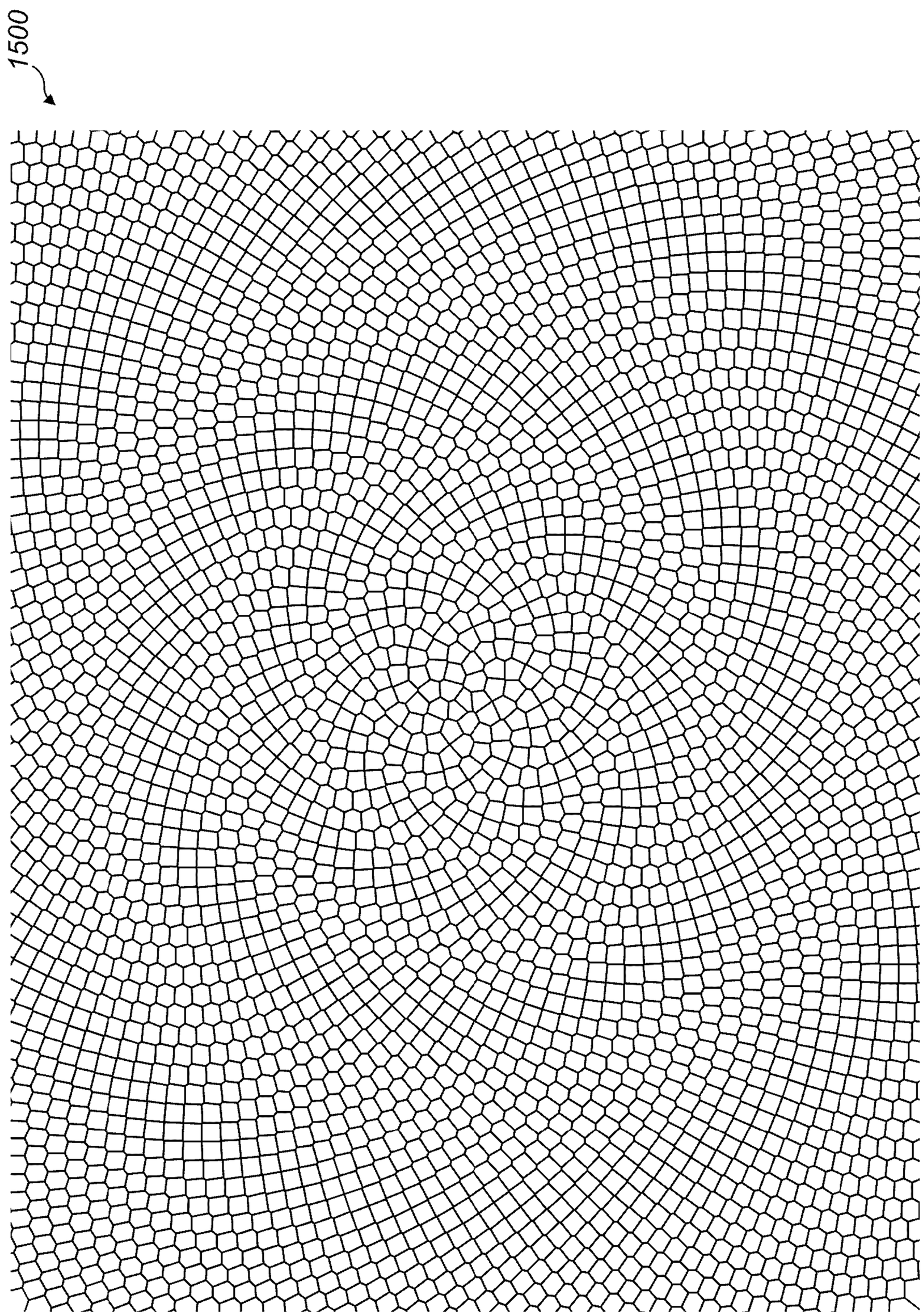


FIG. 15

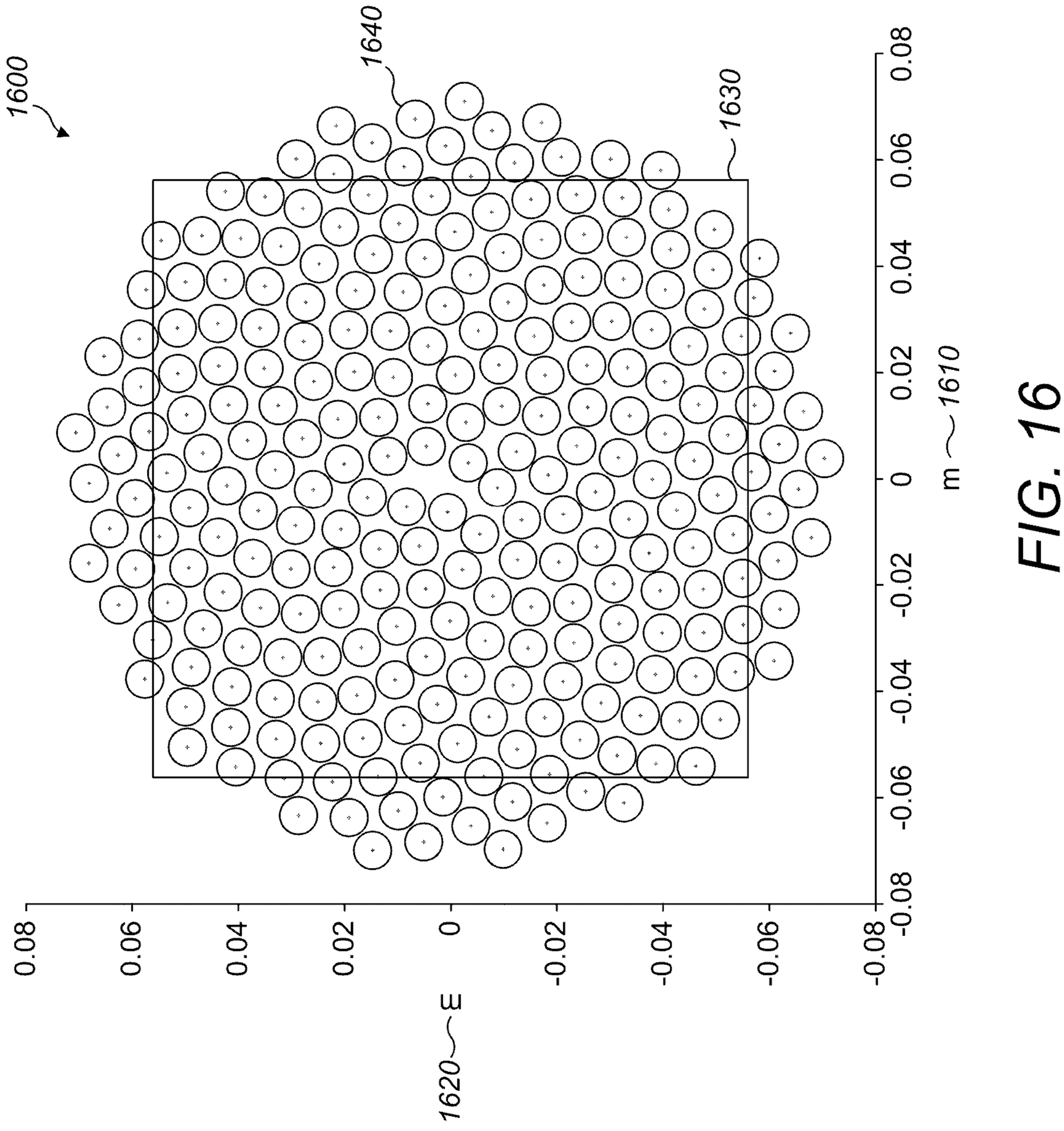


FIG. 16

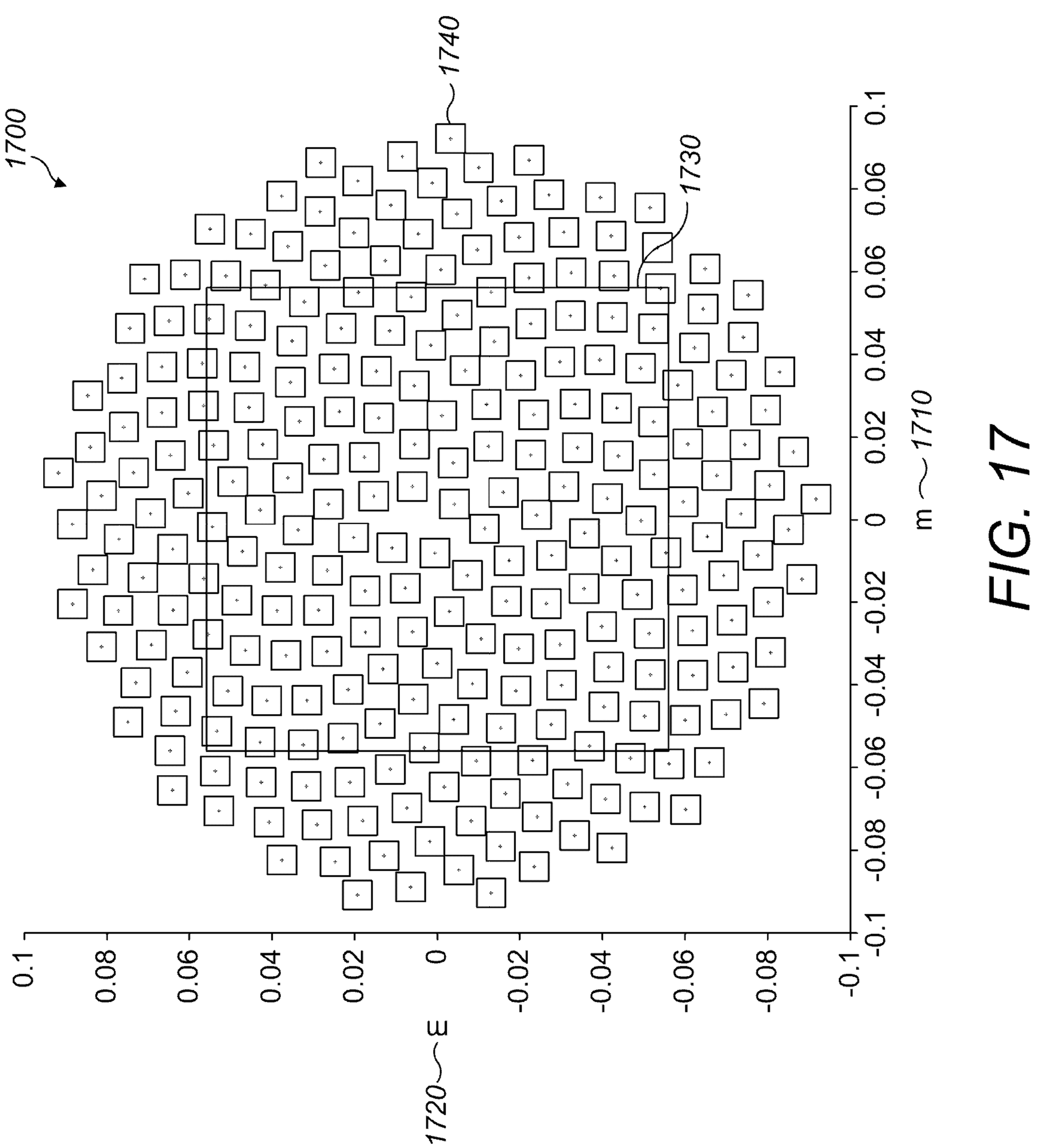

1700
1740
1730
1710
1720
0.1
0.08
0.06
0.04
0.02
0
-0.02
-0.04
-0.06
-0.08
-0.1
ω
m

FIG. 17

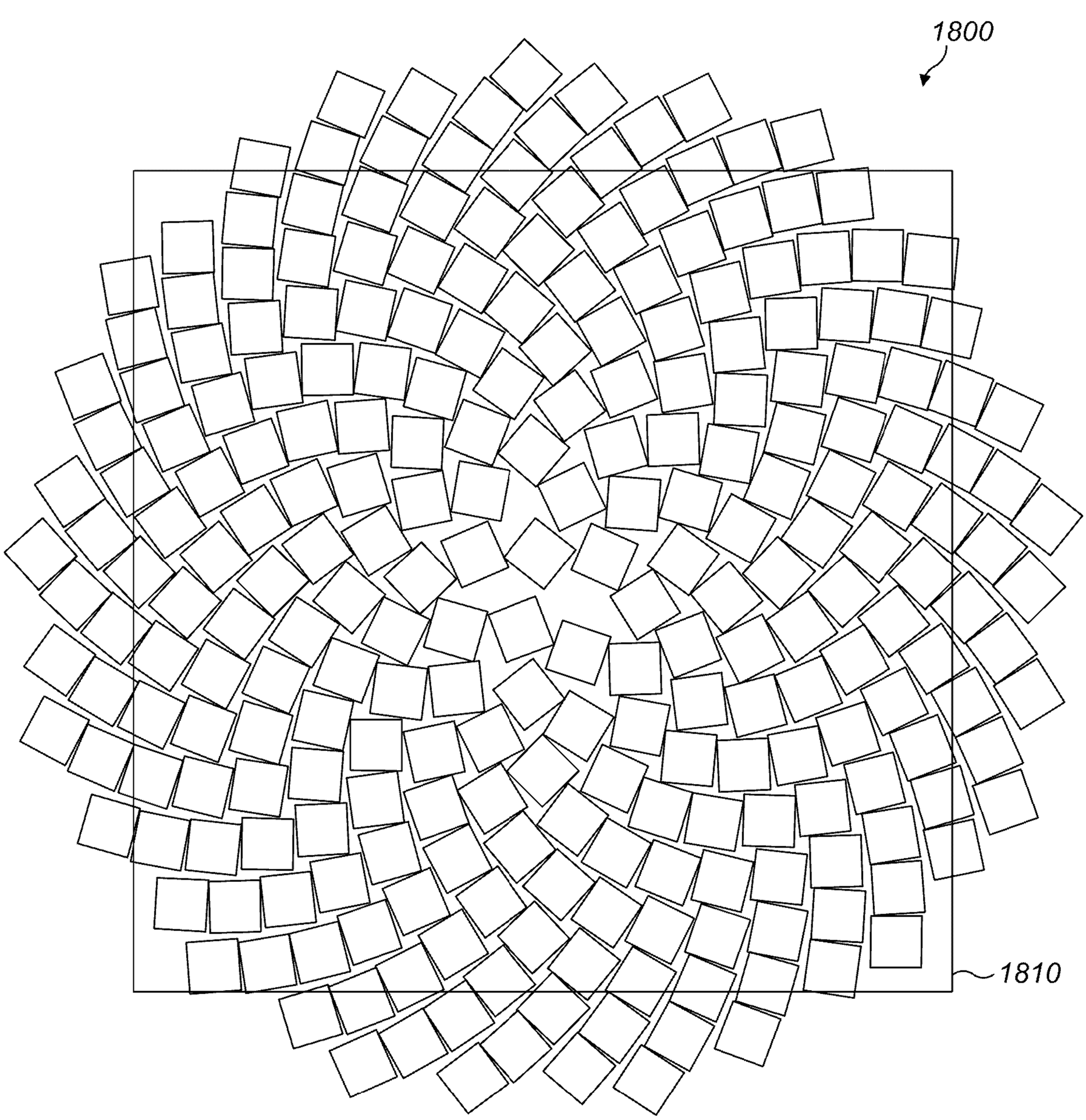


FIG. 18

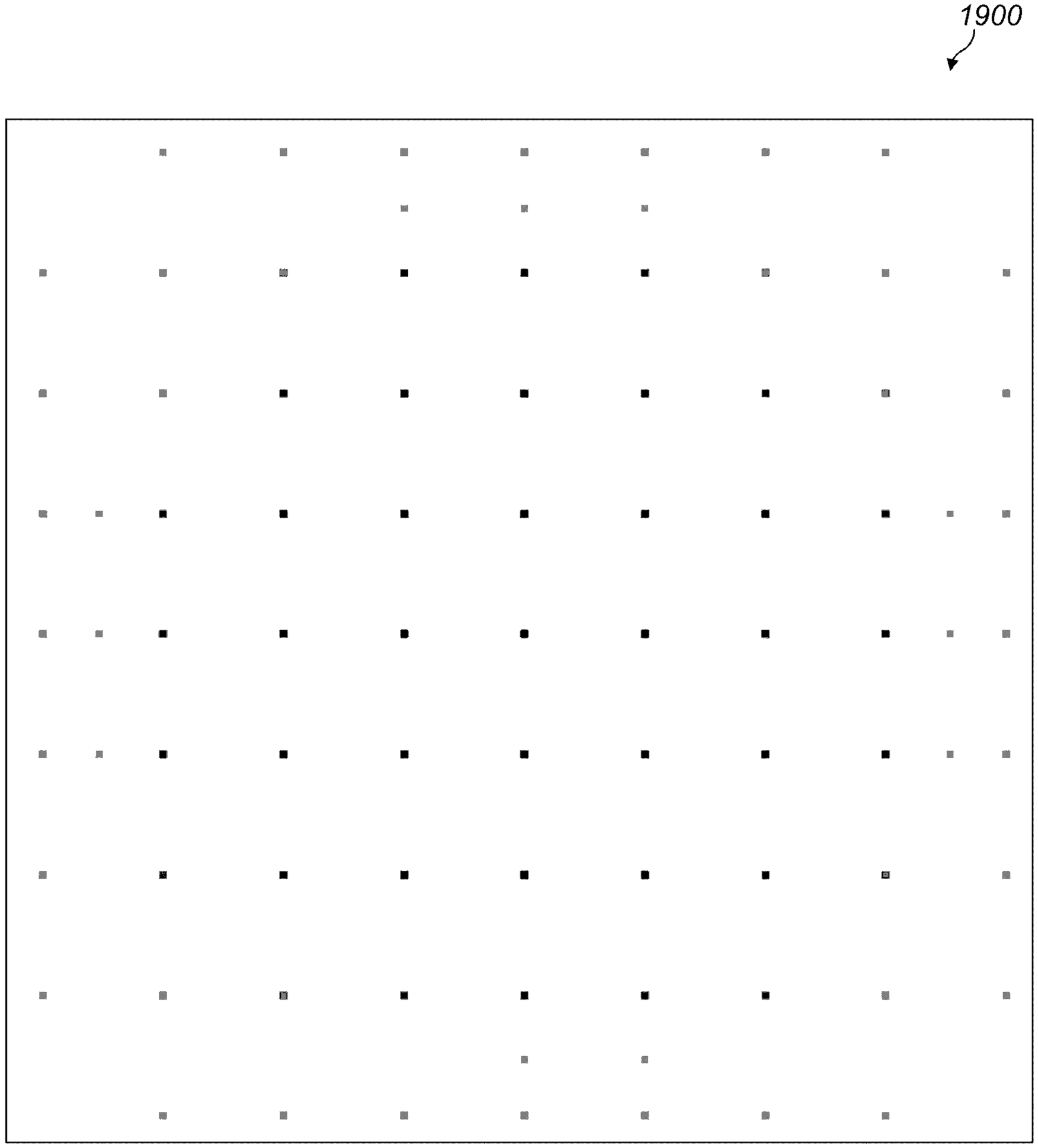


FIG. 19

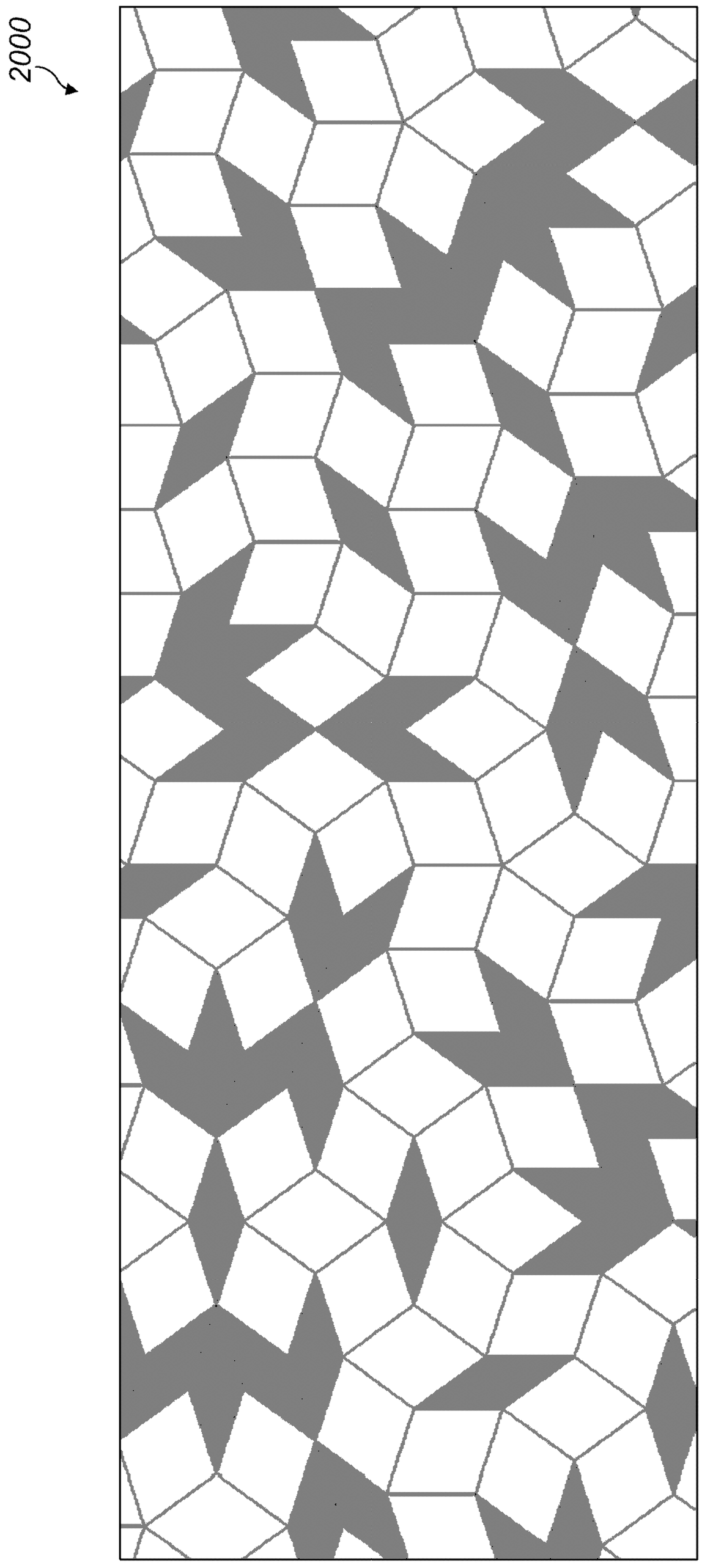


FIG. 20

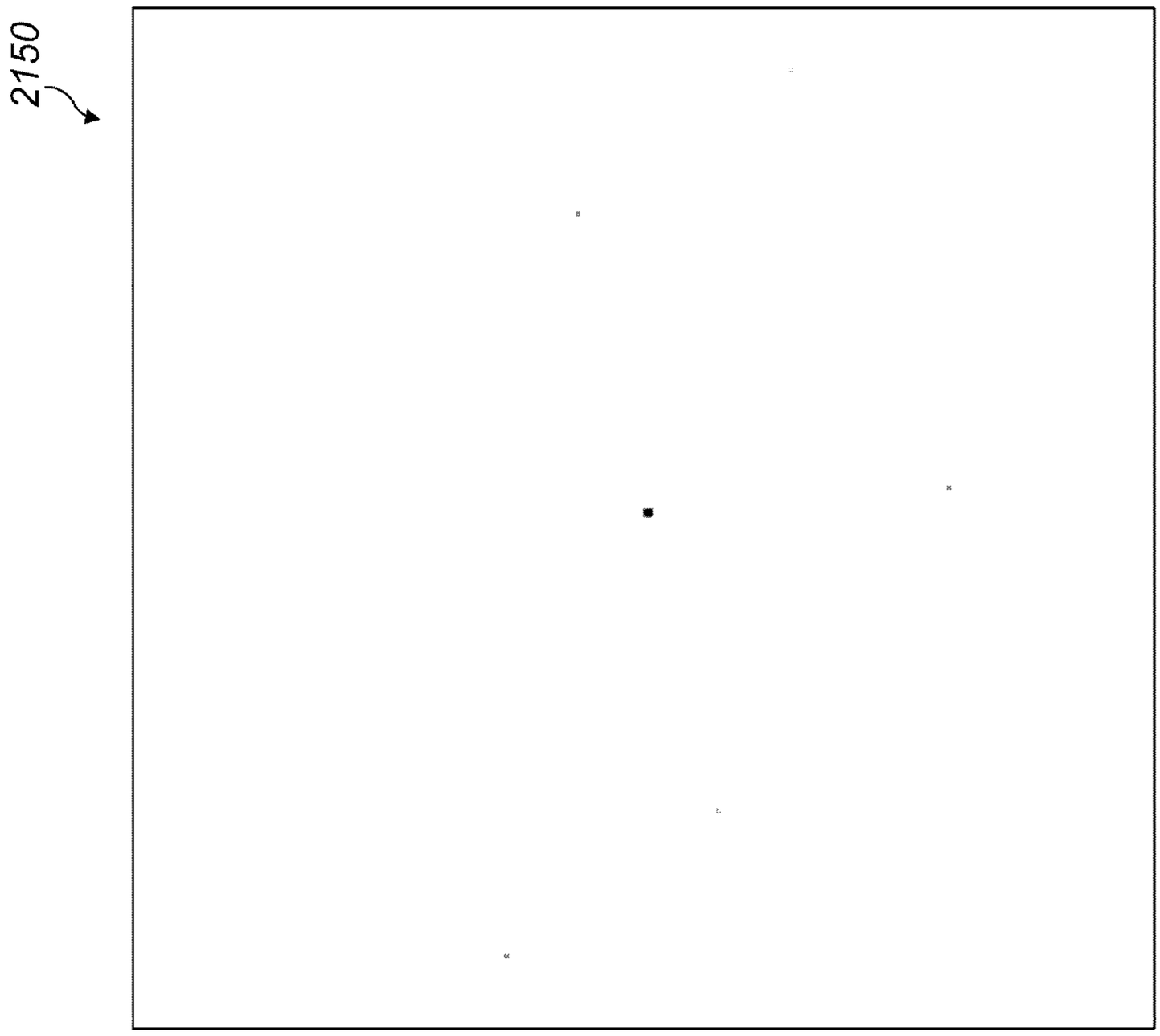


FIG. 21B

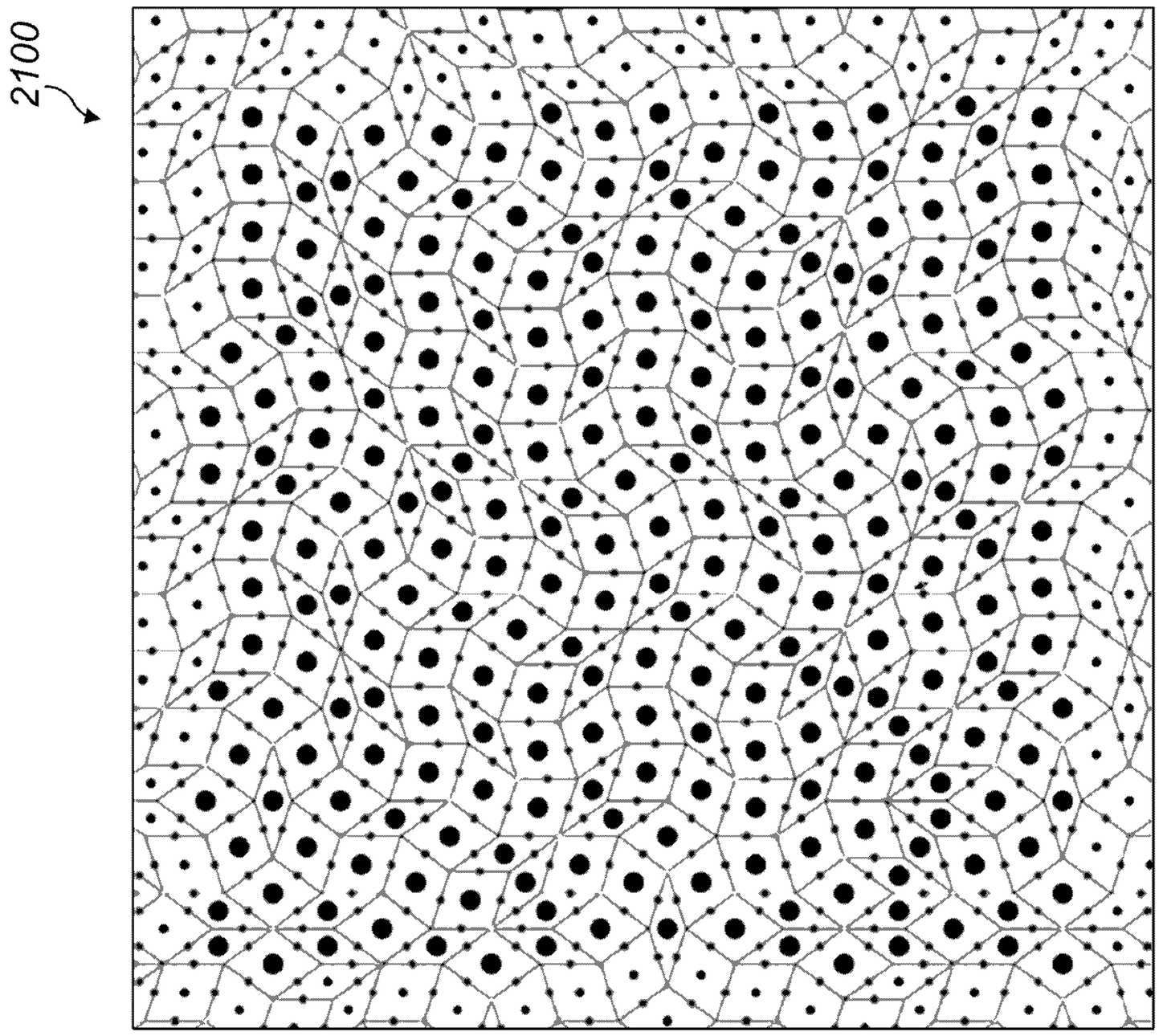


FIG. 21A

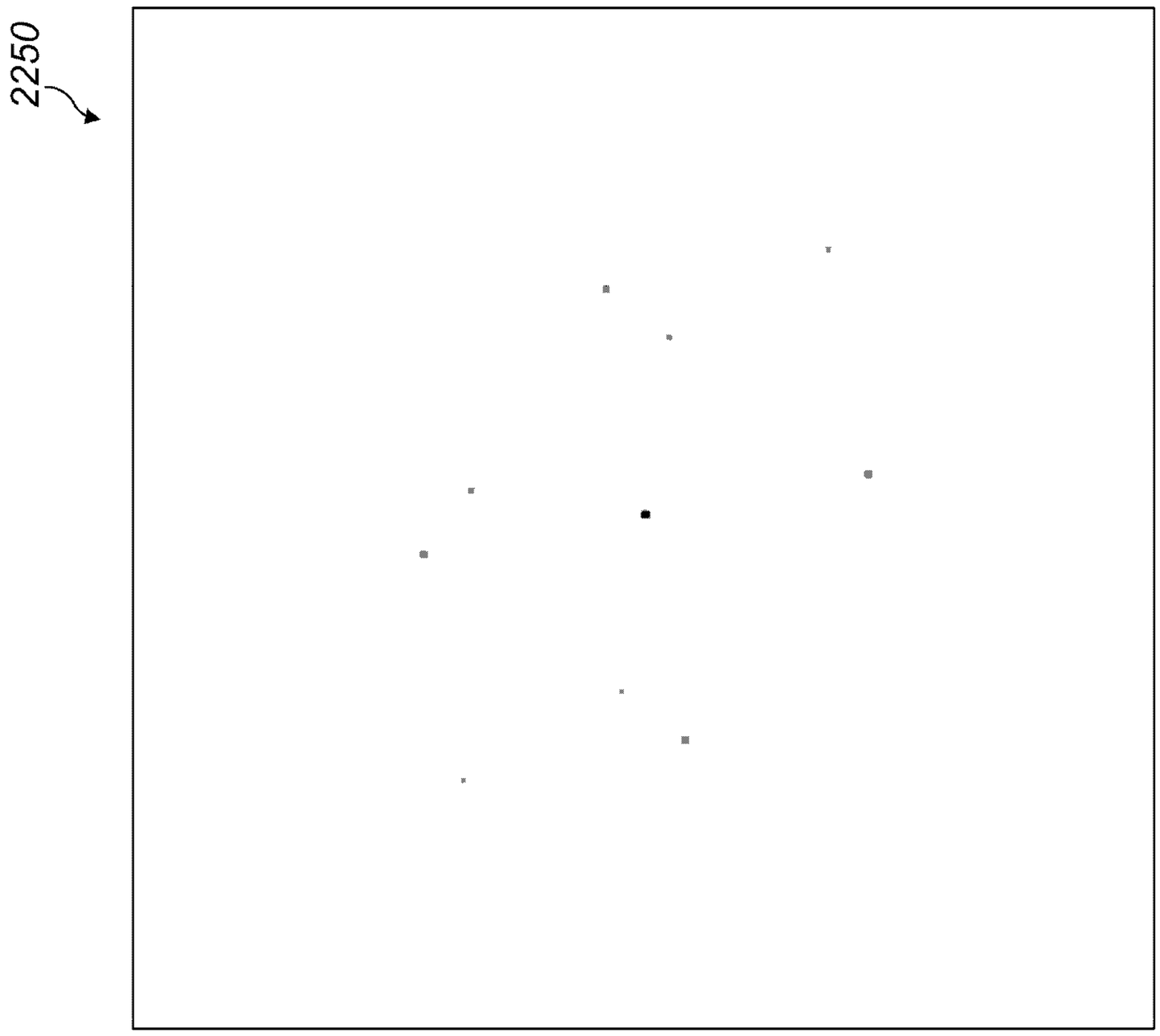


FIG. 22B

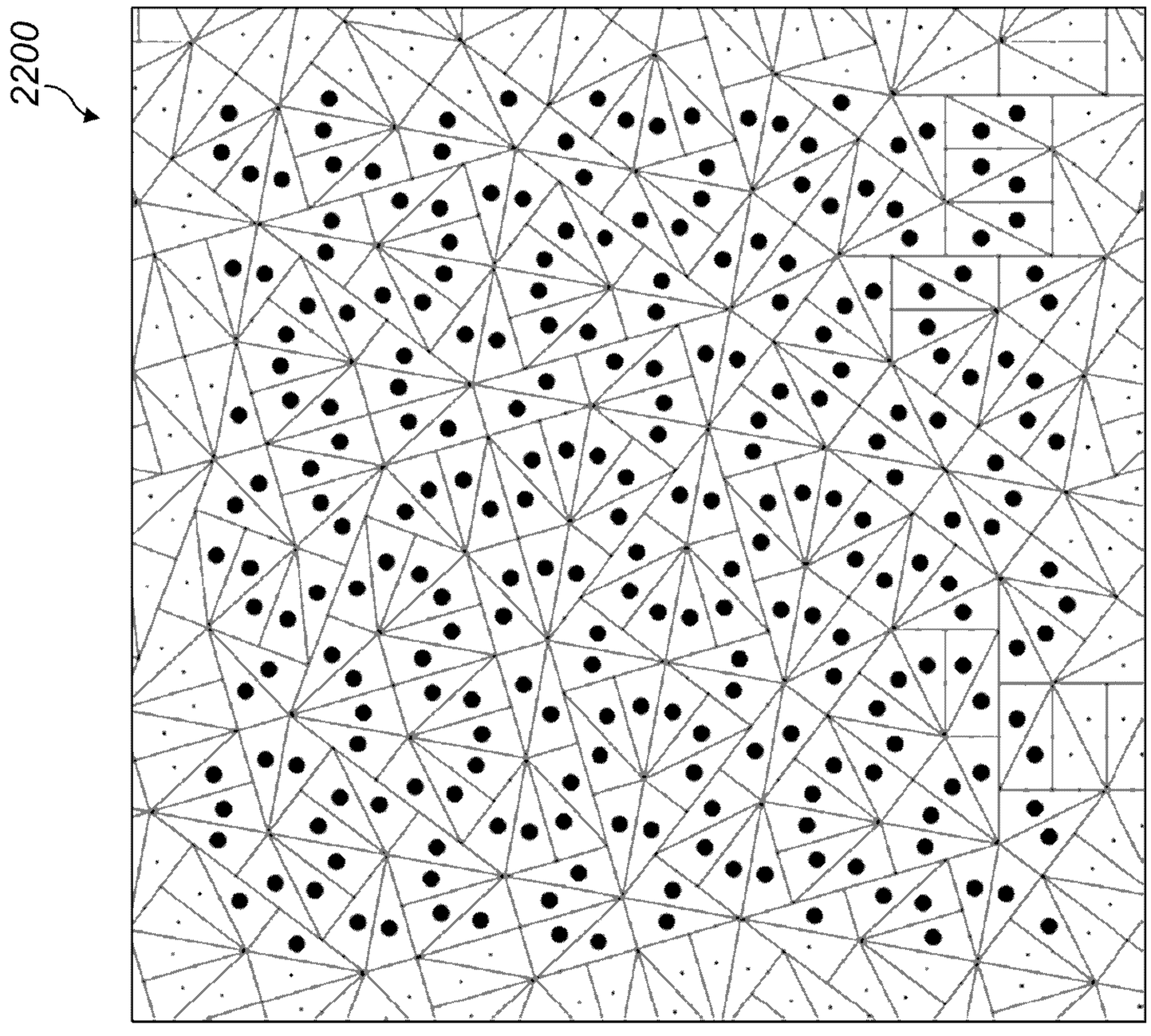


FIG. 22A

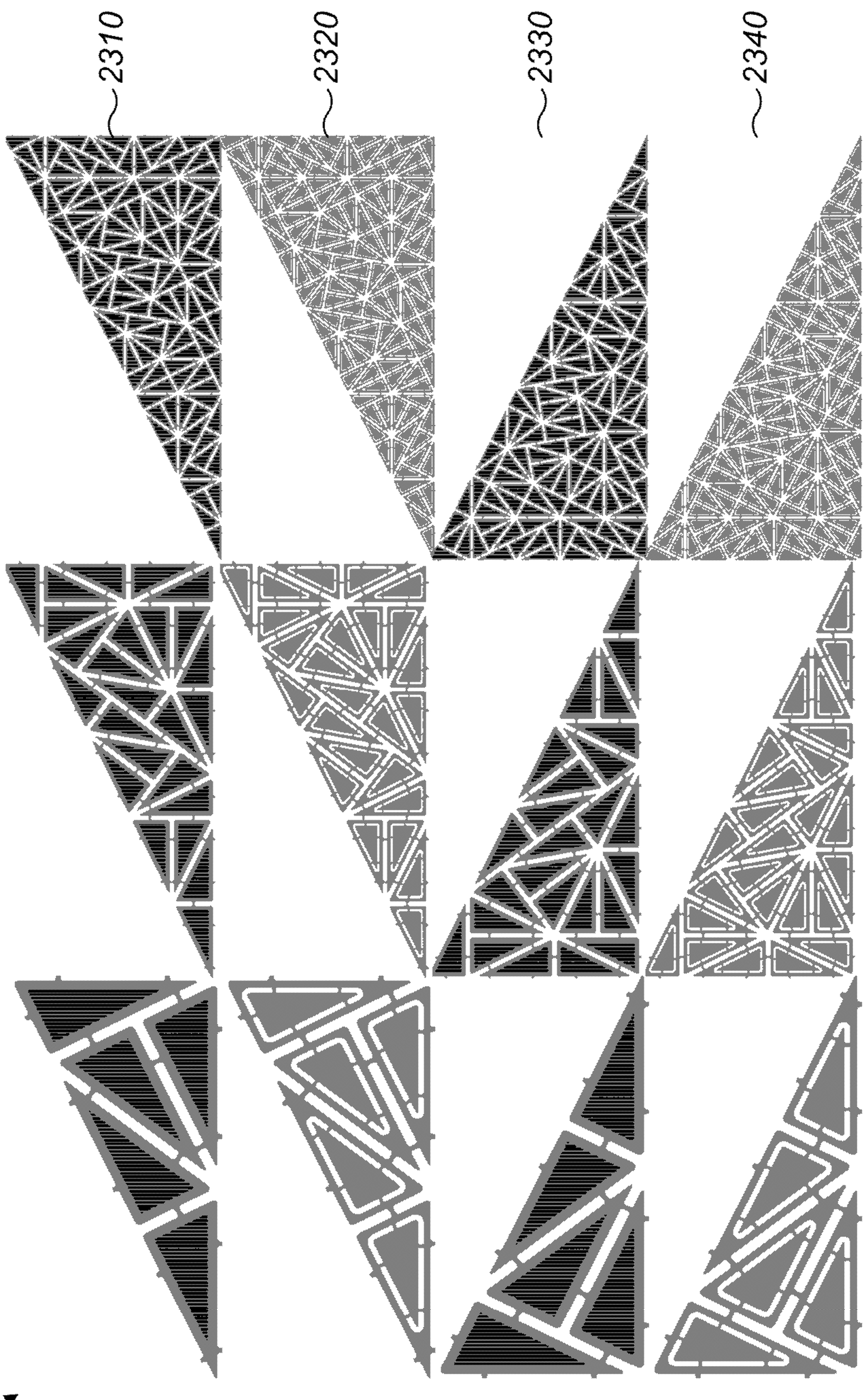


FIG. 23

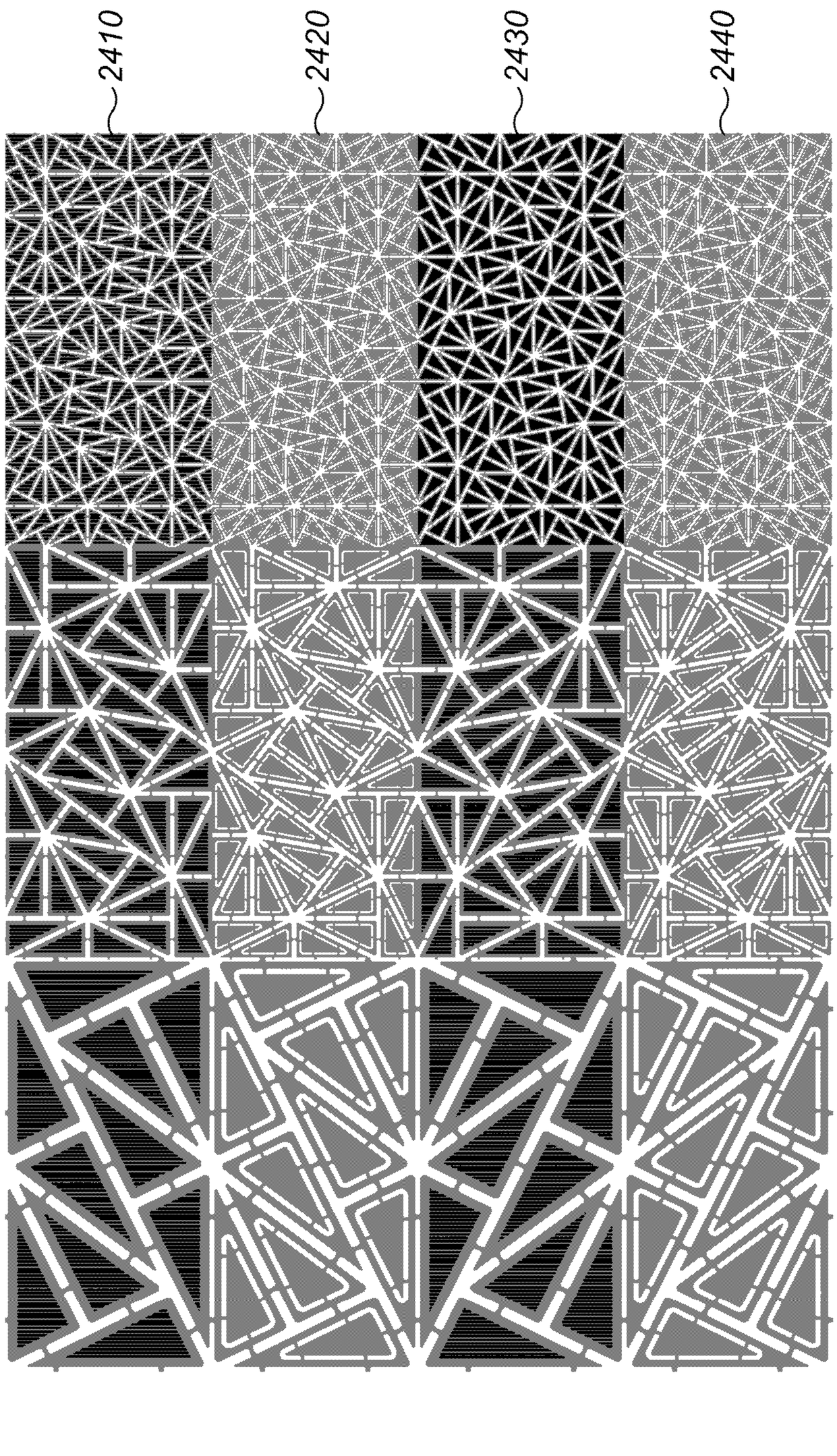


FIG. 24

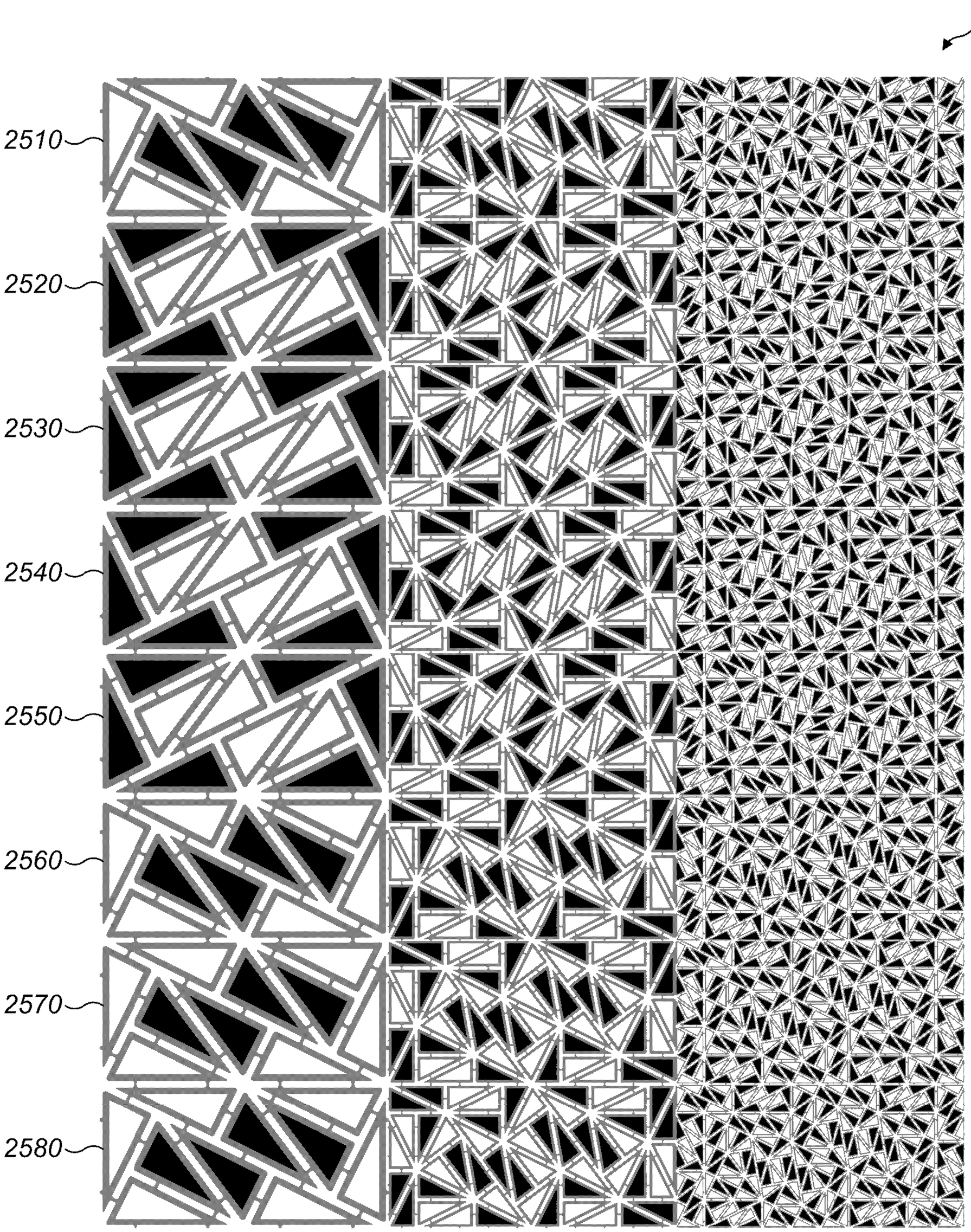


FIG. 25

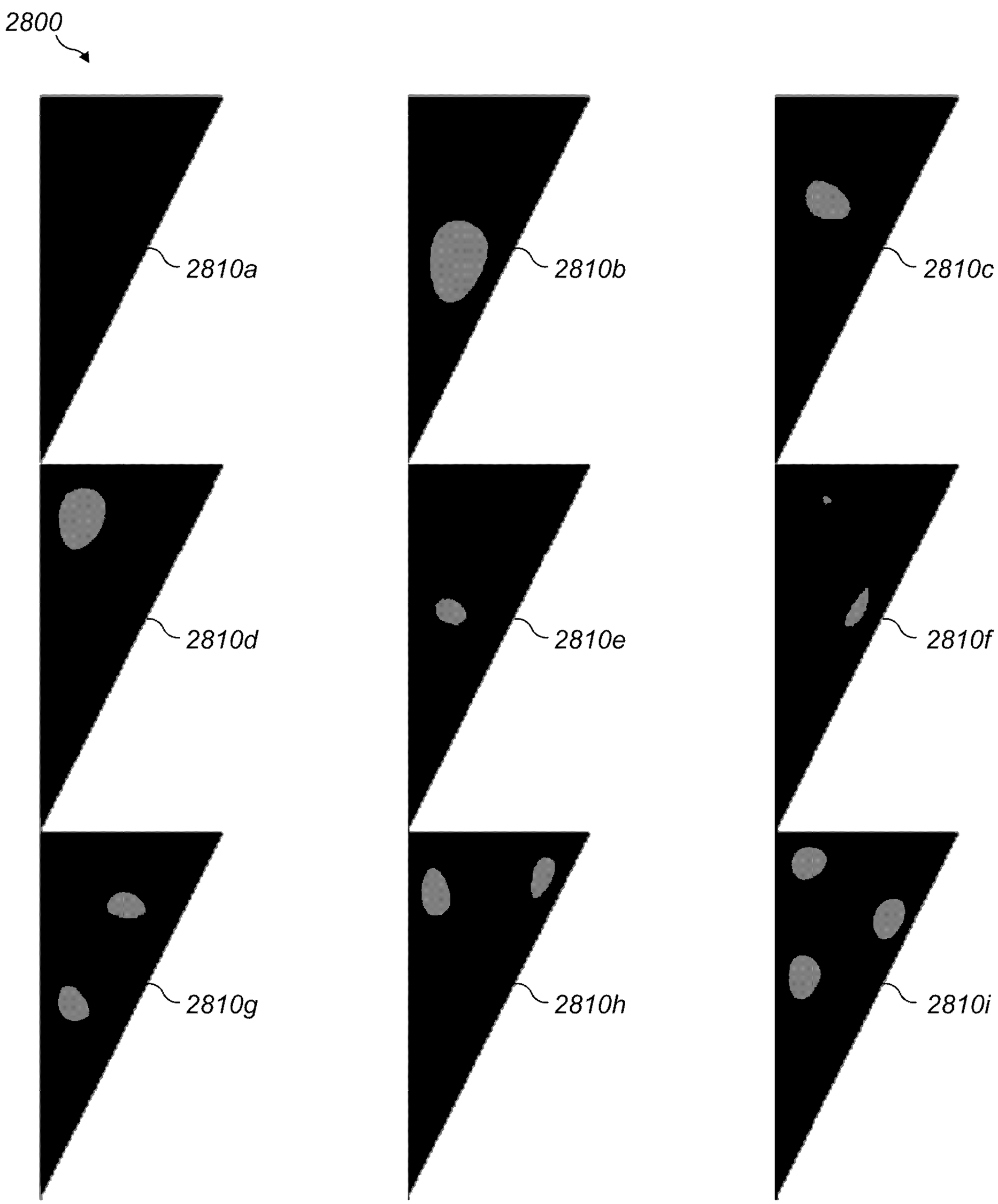


FIG. 26

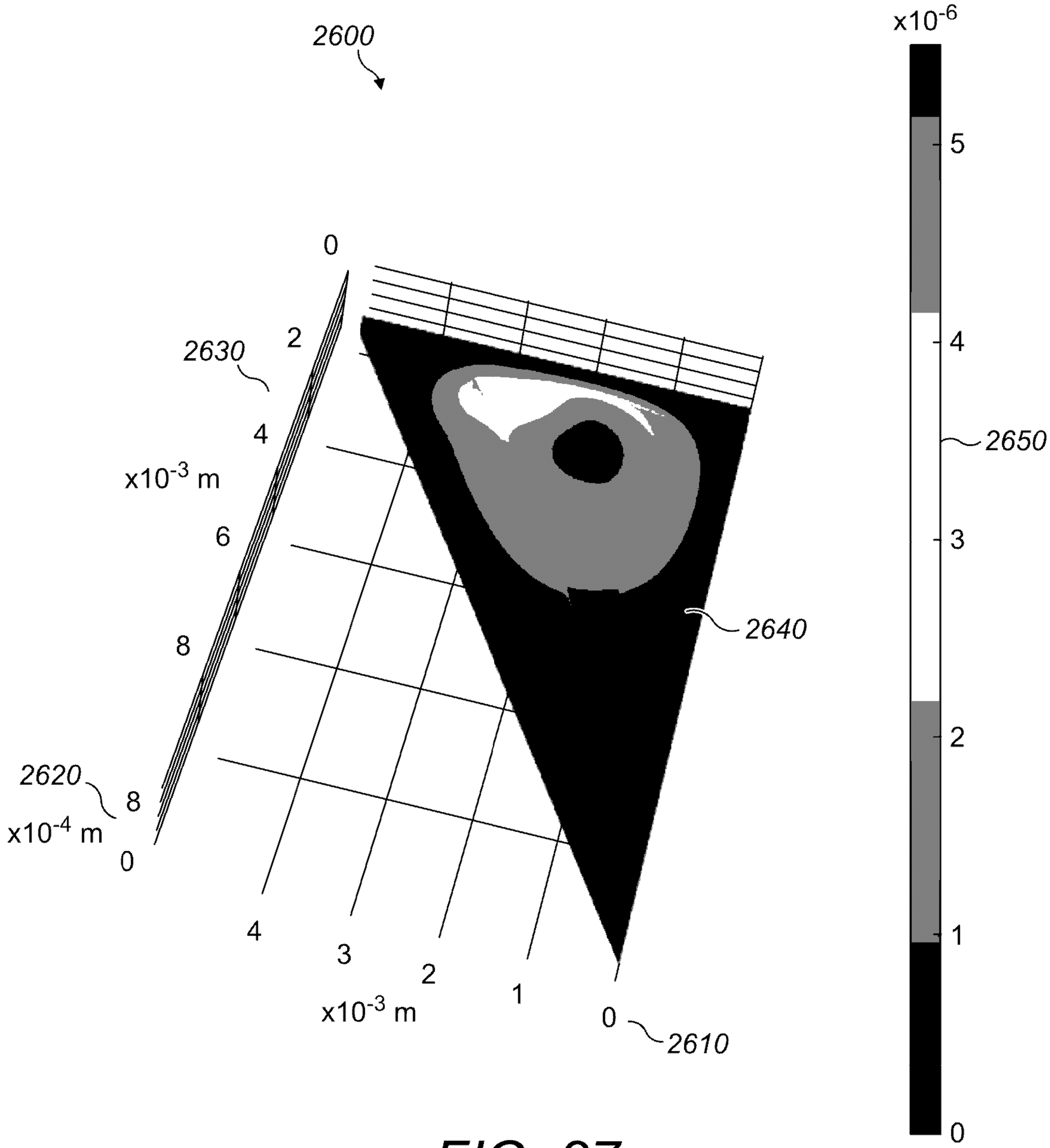

2600
x10-6
5
4
2650
3
2
1
0
2640
0
2630
2
4
x10-3 m
6
8
2620
8
x10-4 m
0
4
3
2
1
0
x10-3 m
2610

FIG. 27

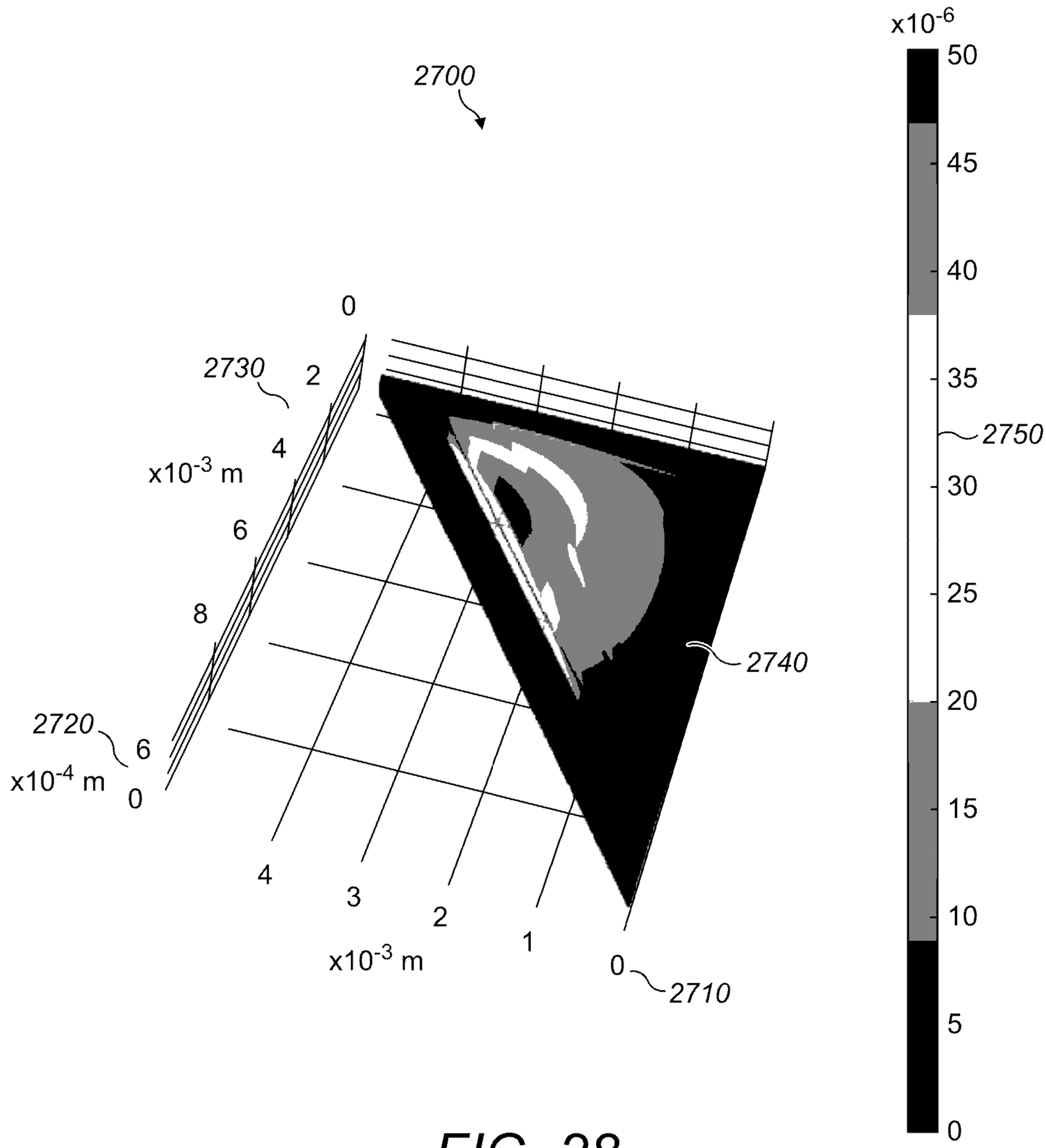

2700
2730
2720
2740
2710
2750
x10-3 m
x10-4 m
x10-3 m
x10-6
0
2
4
6
8
6
0
4
3
2
1
0
50
45
40
35
30
25
20
15
10
5
0

FIG. 28

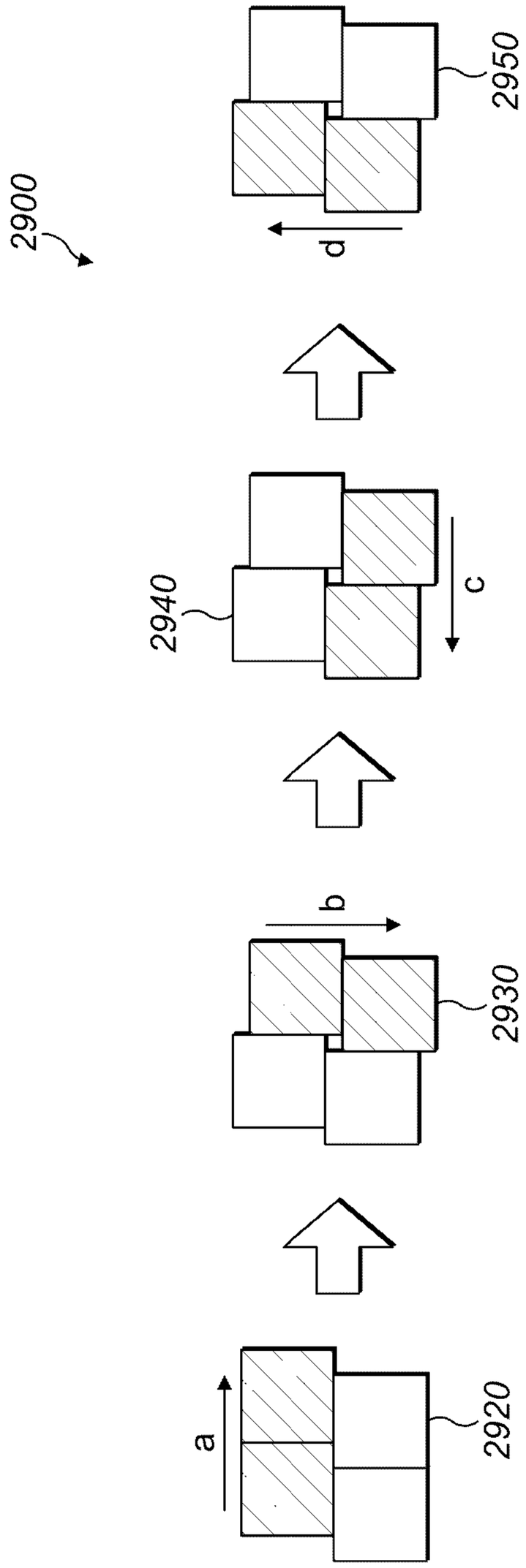


FIG. 29

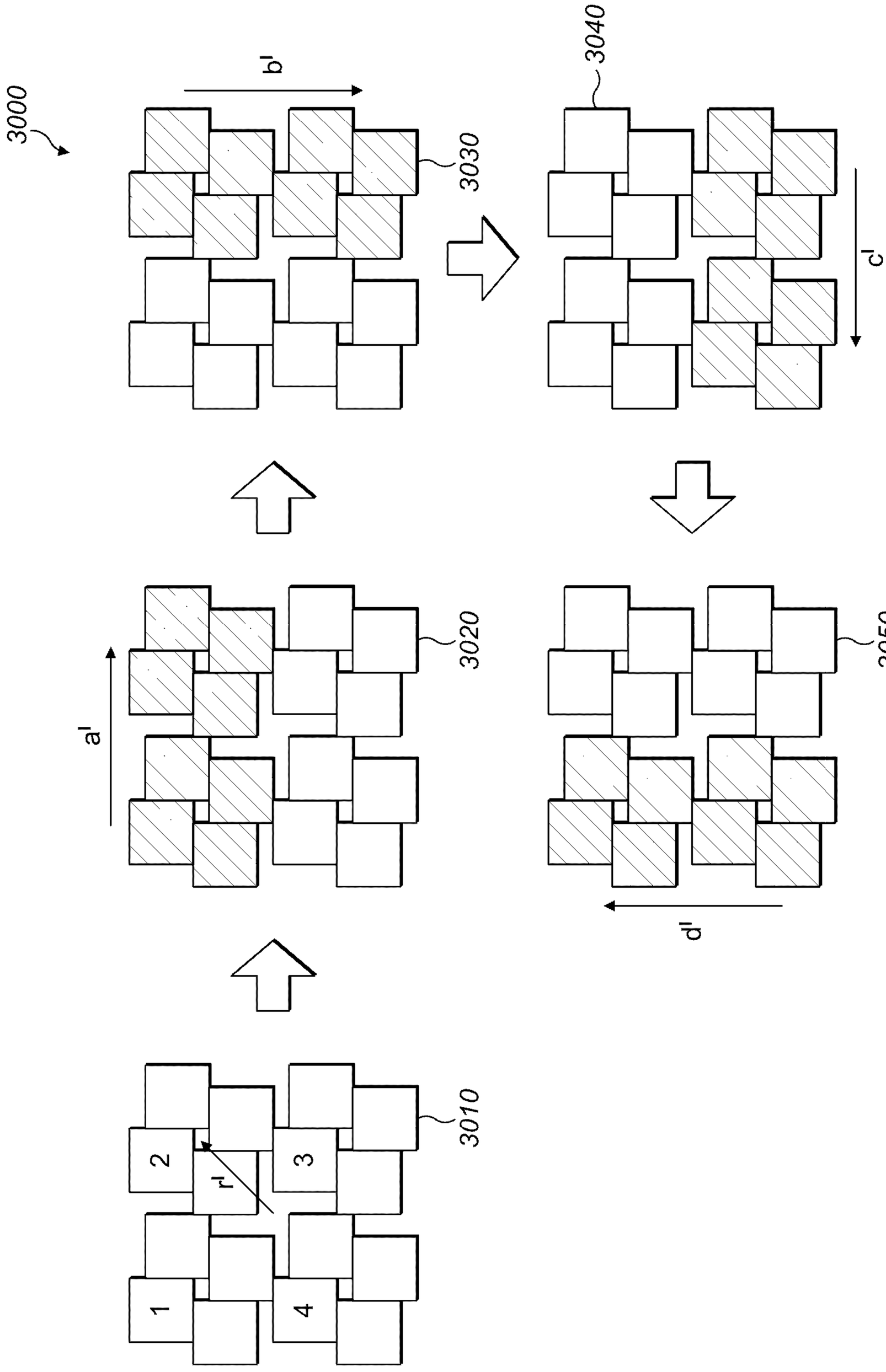


FIG. 30

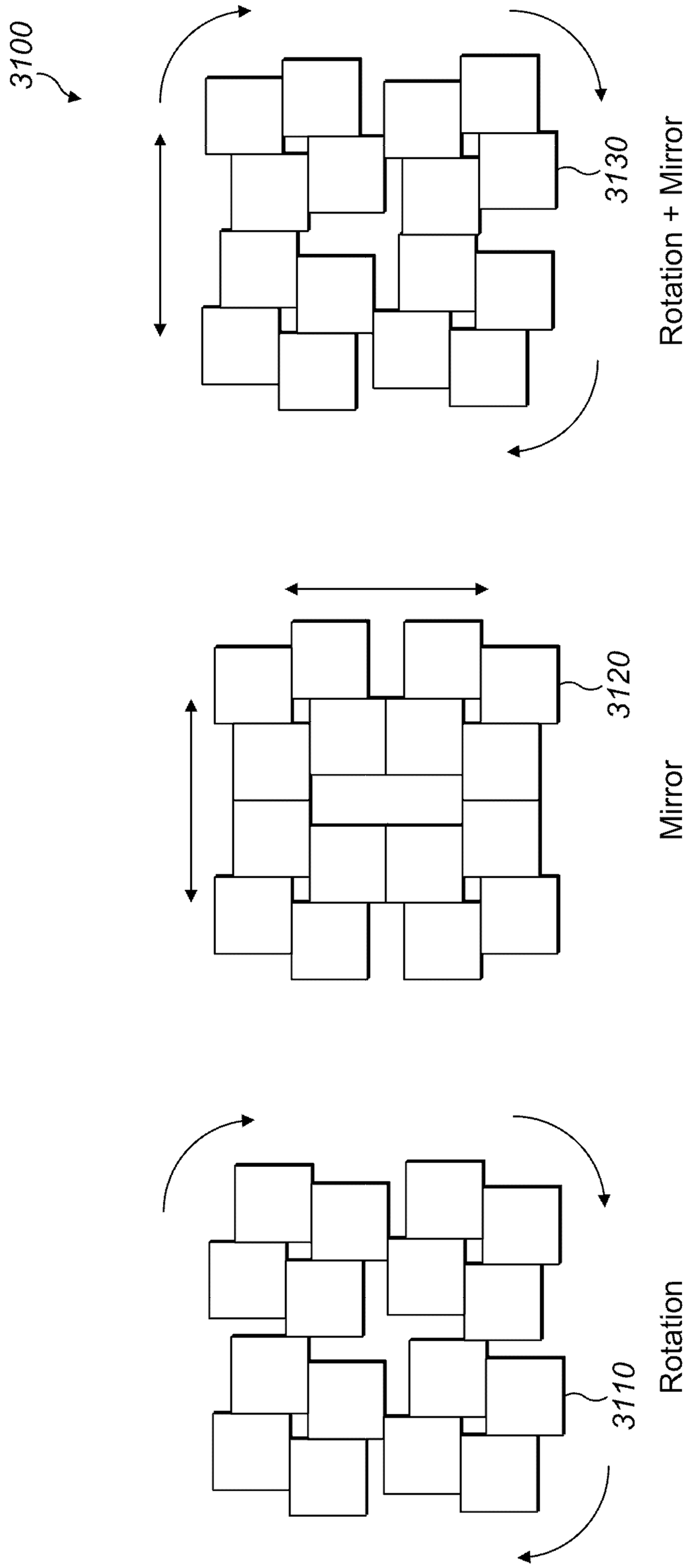


FIG. 31

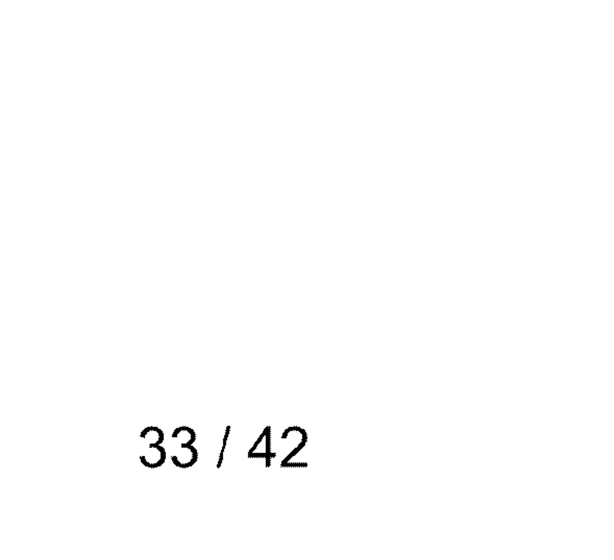


FIG. 32A

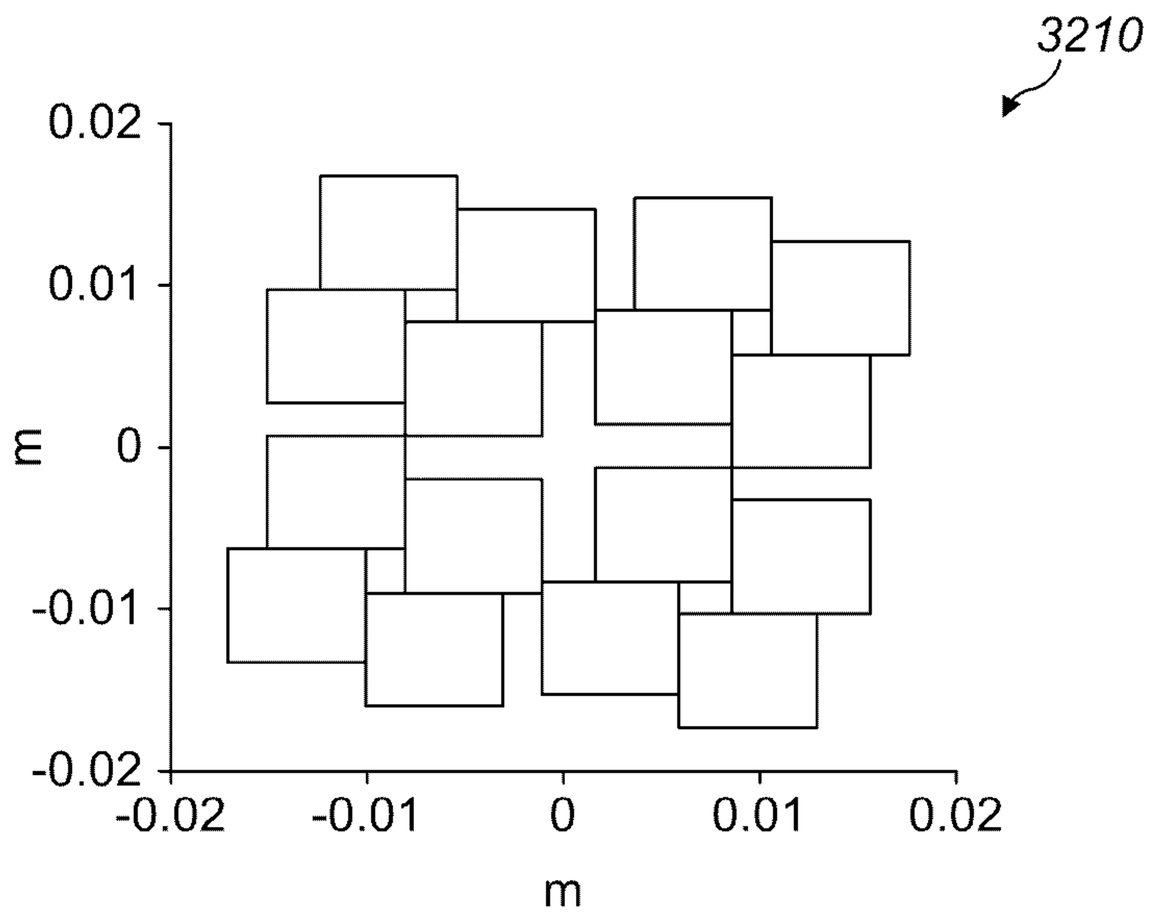


FIG. 32B

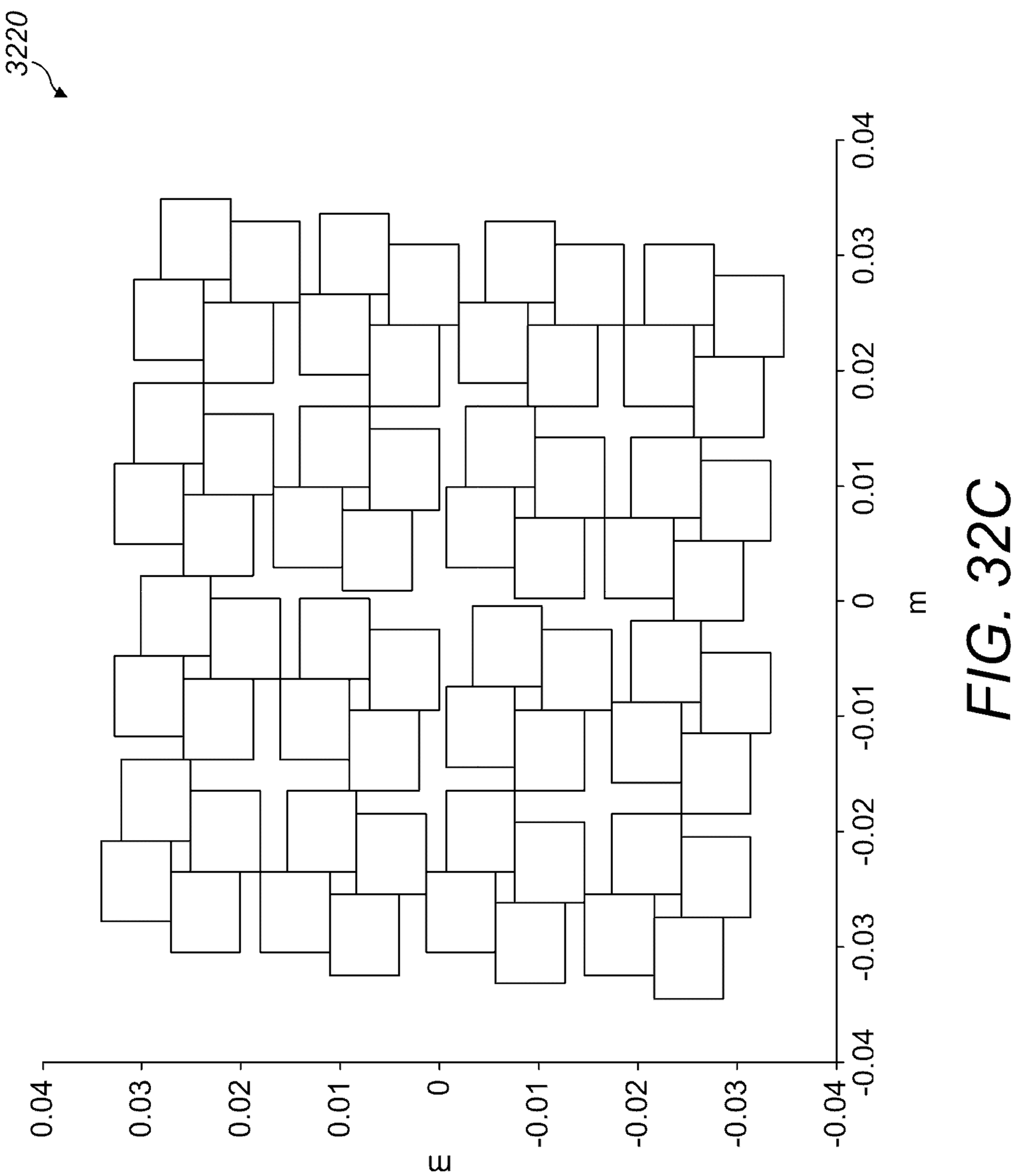

322C
0.04
0.03
0.02
0.01
0
-0.01
-0.02
-0.03
-0.04
m
0.04
0.03
0.02
0.01
0
-0.01
-0.02
-0.03
-0.04
m

FIG. 32C

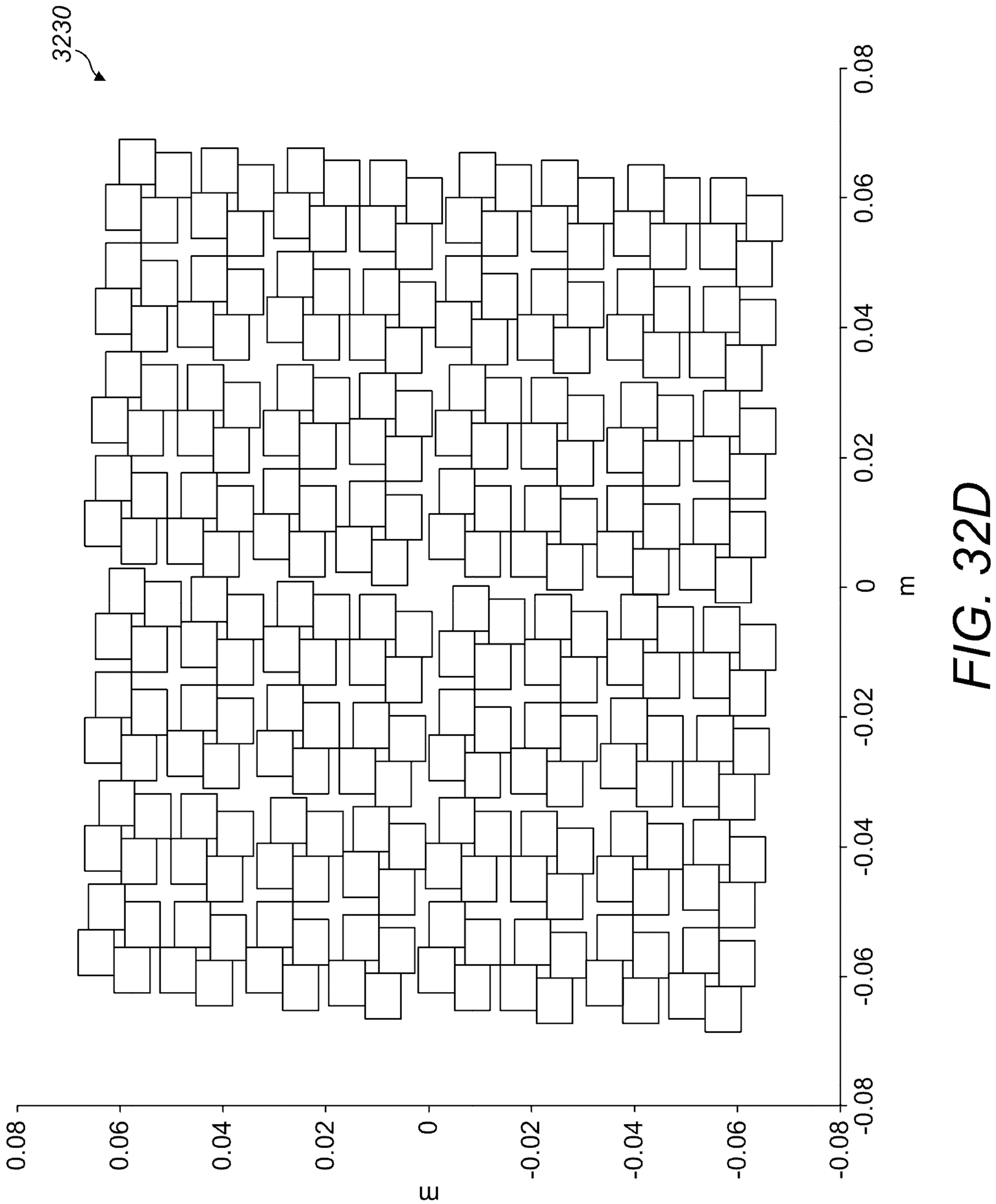

3230
0.08
0.06
0.04
0.02
0
-0.02
-0.04
-0.06
-0.08
m
0.08
0.06
0.04
0.02
0
-0.02
-0.04
-0.06
-0.08
m

FIG. 32D

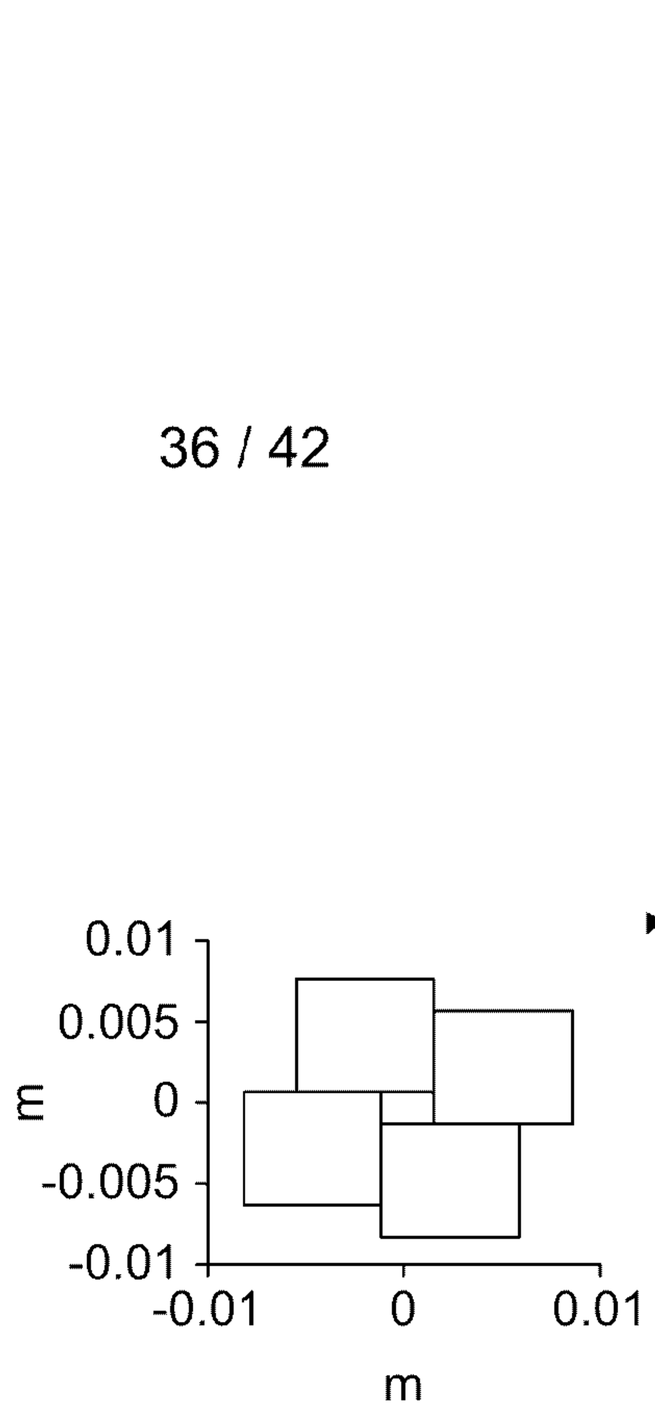


FIG. 33A

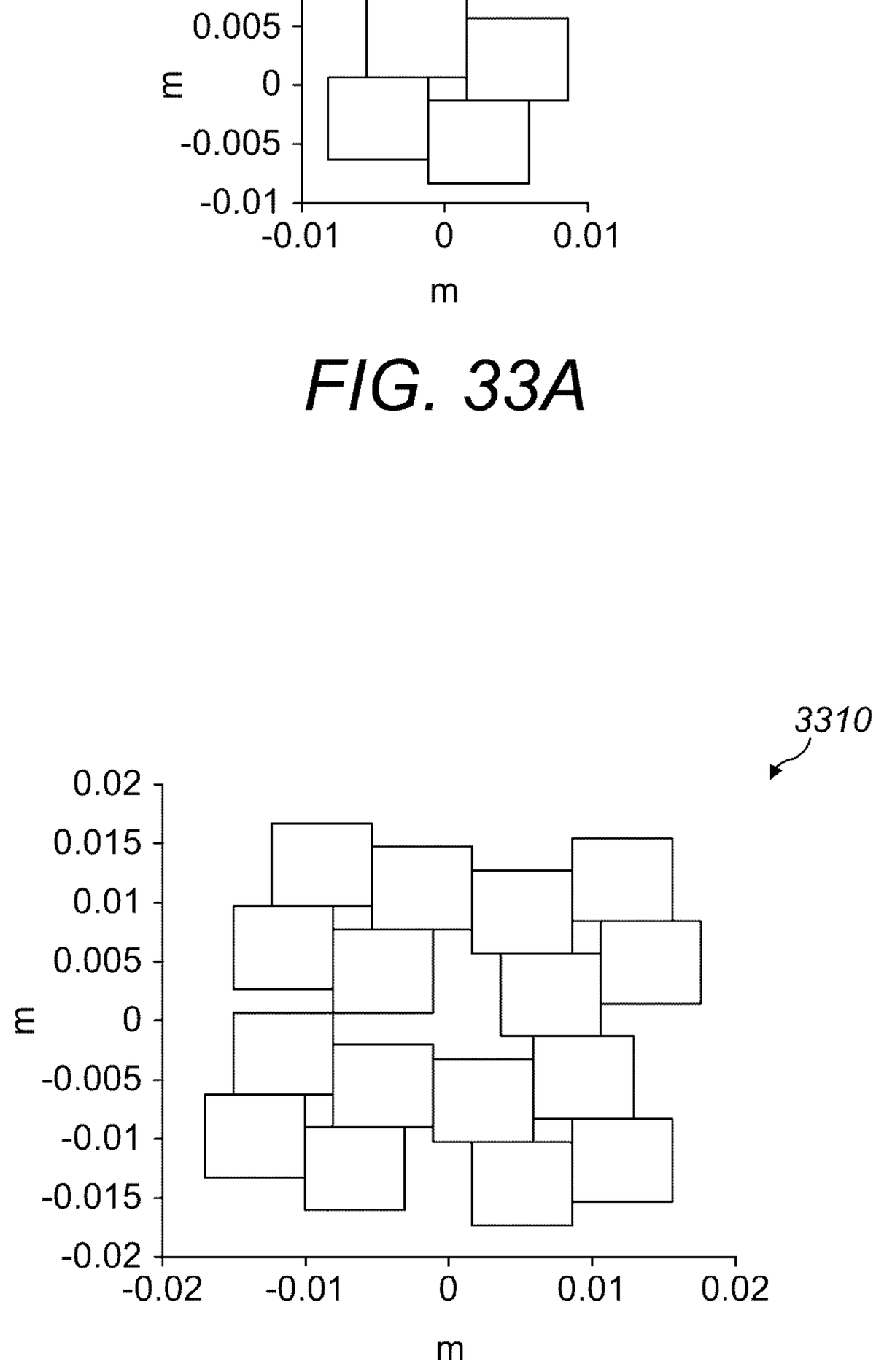


FIG. 33B

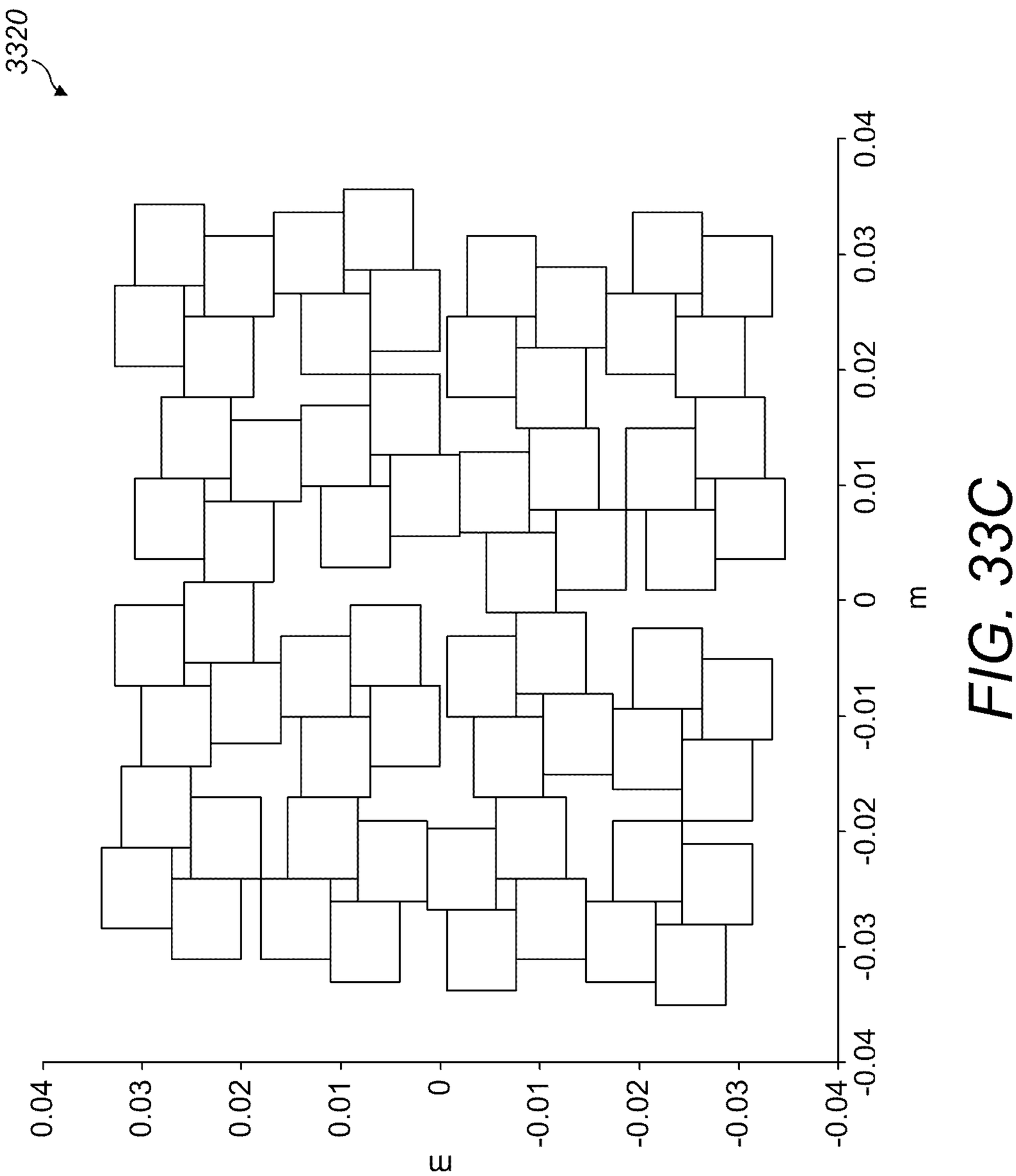

332
0.04
0.03
0.02
0.01
0
-0.01
-0.02
-0.03
-0.04
0.04
0.03
0.02
0.01
0
-0.01
-0.02
-0.03
-0.04
m
m

FIG. 33C

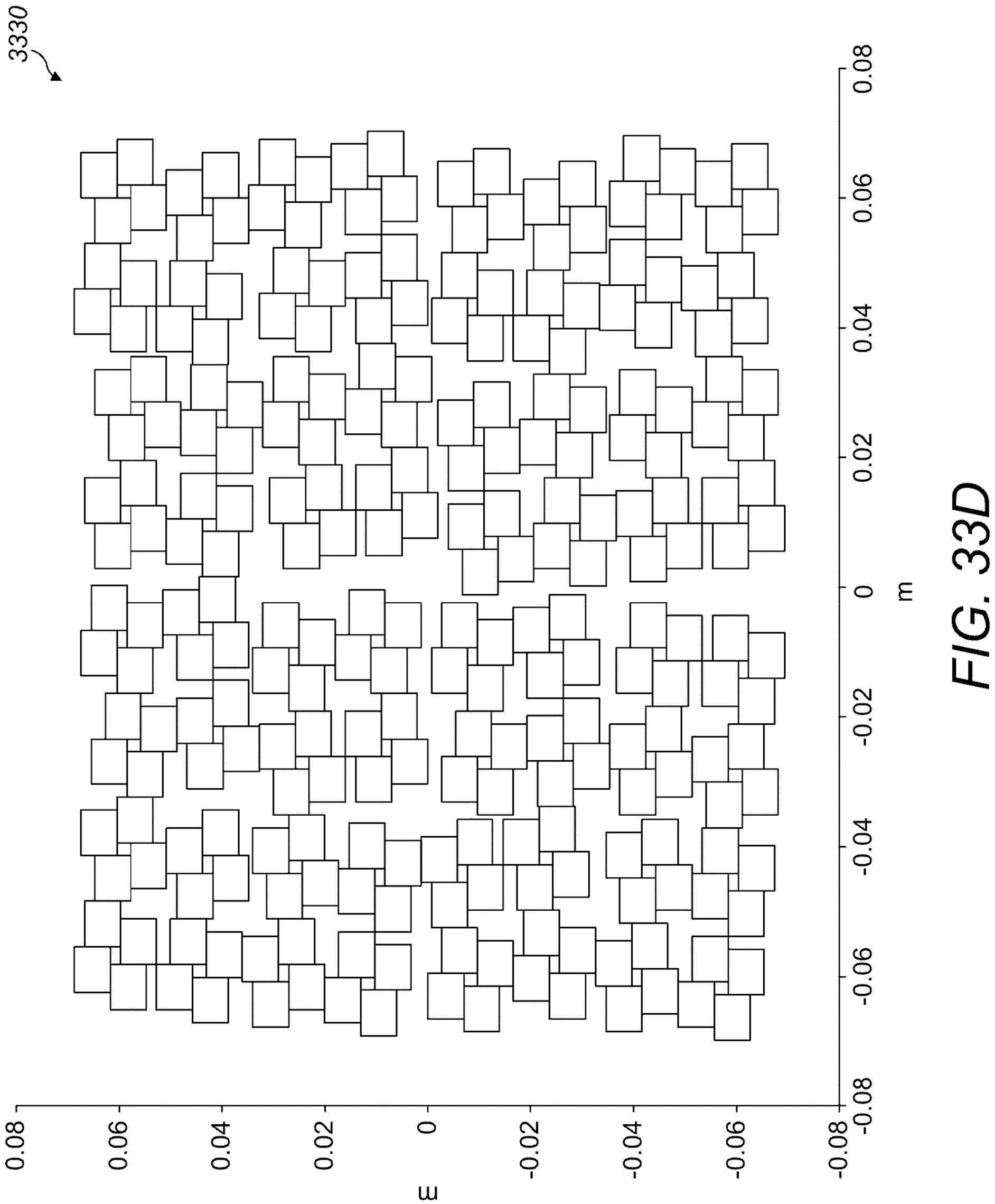

3330
0.08
0.06
0.04
0.02
0
-0.02
-0.04
-0.06
-0.08
m
0.08
0.06
0.04
0.02
0
-0.02
-0.04
-0.06
-0.08
m

FIG. 33D

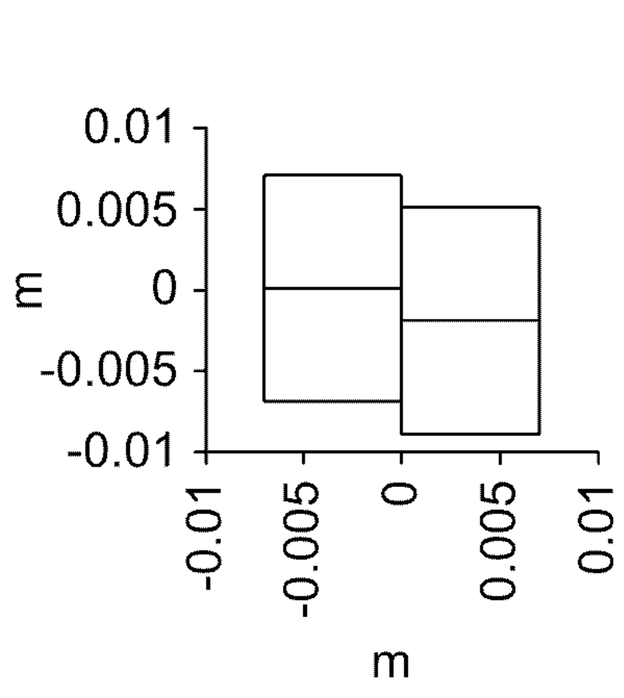


FIG. 34A

FIG. 34B

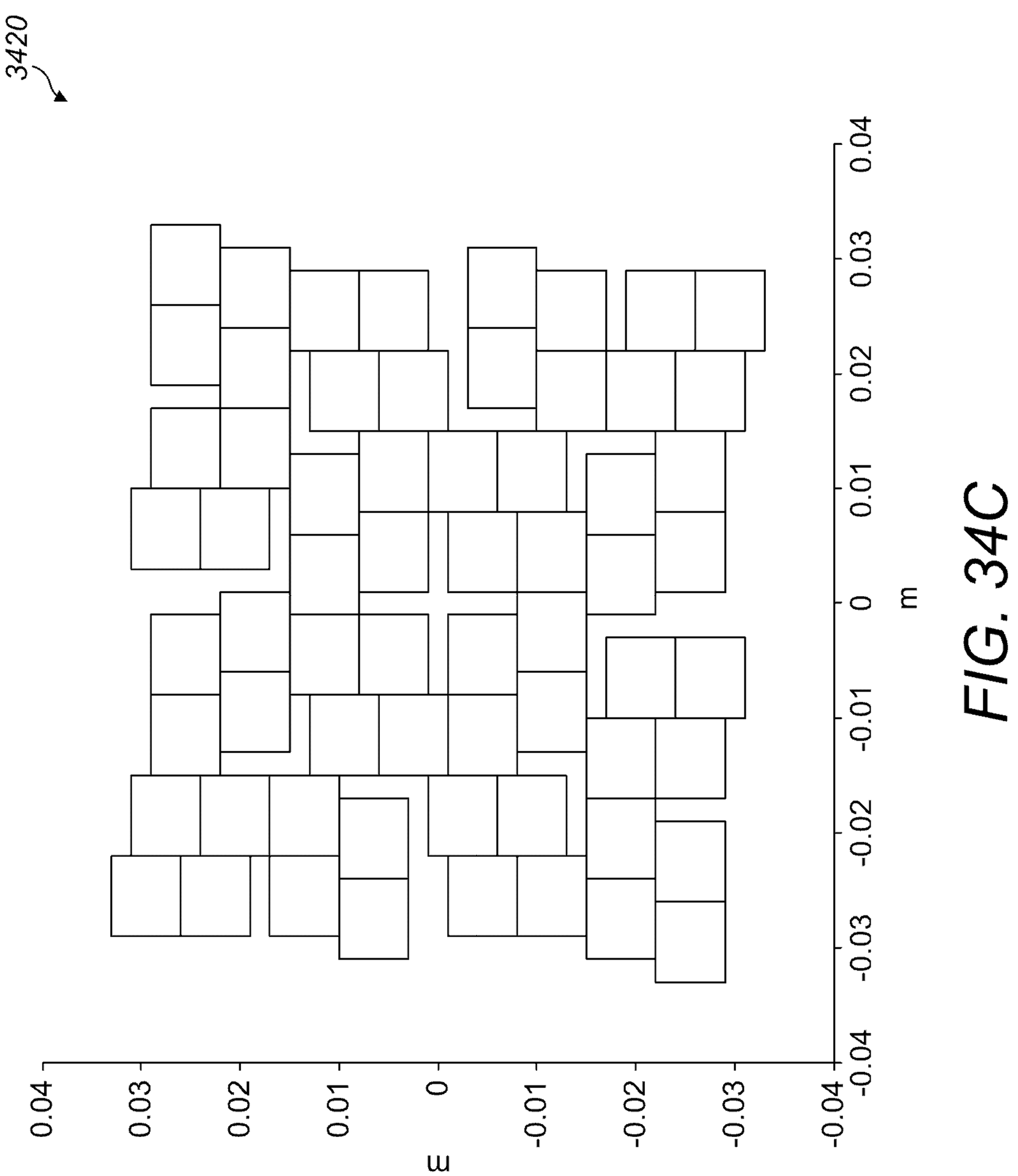

342
0.04
0.03
0.02
0.01
0
-0.01
-0.02
-0.03
-0.04
m
0.04
0.03
0.02
0.01
0
-0.01
-0.02
-0.03
-0.04
m

FIG. 34C

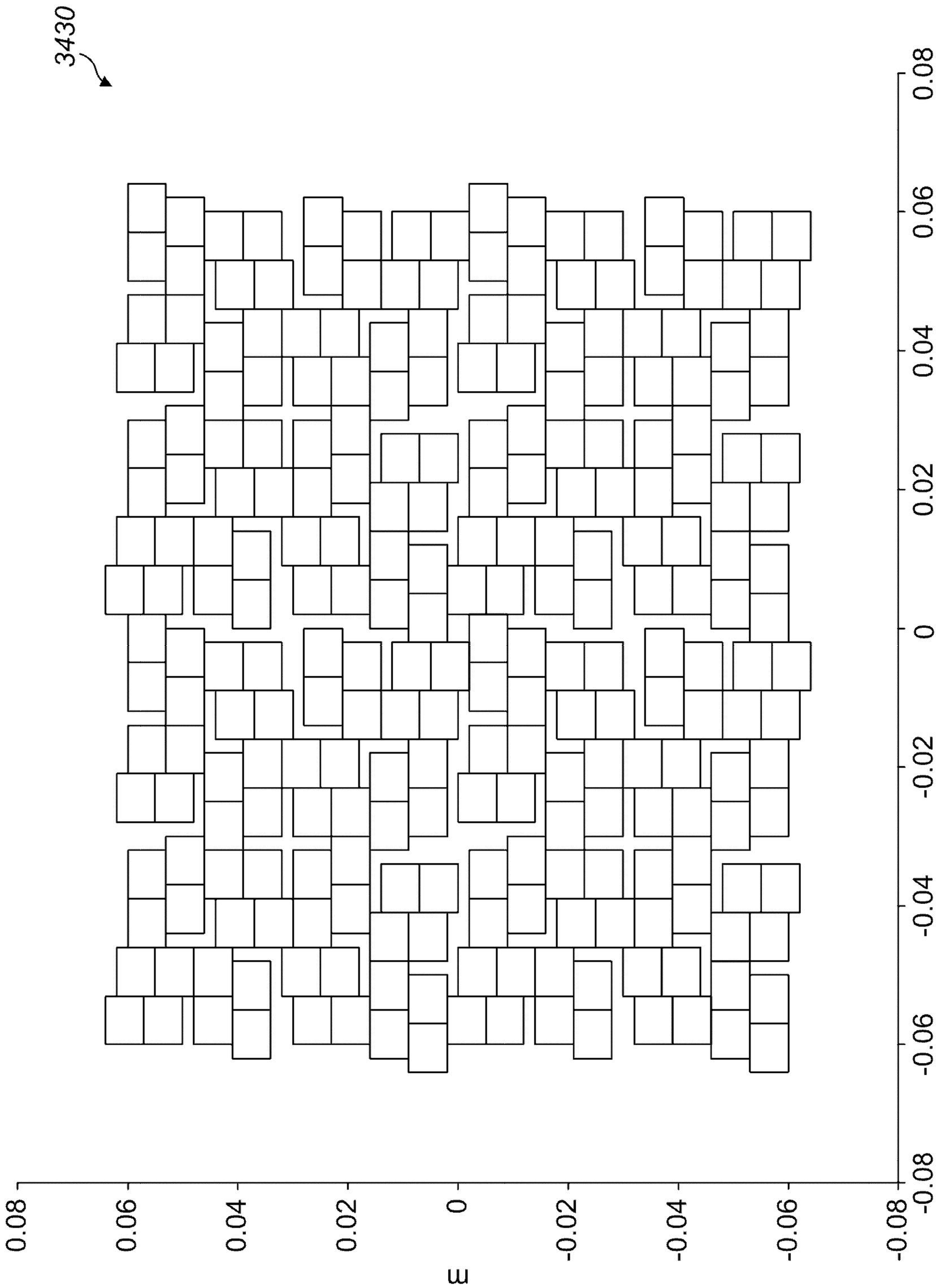

3430
0.08
0.06
0.04
0.02
0
-0.02
-0.04
-0.06
-0.08
m
0.08
0.06
0.04
0.02
0
-0.02
-0.04
-0.06
-0.08
m

FIG. 34D

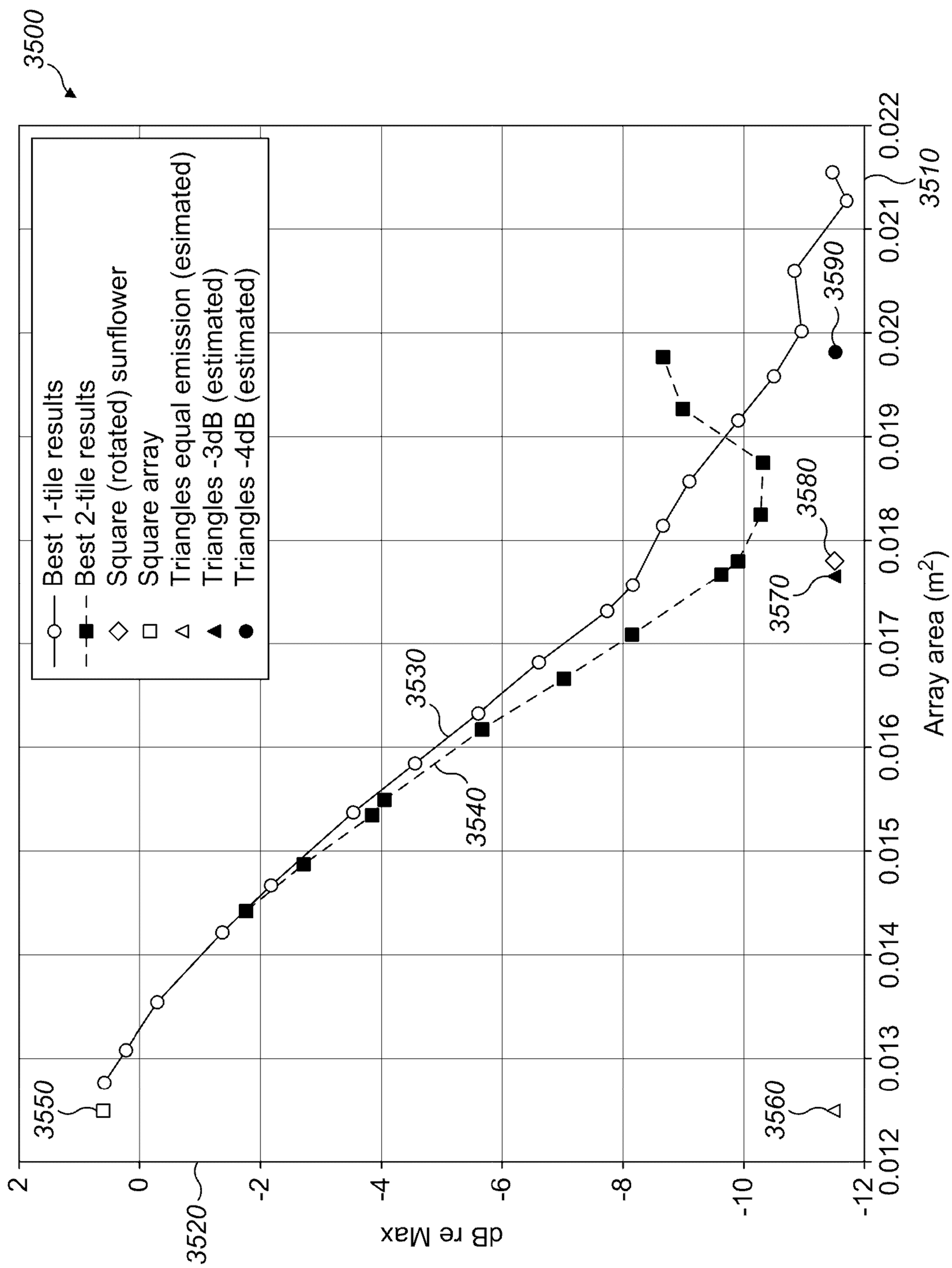

500
Best 1-tile results
Best 2-tile results
Square (rotated) sunflower
Square array
Triangles equal emission (esimated)
Triangles -3dB (estimated)
Triangles -4dB (estimated)
3550
3530
3540
3580
3590
3570
3560
3510
3520
0.012
0.013
0.014
0.015
0.016
0.017
0.018
0.019
0.020
0.021
0.022
Array area (m2)
2
0
-2
-4
-6
-8
-10
-12
dB re Max

FIG. 35

INTERNATIONAL SEARCH REPORT

International application No
PCT/GB2020/053373

A. CLASSIFICATION OF SUBJECT MATTER
INV. B06B1/06 G10K11/34 G10K11/04 G10K11/02 G10K11/22
ADD.

According to International Patent Classification (IPC) or to both national classification and IPC

B. FIELDS SEARCHED

Minimum documentation searched (classification system followed by classification symbols)
B06B G10K A61B

Documentation searched other than minimum documentation to the extent that such documents are included in the fields searched

Electronic data base consulted during the international search (name of data base and, where practicable, search terms used)
EPO-Internal, WPI Data

C. DOCUMENTS CONSIDERED TO BE RELEVANT

Category*	Citation of document, with indication, where appropriate, of the relevant passages	Relevant to claim No.
X Y	WO 2016/073936 A2 (CHIRP MICROSYSTEMS [US]) 13 May 2016 (2016-05-13) paragraphs [0008], [0019], [0026], [0018]; claim 1; figure 3 -----	1,2,5,8, 14,19 3,6,7, 9-13,17, 18,20
X	JAGER AXEL ET AL: "Air-coupled 40-KHZ ultrasonic 2D-phased array based on a 3D-printed waveguide structure", 2017 IEEE INTERNATIONAL ULTRASONICS SYMPOSIUM (IUS), IEEE, 6 September 2017 (2017-09-06), pages 1-4, XP033245009, DOI: 10.1109/ULTSYM.2017.8091892 [retrieved on 2017-10-31] pages 1, 2; figures 1, 2 -----	1,2,4, 14-16

-/--

[X] Further documents are listed in the continuation of Box C.

[X] See patent family annex.

* Special categories of cited documents :

"A" document defining the general state of the art which is not considered to be of particular relevance

"E" earlier application or patent but published on or after the international filing date

"L" document which may throw doubts on priority claim(s) or which is cited to establish the publication date of another citation or other special reason (as specified)

"O" document referring to an oral disclosure, use, exhibition or other means

"P" document published prior to the international filing date but later than the priority date claimed

"T" later document published after the international filing date or priority date and not in conflict with the application but cited to understand the principle or theory underlying the invention

"X" document of particular relevance; the claimed invention cannot be considered novel or cannot be considered to involve an inventive step when the document is taken alone

"Y" document of particular relevance; the claimed invention cannot be considered to involve an inventive step when the document is combined with one or more other such documents, such combination being obvious to a person skilled in the art

"&" document member of the same patent family

Date of the actual completion of the international search	Date of mailing of the international search report
18 March 2021	26/03/2021
Name and mailing address of the ISA/ European Patent Office, P.B. 5818 Patentlaan 2 NL - 2280 HV Rijswijk Tel. (+31-70) 340-2040, Fax: (+31-70) 340-3016	Authorized officer Pitzer, Hanna

2

Form PCT/ISA/210 (second sheet) (April 2005)

INTERNATIONAL SEARCH REPORT

International application No
PCT/GB2020/053373

C(Continuation). DOCUMENTS CONSIDERED TO BE RELEVANT

Category*	Citation of document, with indication, where appropriate, of the relevant passages	Relevant to claim No.
Y	US 2001/033124 A1 (NORRIS ELWOOD G [US] ET AL) 25 October 2001 (2001-10-25) paragraph [0039]	3,9-13
Y	US 2011/066032 A1 (VITEK SHUKI [IL] ET AL) 17 March 2011 (2011-03-17) paragraph [0004]; claim 13	6,7,17, 18
Y	EP 0 309 003 A2 (TRW INC [US]) 29 March 1989 (1989-03-29) figure 9	20

INTERNATIONAL SEARCH REPORT

Information on patent family members

International application No
PCT/GB2020/053373

Patent document cited in search report	Publication date	Patent family member(s)	Publication date
WO 2016073936 A2	13-05-2016	EP 3216231 A2	13-09-2017
		US 2017236506 A1	17-08-2017
		WO 2016073936 A2	12-05-2016
US 2001033124 A1	25-10-2001	NONE	
US 2011066032 A1	17-03-2011	US 2011066032 A1	17-03-2011
		WO 2011024074 A2	03-03-2011
EP 0309003 A2	29-03-1989	NONE	